Electron-withdrawing group modification of thermally-activated delayed fluorescence materials for blue OLEDs with high efficiency and durability

横山, 正幸

2020

Doctor thesis

Electron-withdrawing group modification of thermally-activated delayed fluorescence materials for blue OLEDs with high efficiency and durability

Masayuki Yokoyama

Department of Chemistry and Biochemistry
Graduate School of Engineering
Kyushu University

Contents

Chapter 1

Introduction

1-1. Background and motivation

1-1-1. Organic light-emitting diodes

Organic light-emitting diodes (OLEDs) have attracted a great deal of attention due to their superior advantages that are not provided by conventional inorganic light-emitting diodes (LEDs) and liquid crystal displays (LCDs). They are now gradually being used as light sources for not only large-sized displays but also lighting.[1,2] **Figure 1-1** a shows the basic structure of an OLED having the multiple organic thin-film stacks consisting of the hole transport, emission, and electron transport layers between the transparent (Indium-tin-oxide: ITO) and metal electrodes. When a voltage is applied between the two electrodes, holes and electrons are injected into the hole transport layer and electron transport layer, respectively. By the applied electric field between the electrodes, the injected charges are transported, then the holes and electrons recombine in the emission layer, leading to the formation of excitons. Each organic layer in OLEDs is fabricated usually less than 100 nm thickness with the methods such as vacuum deposition and inkjet printing (**Figure 1-1** b).[3,4]

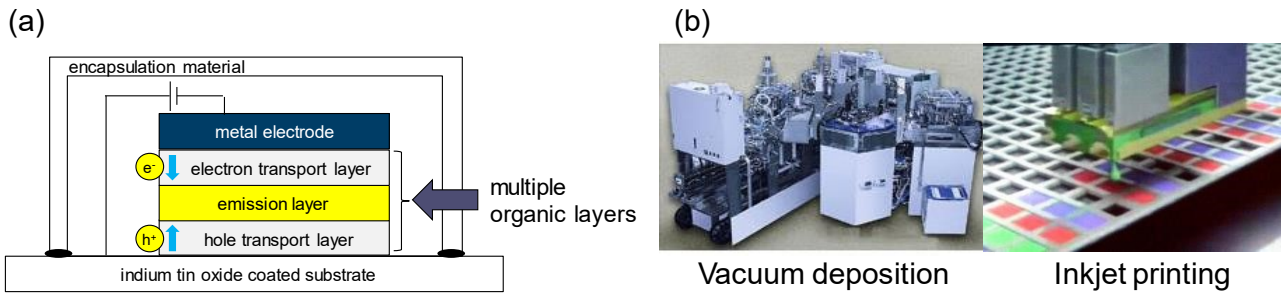

Figure 1-1 (a) Typical device structure of OLEDs, (b) Manufacturing method of OLEDs.

The features of OLEDs are the thinness and flexibility, utilizing the softness and low-temperature processing characteristics of organic materials, and the high image quality (high contrast and short response time) comes from the superior emission properties of organic emitters. This makes it possible to design high-quality displays and lighting in a variety of forms, regardless of whether flat, curved, rollable, or transparent. OLEDs are expected to be used in all parts of our daily lives in the near future. However, OLEDs have not yet established a competitive advantage over inorganic LEDs and LCDs in terms of power consumption, durability, and manufacturing costs at present. This prevents the OLED market from further expanding.

The key component that determines the power consumption and durability of OLEDs is the emitting materials. OLED display normally uses three emitters: blue, green, and red, corresponding to the three primary colors of light. As described below, the biggest bottleneck is blue OLEDs. Compared to green and red OLEDs, blue OLEDs are inferior in terms of luminescence efficiency, maximum brightness, and stability. These problems are mainly caused by the high excited state energy of the blue emitters. When I succeed to develop a promising blue emitter, therefore, it will improve greatly in the power consumption and device lifetime, and enhance the further expansion of the OLED market.

1-1-2. Emitting materials

In order to obtain highly efficient electroluminescence (EL), it is essential to utilize an electrically generated triplet excitons as an EL because 25% of singlet and 75% of triplet excitons are directly generated according to the spin statistical law due to the random injection of electron spin of the carriers.[5,6] The emitting materials for OLEDs are generally categorized into three types by the emission mechanisms; that are the fluorescent, phosphorescent, and thermally-activated delayed fluorescence (TADF) materials (**Figure 1-2**).

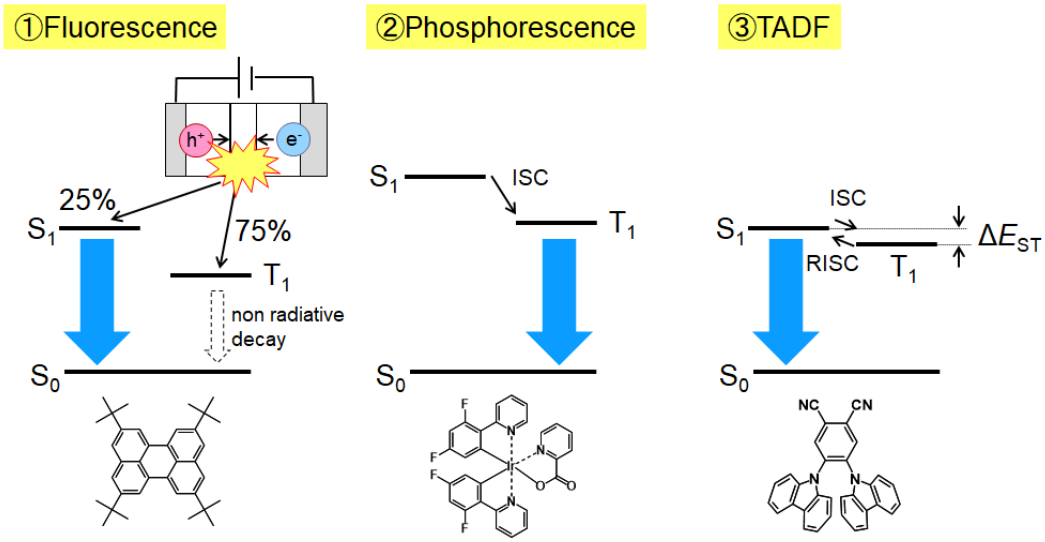

Figure 1-2 Emitting mechanisms of fluorescence, phosphorescence, and TADF materials.

Fluorescent molecules can use only 25% of the generated excitons under the current excitation because the radiative transition from the lowest triplet excited state (T_1) to the singlet ground state (S_0) is strictly prohibited by spin conservation law. Therefore, the internal EL quantum efficiency (IQE) is limited to 25%. Thus, many researchers have applied other approaches to harvest triplet energy for fluorescent emission. One possible way is a utilization of up-conversion process *via* triplet-triplet annihilation (TTA). In the TTA process, two triplet excitons combine their energy to yield one highly lying singlet exciton, whose energy is close to twice that of the triplet exciton. The production of additional singlet exciton can increase the efficiency between 15% and 37.5% depending on the up-conversion mechanism.[7] However, the maximum IQE is still limited to 62.5%. Meanwhile, IQE of phosphorescent materials can achieve 100% through the intersystem crossing (ISC).[8] Although the transition probability from triplet to the ground state is quite low in conventional purely organic compounds, heavy metals such as iridium can strongly mix singlet and triplet states by strong spin-orbit coupling and then promote the ISC with high probability even at room temperature; it is called an internal heavy atomic effect. This effectively converts singlet excitons into triplet excitons and also allows the effective radiative transition from T_1 to S_0, resulting in an ideal IQE (100%). Since room-temperature phosphorescent materials such as iridium complexes show very high IQE close to the theoretical limit and green and red-emitting materials are highly stable, they have already been used for practical applications. However, the stable phosphorescent materials for deep blue OLEDs have not developed yet because of the difficulty of material design to obtain deep blue emission from T_1. Fluorescent materials are still used as blue emitters for the commercial OLED displays. Whereas the fluorescent materials are less expensive compared with the phosphorescent materials because they do not contain any rare metals, their low EL efficiency is the critical factor that restricts exploiting the full potential of OLEDs.

As a next-generation high-efficiency luminescent material under the current excitation, our group extensively developed highly emissive molecules based on TADF.[9] TADF materials show 100% IQE by the harvesting of triplet exciton as delayed fluorescence through the reverse intersystem

crossing (RISC) from T_1 to the lowest singlet excited state (S_1) without any heavy metals. According to a classical understanding of the TADF process, the RISC rate constant (k_{RISC}) is expressed by the Arrhenius equation.

$$\boldsymbol{k_{RISC} \approx A \times \exp(-\Delta E_{ST}/k_B T)}$$

where A is the pre-factor including the spin-orbit coupling (SOC) element value, ΔE_{ST} is the energy difference between the S_1 and T_1, k_B is the Boltzmann constant and T is temperature. Therefore, small ΔE_{ST} is essential for effective RISC.[10] To obtain TADF materials having small ΔE_{ST}, the most effective strategy is the reduction of a spatial overlap between the highest occupied molecular orbital (HOMO) and the lowest unoccupied molecular orbital (LUMO). Therefore, most TADF materials are developed based on the donor-acceptor linkage with the large dihedral angle between them. Because of its restricted π-conjugation, HOMO and LUMO are effectively separated on donor and acceptor units, respectively. Based on this molecular design, many TADF materials with IQE ~ 100% have been reported.[11,12] However, the reports for deep-blue TADF materials are limited to only a few literatures and most of the blue TADF materials are actually sky-blue.[13–15] In addition, blue TADF-OLEDs show a shorter device operational lifetime than those of green TADF-OLEDs. The half device operational lifetime (LT_{50}) of blue TADF-OLEDs is typically several hundred hours or less,[16–19] while that of green TADF OLEDs is exceeding 1000 hours.[20–22]

Despite the industrial need, simultaneous achievement of high EL efficiency and high operational device stability, the materials to meet the market requirements (IQE ~ 100%, LT_{95} > 100 h) have not been developed yet (**Figure 1-3**). Device degradation is a complicated issue influenced by several factors, for example, materials (features of the excited states, bond dissociation energy, and impurities), device structures (exciton quenching, energy transfer, density and energy of the charge carriers, and carrier traps), and external environments (temperature, oxygen, and moisture).[23] Since extrinsic degradation can be suppressed by the strict encapsulation of OLEDs, intrinsic degradation processes have attracted much interest.[24,25] The reason for the intrinsic degradation phenomenon is widely accepted to be the chemical dissociation or addition of organic materials during device operations. Especially, unstable triplet states concern the formation of molecular

fragments (i.e., defects), which may trap charge carriers, quench excitons, or lead to nonradiative recombination.[26–28] This is because hot excitons are generated by TTA or triplet-polaron annihilation (TPA) processes.[27–29] Compared to fluorescent materials, blue phosphorescent and TADF materials have relatively high triplet excited state energies and long exciton lifetime, resulting in reduced device stability and a significant efficiency roll-off. Intensive researches are undergoing both in phosphorescent and TADF materials, but the guidelines for a molecular design satisfying all the requirements of high efficiency, durability, and blue light emission are insufficient.

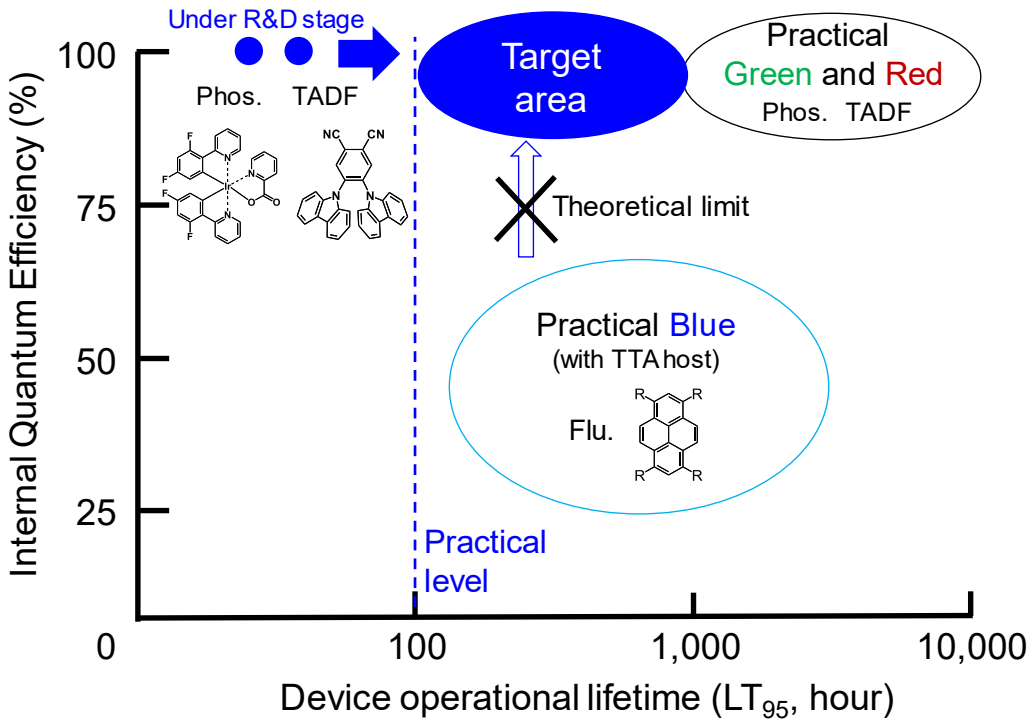

Figure 1-3 Current performance of fluorescent, phosphorescent, and TADF materials of each color and research target area.

1-2. Purpose and outline

The purpose of this thesis is to develop blue TADF materials with high photoluminescence quantum yield (PLQY) and durability by controlling HOMO-LUMO levels and the excited-state stability through the modification of an electron-withdrawing group on the electron donor moiety. A simple molecular modification that allows controlling the emission color, efficiency, and durability of blue emitters contributes significantly to improving the performance of blue OLEDs. This thesis is organized as follows.

In **Chapter 2**, I demonstrated a new strategy for a wide HOMO-LUMO energy gap to obtain blue-shifted emission. When I employ an electron donor moiety having a weak electron-donating ability, TADF materials having wide HOMO-LUMO gaps should be obtained. To demonstrate this strategy, I selected 2,4,5,6-tetra(9*H*-carbazol-9-yl)isophthalonitrile (**4CzIPN**) and 2,3,5,6-tetra(9*H*-carbazol-9-yl)terephthalonitrile (**4CzTPN**) as a platform. As an electron-withdrawing group for weakening the donor nature, I selected the trifluoromethyl (CF_3) group and introduced it to the 2,7- (β-) or 3,6- (γ-) position of all carbazoles (Cz) on **4CzIPN** and **4CzTPN**. The modification with the electron-withdrawing group on the donor moiety showed deepened HOMO levels of the emitters and blue-shifted emission. The modification position of the CF_3 group affected the color purity (full width at half maximum, FWHM), emission efficiency of emitters.

In **Chapter 3**, I used a platform of 2,3,4,5,6-penta(9*H*-carbazol-9-yl)benzonitrile (**5CzBN**) to demonstrate the full and partial CF_3 modification strategies. **5CzBN** has been often used to demonstrate the new strategies, e.g. hetero-donor, and multi-donor strategies.[30,31] Fully CF_3 modified emitter (**5CF5**), in which all Cz constituting **5CzBN** were modified with CF_3 groups, exhibited highly efficient deep blue emission, as predicted from the discussion in **Chapter 2**. On the other hand, the partially CF_3 modified **5CzBN** derivatives showed red-shifted emission. Interestingly, the modification position of CF_3 on Cz had a critical effect on their photostability in spite of their HOMOs were distributed on the unmodified Cz. The modification on the β-position enhanced the photostability but on the γ-position contrastingly worsened. The stability of the excited states also

affected the device lifetime. **5CF1** having a CF_3 modified Cz at the *para*-position of the benzonitrile showed higher external quantum efficiency (EQE) of 17.6% and 3.2 times longer LT_{50} of 276 h than naked **5CzBN** (14.1%, 86 h).

In **Chapter 4**, partial CF_3 modification was applied to 2,3,5,6-tetra(9*H*-carbazol-9-yl)benzonitrile (**4CzBN**). **4CzBN** is a deep-blue TADF material and can be expected to emit in blue even when the emission color is red-shifted by the partial CF_3 modification. **4CF1** in which one Cz of **4CzBN** was replaced by CF_3 modified Cz, showed blue emission with higher PLQY and photostability compared with **4CzBN**. The EQE and LT_{50} of OLEDs using these emitters were 5.9% and 3 h for **4CzBN**, and 11.7% and 33 h for **4CF1**. I succeeded in the enhancement of the efficiency and lifetime of the blue TADF device with the partial modification strategy using the carbazole having CF_3 groups on its β-position.

Finally, **Chapter 5** concludes and summarizes this study.

References

(1) Tang, C. W.; Vanslyke, S. A. Organic Electroluminescent Diodes. *Appl. Phys. Lett.* **1987**, *51* (12), 913–915.

(2) Forrest, S. R. The Path to Ubiquitous and Low-Cost Organic Electronic Appliances on Plastic. *Nature* **2004**, *428* (6986), 911–918.

(3) 有機EL成膜装置 SOLCIET, SATELLA, ZELDAシリーズ | 株式会社アルバック | 製品サイト https://www.ulvac.co.jp/products_j/equipment/products/vacuum-evaporation-system/solciet_satella_new-zelda.

(4) 「世界最大」の秘密は“高分子”と“インクジェット技術”―エプソン、40インチ有機EL (2/2) - ITmedia NEWS https://www.itmedia.co.jp/lifestyle/articles/0405/18/news033_2.html.

(5) Forrest, S. R.; O'Brien, D. F. Excitonic Singlet-Triplet Ratio in a Semiconducting Organic Thin Film. *Phys. Rev. B - Condens. Matter Mater. Phys.* **1999**, *60* (20), 14422–14428.

(6) Segal, M.; Baldo, A.; Holmes, J.; Forrest, R.; Soos, G. Excitonic Singlet-Triplet Ratios in Molecular and Polymeric Organic Materials. *Phys. Rev. B - Condens. Matter Mater. Phys.* **2003**, *68* (7), 075211.

(7) Kondakov, D. Y.; Pawlik, T. D.; Hatwar, T. K.; Spindler, J. P. Triplet Annihilation Exceeding Spin Statistical Limit in Highly Efficient Fluorescent Organic Light-Emitting Diodes. *J. Appl. Phys.* **2009**, *106* (12), 124510.

(8) Baldo, M. A.; O'Brien, D. F.; You, Y.; Shoustikov, A.; Sibley, S.; Thompson, M. E.; Forrest, S. R. Highly Efficient Phosphorescent Emission from Organic Electroluminescent Devices. *Nature* **1998**, *395* (6698), 151–154.

(9) Uoyama, H.; Goushi, K.; Shizu, K.; Nomura, H.; Adachi, C. Highly Efficient Organic Light-Emitting Diodes from Delayed Fluorescence. *Nature* **2012**, *492* (7428), 234–238.

(10) Parker, C. Triplet State Processes in Fluid Solution. *Berichte der Bunsengesellschaft für Phys. Chemie* **1969**, *73* (8-9), 764–772.

(11) Yang, Z.; Mao, Z.; Xie, Z.; Zhang, Y.; Liu, S.; Zhao, J.; Xu, J.; Chi, Z.; Aldred, M. P. Recent Advances in Organic Thermally Activated Delayed Fluorescence Materials. *Chem. Soc. Rev.* **2017**, *46* (3), 915–1016.

(12) Wong, M. Y.; Zysman-Colman, E. Purely Organic Thermally Activated Delayed Fluorescence Materials for Organic Light-Emitting Diodes. *Adv. Mater.* **2017**, *29* (22), 1605444.

(13) Zhang, Q.; Li, J.; Shizu, K.; Huang, S.; Hirata, S.; Miyazaki, H.; Adachi, C. Design of Efficient Thermally Activated Delayed Fluorescence Materials for Pure Blue Organic Light Emitting Diodes. *J. Am. Chem. Soc.* **2012**, *134* (36), 14706–14709.

(14) Hatakeyama, T.; Shiren, K.; Nakajima, K.; Nomura, S.; Nakatsuka, S.; Kinoshita, K.; Ni, J.; Ono, Y.; Ikuta, T. Ultrapure Blue Thermally Activated Delayed Fluorescence Molecules: Efficient HOMO-LUMO Separation by the Multiple Resonance Effect. *Adv. Mater.* **2016**, *28* (14), 2777–2781.

(15) Godumala, M.; Choi, S.; Cho, M. J.; Choi, D. H. Thermally Activated Delayed Fluorescence Blue Dopants and Hosts: From the Design Strategy to Organic Light-Emitting Diode Applications. *J. Mater. Chem. C* **2016**, *4* (48), 11355–11381.

(16) Zhang, D.; Cai, M.; Zhang, Y.; Zhang, D.; Duan, L. Sterically Shielded Blue Thermally Activated Delayed Fluorescence Emitters with Improved Efficiency and Stability. *Mater. Horiz.* **2016**, *3* (2), 145–151.

(17) Kim, M.; Jeon, S. K.; Hwang, S. H.; Lee, J. Y. Stable Blue Thermally Activated Delayed Fluorescent Organic Light-Emitting Diodes with Three Times Longer Lifetime than Phosphorescent Organic Light-Emitting Diodes. *Adv. Mater.* **2015**, *27* (15), 2515–2520.

(18) Cui, L. S.; Deng, Y. L.; Tsang, D. P. K.; Jiang, Z. Q.; Zhang, Q.; Liao, L. S.; Adachi, C. Controlling Synergistic Oxidation Processes for Efficient and Stable Blue Thermally Activated Delayed Fluorescence Devices. *Adv. Mater.* **2016**, *28* (35), 7620–7625.

(19) Lee, D. R.; Kim, M.; Jeon, S. K.; Hwang, S. H.; Lee, C. W.; Lee, J. Y. Design Strategy for 25% External Quantum Efficiency in Green and Blue Thermally Activated Delayed Fluorescent Devices. *Adv. Mater.* **2015**, *27* (39), 5861–5867.

(20) Tsang, D. P. K.; Adachi, C. Operational Stability Enhancement in Organic Light-Emitting Diodes with Ultrathin Liq Interlayers. *Sci. Rep.* **2016**, *6*, 22463.

(21) Nakanotani, H.; Masui, K.; Nishide, J.; Shibata, T.; Adachi, C. Promising Operational Stability of High-Efficiency Organic Light-Emitting Diodes Based on Thermally Activated Delayed Fluorescence. *Sci. Rep.* **2013**, *3*, 2127.

(22) Kamata, T.; Sasabe, H.; Igarashi, M.; Kido, J. A Novel Sterically Bulky Hole Transporter to Remarkably Improve the Lifetime of Thermally Activated Delayed Fluorescent OLEDs at High Brightness. *Chem. - A Eur. J.* **2018**, *24* (18), 4590–4596.

(23) Song, W.; Lee, J. Y. Degradation Mechanism and Lifetime Improvement Strategy for Blue Phosphorescent Organic Light-Emitting Diodes. *Adv. Opt. Mater.* **2017**, *5* (9), 1600901.

(24) Wu, J.; Fei, F.; Wei, C.; Chen, X.; Nie, S.; Zhang, D.; Su, W.; Cui, Z. Efficient Multi-Barrier Thin Film Encapsulation of OLED Using Alternating Al2O3 and Polymer Layers. *RSC Adv.* **2018**, *8* (11), 5721–5727.

(25) Freidzon, A. Y.; Safonov, A. A.; Bagaturyants, A. A.; Krasikov, D. N.; Potapkin, B. V.; Osipov, A. A.; Yakubovich, A. V.; Kwon, O. Predicting the Operational Stability of Phosphorescent OLED Host Molecules from First Principles: A Case Study. *J. Phys. Chem. C* **2017**, *121* (40), 22422–22433.

(26) Zhao, C.; Li, C.; Li, Y.; Qiu, Y.; Duan, L. Understanding the Operational Lifetime Expansion Methods of Thermally Activated Delayed Fluorescence Sensitized OLEDs: A Combined Study of Charge Trapping and Exciton Dynamics. *Mater. Chem. Front.* **2019**, *3* (6), 1181–1191.

(27) Giebink, N. C.; D'Andrade, B. W.; Weaver, M. S.; MacKenzie, P. B.; Brown, J. J.; Thompson, M. E.; Forrest, S. R. Intrinsic Luminance Loss in Phosphorescent Small-Molecule Organic Light Emitting Devices Due to Bimolecular Annihilation Reactions. *J. Appl. Phys.* **2008**, *103* (4), 044509.

(28) Giebink, N. C.; D'Andrade, B. W.; Weaver, M. S.; Brown, J. J.; Forrest, S. R. Direct Evidence for Degradation of Polaron Excited States in Organic Light Emitting Diodes. *J. Appl. Phys.* **2009**, *105* (12), 124514.

(29) Wang, Q.; Aziz, H. Degradation of Organic/Organic Interfaces in Organic Light-Emitting Devices Due to Polaron-Exciton Interactions. *ACS Appl. Mater. Interfaces* **2013**, *5* (17), 8733–8739.

(30) Noda, H.; Nakanotani, H.; Adachi, C. Excited State Engineering for Efficient Reverse Intersystem Crossing. *Sci. Adv.* **2018**, *4* (6), eaao6910.

(31) Balijapalli, U.; Tanaka, M.; Auffray, M.; Chan, C. Y.; Lee, Y. T.; Tsuchiya, Y.; Nakanotani, H.; Adachi, C. Utilization of Multi-Heterodonors in Thermally Activated Delayed Fluorescence Molecules and Their High Performance Bluish-Green Organic Light-Emitting Diodes. *ACS Appl. Mater. Interfaces* **2020**, *12* (8), 9498–9506.

Chapter 2

Trifluoromethyl modification of thermally-activated delayed fluorescence molecules for high-efficiency blue organic light-emitting diodes

Yokoyama, M.; Inada, K.; Tsuchiya, Y.; Nakanotani, H.; Adachi, C.

Chemical Communications **2018**, *54*, 8261-8264.

Abstract

Highly efficient blue and green TADF molecules bearing trifluoromethyl-modified carbazole groups were developed. The trifluoromethyl groups on carbazole induced blue-shifted emission and improved the PLQY. The modification position on carbazole affected spectral shape and PLQY.

2-1. Introduction

To obtain deep blue emission, a wide HOMO-LUMO energy gap of the emitters is necessary. In the case of donor-acceptor TADF materials, HOMO and LUMO are mainly distributed on the donor and acceptor skeletons, respectively. Therefore, a donor with a deep HOMO (weak donor) and an acceptor with a shallower LUMO (weak acceptor) would be required as components of materials exhibiting deep-blue TADF. Focusing on the structures of blue TADF materials in previous reports, many acceptors, e.g., cyanobenzene, triazine, pyrimidine, triazole, ketone, sulfone, and phenoxaborin, have been used for blue TADF materials, whereas the donors have been limited to Cz, acridine, and phenoxazine, etc.[1] In terms of device stability, the most promising donor among these candidates should be Cz, because most OLEDs containing blue TADF molecules with Cz groups have displayed rather longer device lifetimes than OLEDs containing TADF molecules with other donors.[2–4] In this study, I investigated the effect of chemical modification on Cz to develop highly efficient blue TADF emitters. To protect the electroactive 3,6- (γ-) positions of Cz, methyl or *tert*-butyl groups are generally introduced.[2] In this case, the emission color is red-shifted because the electron-donating nature of Cz is increased. Therefore, the modification of Cz with an electron-withdrawing group should make its HOMO level deeper than that of unmodified Cz because its electron-donating ability should decrease. It should make blue-shifted emission from a charge-transfer (CT) excited state formed between the donor-acceptor pair.

Here, I synthesized CF_3-modified emitters based on green and yellow TADF materials (**4CzIPN** and **4CzTPN**, respectively). CF_3 groups were introduced at the 2,7- (β-) or γ-position on all Cz of these TADF materials (**Figure 2-1**). As a result, I found that CF_3 modification on Cz provides blue-shifted emission with maintaining a high PLQY (ϕ_{PL}).

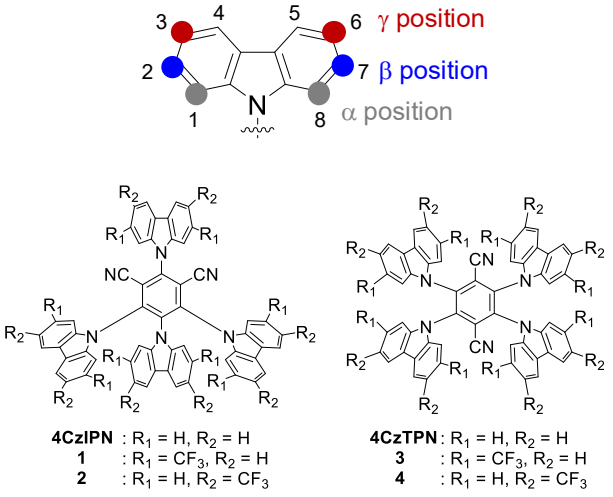

Figure 2-1 Chemical structures of **4CzIPN**, **4CzTPN**, and **1**–**4**.

2-2. Results and discussion

2-2-1. DFT calculations

To investigate the effect of CF_3 modification on the electronic state, HOMO-LUMO levels, and S_1 / T_1 energy were calculated using the Gaussian 16 program package. The S_0 geometry was optimized at the B3LYP/6-31G(d) level of theory, and the S_1 and T_1 were calculated with time-dependent density functional theory (TD-DFT) and B3LYP/6-31G(d, p) methods using the optimized S_0 geometry. According to DFT calculations, all of the CF_3-modified materials **1**–**4** showed deeper HOMO and LUMO levels, and higher S_1 and T_1 energies compared with those of the unmodified materials (**4CzIPN** and **4CzTPN**). Nevertheless, the HOMO and LUMO distributions and ΔE_{ST} values of **1**–**4** were quite similar to those of the unmodified materials (**Table 2-1** and **Figure 2-2**). These calculation results indicate that the emission wavelength can be shortened by CF_3 modification while maintaining TADF activity.

Table 2-1 DFT calculations of **4CzIPN**, **1**, **2**, **4CzTPN**, **3**, and **4** (B3LYP/6-31G(d, p)) using Gaussian 16, Rev. A.03.

Emitter	HOMO (eV)	LUMO (eV)	E_g (eV)	S_1 (eV)	T_1 (eV)	ΔE_{ST} (eV)	f
4CzIPN	−5.67	−2.56	3.11	2.44	2.32	0.12	0.094
1	−6.43	−3.32	3.11	2.45	2.37	0.09	0.074
2	−6.78	−3.57	3.20	2.60	2.49	0.11	0.091
4CzTPN	−5.73	−2.82	2.91	2.25	2.15	0.10	0.101
3	−6.42	−3.50	2.92	2.27	2.17	0.10	0.099
4	−6.83	−3.81	3.02	2.43	2.33	0.10	0.099

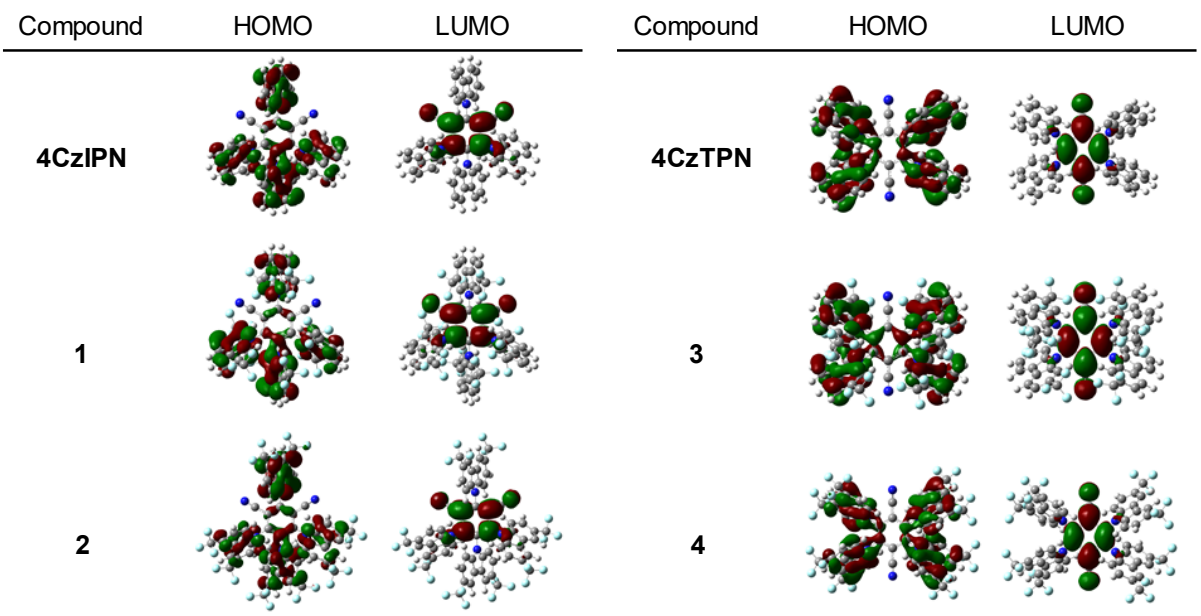

Figure 2-2 HOMO and LUMO distributions for **1**–**4**, **4CzIPN**, and **4CzTPN** (B3LYP/6-31G(d, p)) using Gaussian 16, Rev. A.03.

2-2-2. HOMO and LUMO levels

To estimate the HOMO levels of each compound, photoelectron yield spectroscopy in N_2 was applied to the pristine films (**Figure 2-3**). Large HOMO values were obtained upon the introduction of electron-withdrawing CF_3 onto Cz; that is, HOMO levels were −5.80, −6.40, −6.40, −5.95, −6.40, and −6.40 eV for **4CzIPN**, **1**, **2**, **4CzTPN**, **3**, and **4**, respectively. These results mean that CF_3 modification of Cz deepens the HOMO levels of the emitters because it lowers their electron-donating ability. The LUMO levels of these materials were also estimated from HOMO levels and the optical energy bandgap determined from the onset absorption wavelength of the pristine films. The LUMO levels were −3.35, −3.65, −3.70, −3.70, −3.95, and −3.95 eV for **4CzIPN**, **1**, **2**, **4CzTPN**, **3**, and **4**, respectively. The LUMO levels also increased following the CF_3 modification of Cz. This means that CF_3 groups on the donor units affected the electron density on the acceptor unit indirectly.

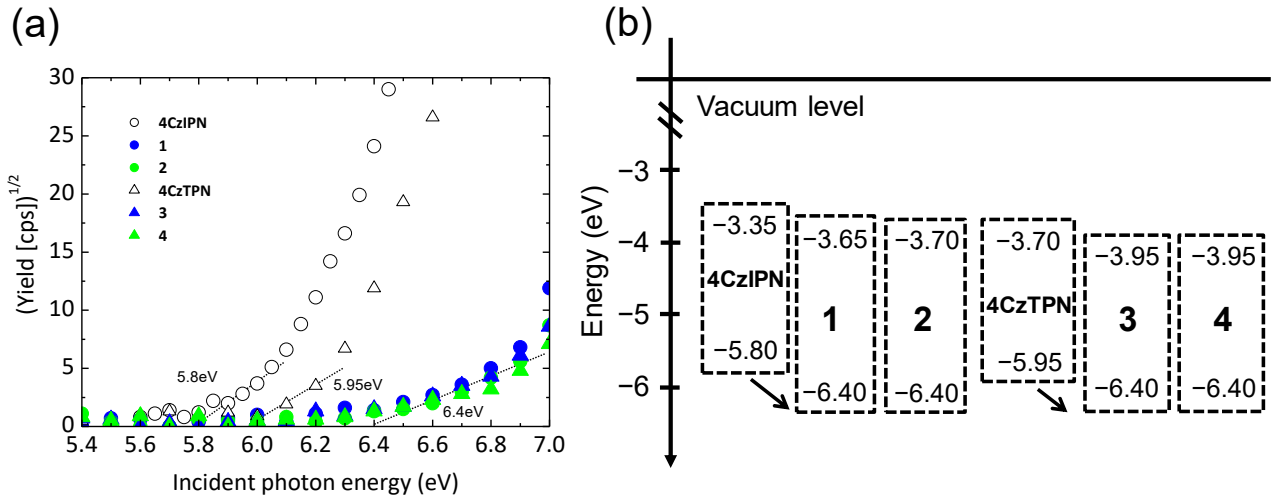

Figure 2-3 (a) Photoelectron yield spectroscopy in N_2 of **1**–**4**, **4CzIPN**, and **4CzTPN** pristine films (UV light source intensity, 10 nW), (b) Energy diagram.

2-2-3. Photophysical properties

Confirming the emission color shift predicted from the DFT calculations, the ultraviolet–visible (UV–vis) absorption and photoluminescence (PL) spectra of **1**–**4** and unmodified materials of **4CzIPN** and **4CzTPN** in toluene were measured (**Figure 2-4**). The broad absorption at 400–500 nm was assigned to a CT transition from the electron-donating Cz moiety to the electron-accepting phthalonitrile group in all compounds. The onset absorption wavelengths of **1**–**4** shifted to shorter wavelengths than those of the unmodified materials; this indicates that wider HOMO-LUMO energy gaps were achieved by CF_3 modification of the donor moiety. In addition, the compounds with the same skeleton (the group of **1**, **2**, and **4CzIPN** or that of **3**, **4**, and **4CzTPN**) showed CT absorption bands with similar absorbance indices. This means that the CF_3 modification of Cz does not influence its oscillator strength. In the fluorescence spectra, **1** and **2** showed blue emission (the emission maximum (λ_{em}) = 456 and 453 nm, respectively), and **3** and **4** emitted green (λ_{em} = 510 and 492 nm, respectively). Compounds **1**–**4** all showed relatively broad emission spectra without vibronic structure, indicating that the emission mainly occurs from not the locally excited state but the CT state. The emission spectra were blue-shifted compared with those of the unmodified materials of **4CzIPN** and **4CzTPN** (λ_{em} = 471 and 521 nm, respectively). This trend is different from the halogen

(Cl, Br, and I) modification of the Cz groups of **4CzIPN** and **4CzTPN** reported by Bunz et al.[5] Halogen-modified **4CzIPN** and **4CzTPN** show red-shifted emission despite the electron-withdrawing nature of halogens. This is caused by the electron-donating unshared electron pair on the halogen atom, which can stabilize the carbazolyl radical cation in their CT excited states.[6]

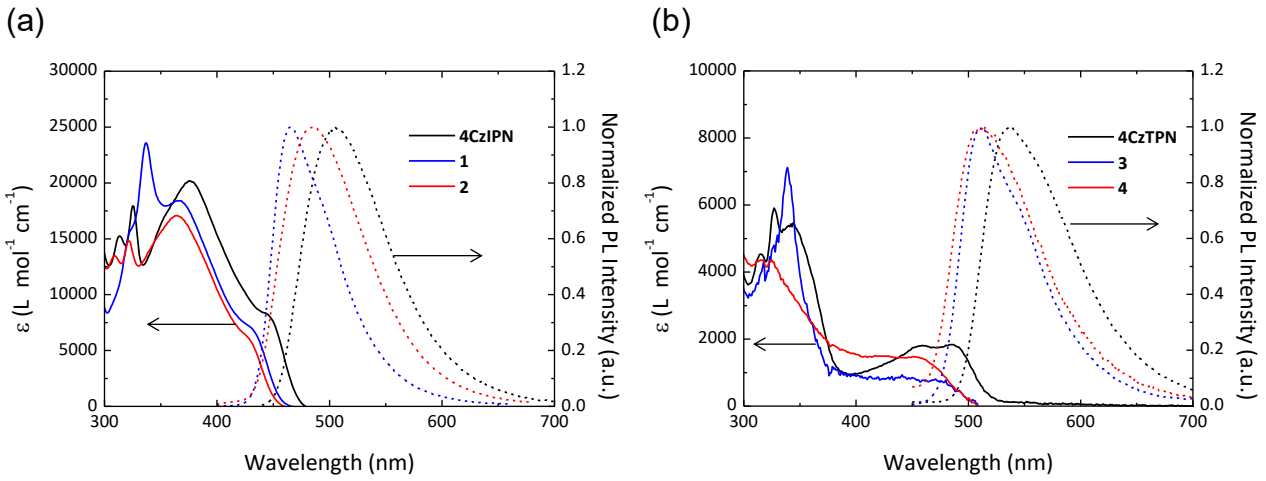

Figure 2-4 UV–vis absorption (solid line) and PL spectra (dashed line) in toluene (1.0×10^{-5} mol L^{-1}) of (a) **4CzIPN**, **1**, and **2**, (b) **4CzTPN**, **3**, and **4**.

PLQY and transient PL decay measurements were performed in the air- or N_2-saturated toluene. All compounds showed dramatic increases in PLQY after N_2 bubbling (**Table 2-2**). The transient PL decay curves contained prompt and delayed components (**Figure 2-5**). For all compounds, the lifetime of the delayed component dramatically increased after N_2 bubbling. These results indicate that the triplet excitons, which are quenched by oxygen, contribute to the delayed emission. In addition, the CF_3 modification of Cz extended the lifetime of the delayed component. This trend was more obvious for β-modification than for γ-modification. In addition, the emission properties were affected by the modification position of the CF_3 group; that is, the compounds with β-substituents (**1** and **3**) showed a smaller FWHM values and higher PLQYs than those of the materials with γ-substituents (**2** and **4**). This may be induced by the F-π repulsion between CF_3-modified Cz units. From the calculated structures (**Table 2-3**), it seems that the β-substituted Cz has larger steric overlap between Cz and CF_3 groups than that of the γ-substituted Cz in these TADF materials. The large steric hindrance of CF_3 arising from its F-π repulsion would lead to weak

intermolecular π-π interactions between Cz groups and fix the position of each Cz group,[7] resulting in the narrow FWHM and high PLQY.

Table 2-2 Photophysical properties of emitters in toluene solution and doped films.

	Toluene solution (1.0×10^{-5} mol L^{-1})						Doped film (10 wt% emitter in **PPT**)							
Emitter	λ_{abs} [a] (nm)	λ_{PL} [b] (nm)	FWHM (nm)	ϕ_{PL} [c] (%)	τ_P (ns)	τ_d [c] (μs)	λ_{PL} [b] (nm)	FWHM (nm)	ϕ_{PL} (%)	τ_P (ns)	τ_d (μs)	S_1 [d] (eV)	T_1 [d] (eV)	ΔE_{ST} (eV)
4CzIPN	471	505	86	93 (23)	13.6	4.71 (0.36)	524	98	85	12.5	3.34	2.71	2.68	0.03
1	456	465	62	98 (14)	3.56	15.1 (0.46)	469	75	95	4.78	11.9	2.99	2.86	0.13
2	453	485	87	90 (27)	15.6	7.97 (2.59)	482	94	86	9.25	6.04	2.92	2.86	0.06
4CzTPN	521	539	91	97 (25)	6.38	2.52 (0.50)	557	97	48	6.89	2.47	2.49	2.44	0.05
3	510	512	74	99 (33)	2.60	4.02 (1.49)	504	82	86	3.55	6.58	2.73	2.63	0.10
4	510	515	87	77 (38)	11.1	2.59 (1.06)	507	90	78	8.15	3.08	2.73	2.72	0.01

[a] Absorption onset; [b] peak maximum; [c] after N_2-saturation, values before deoxygenation are shown in parenthesis; [d] estimated from the emission onset values at 300 or 6 K obtained by streak camera measurements.

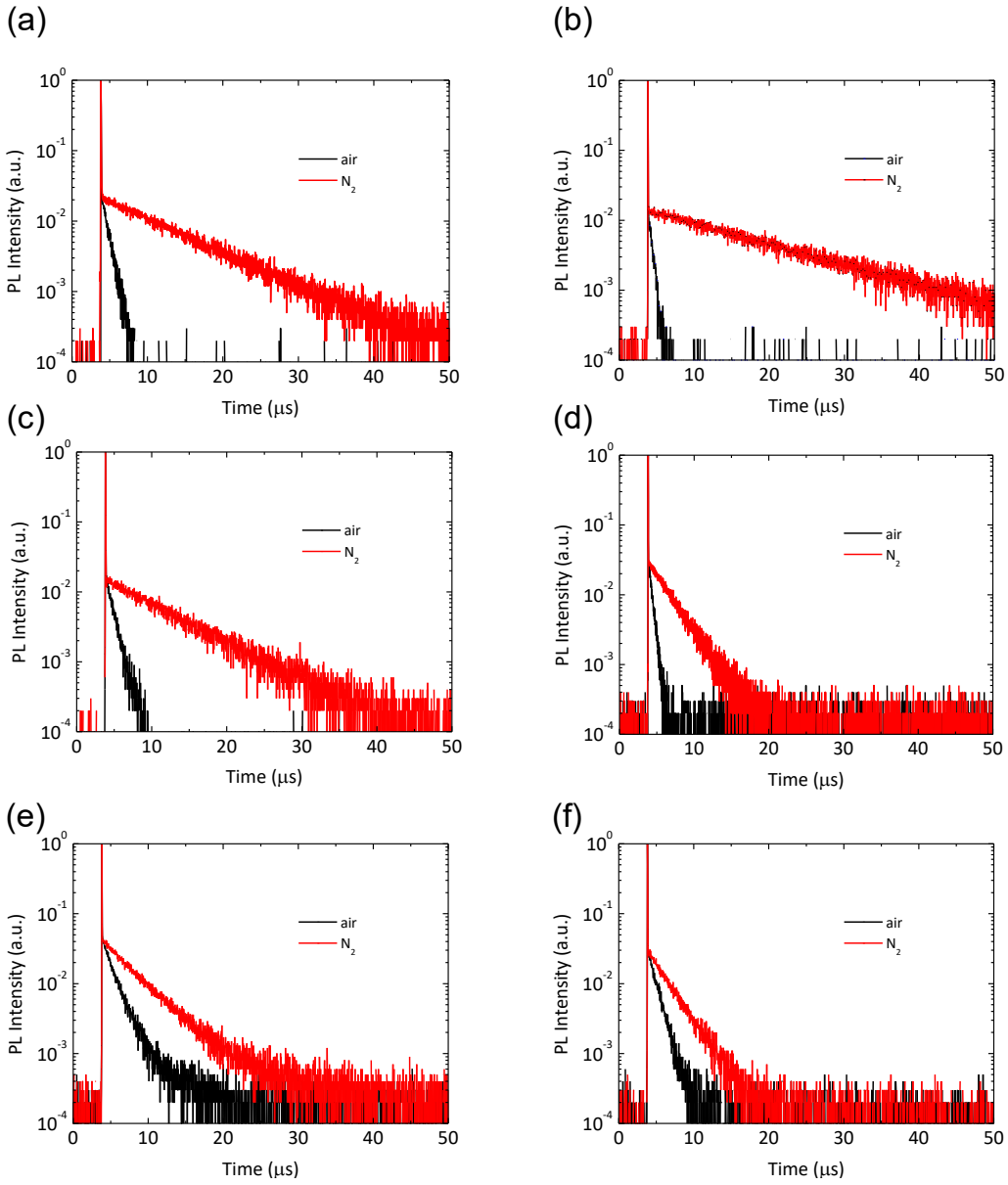

Figure 2-5 Transient PL decay curve of **4CzIPN** (a), **1** (b), **2** (c), **4CzTPN** (d), **3** (e), and **4** (f) in toluene (1.0×10^{-5} mol L^{-1}); black line; air-saturated, red line; N_2-saturated.

Table 2-3 Optimized structures of **1**–**4**, **4CzIPN**, and **4CzTPN**.

Emitter	Θ_1 (°)	Θ_2 (°)	Θ_3 (°)	Θ_4 (°)
4CzIPN	70	65	63	63
1	66	70	68	70
2	71	65	64	64
4CzTPN	67	67	67	67
3	67	70	71	69
4	67	67	67	67

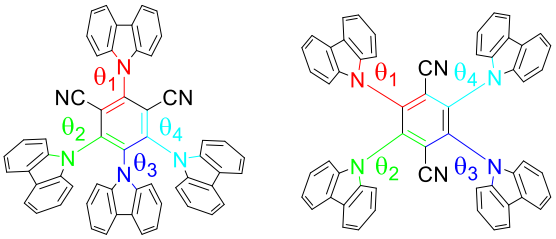

The photophysical properties of the compounds in the solid-state were also studied using thermally evaporated films. To explore available host materials, 10 wt% **1** doped **PPT** or ***m*CBP** films were prepared and their emission spectra were evaluated (**Figure 2-6**). In the case of ***m*CBP** (HOMO = −6.0 eV) film, the emission spectra shifted to much longer wavelength and the PLQY (25%) decreased compared to the solution state (98%). This should be caused by exciplex formation between **1** and ***m*CBP**. On the other hand, using the wide gap host, **PPT** (HOMO = −6.5 eV), a highly efficient blue emission (PLQY = 95%) was obtained as well as the solution state. This result indicates that deep HOMO levels are also required for the combined host and peripheral materials.

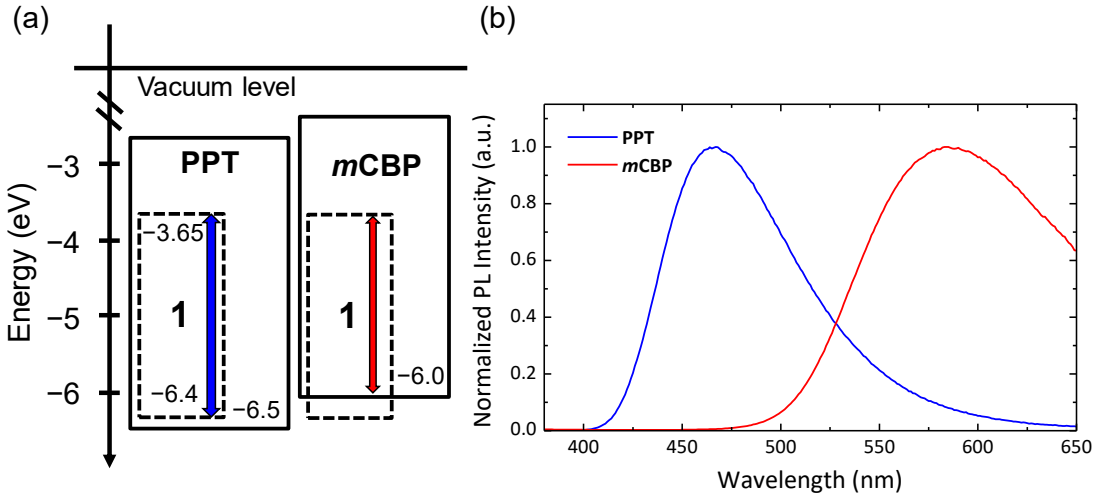

Figure 2-6 (a) Energy diagram, (b) PL spectra of 10wt% **1** doped **PPT** film (blue line) and ***m*CBP** film (red line).

The emission properties of 10wt% **1**–**4** doped **PPT** films are summarised in **Table 2-2**. All trends induced by CF_3 modification found in solution were also observed in the **PPT** films; that is,

blue-shifted emission, elongation of the delayed lifetime, smaller emission FWHM, and PLQY improvement. I confirmed the temperature dependence of the transient emission decay curves for each CF_3 modified emitter in a **PPT** film (**Figure 2-7**). For all compounds of **1**–**4**, the intensity of the delayed components in the decay curves clearly increased with temperature increased. The fluorescence and phosphorescence spectra of the doped **PPT** films were used to estimate S_1, T_1, and ΔE_{ST} for each emitter (**Table 2-2**). All of the CF_3 modified emitters showed small ΔE_{ST} values (≤0.13 eV), which were sufficient to provide RISC from T_1 to S_1. From these characteristics, I concluded that all the CF_3 modified compounds possess TADF activity.

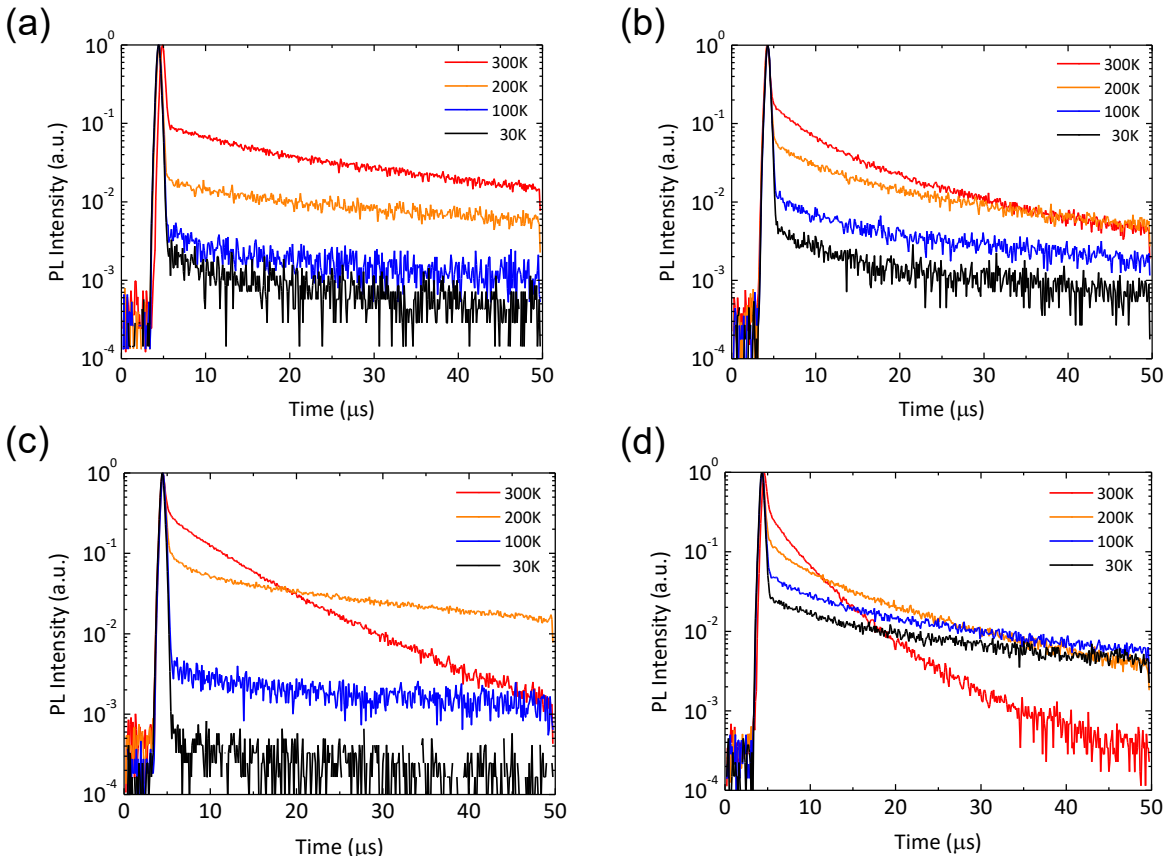

Figure 2-7 Transient PL decay curves of 10 wt% doped **PPT** films for **1** (a), **2** (b), **3** (c), and **4** (d) at 30, 100, 200, 300 K.

With increasing the doping concentration, the films of CF_3 modified emitters **1**–**4** showed smaller red-shifts of their emission peaks and PLQY decreases in comparison to the unmodified emitters of **4CzIPN** and **4CzTPN** (**Figure 2-8**, **2-9**). This behavior would be caused by the decreased intermolecular interaction between emitters following CF_3 modification.

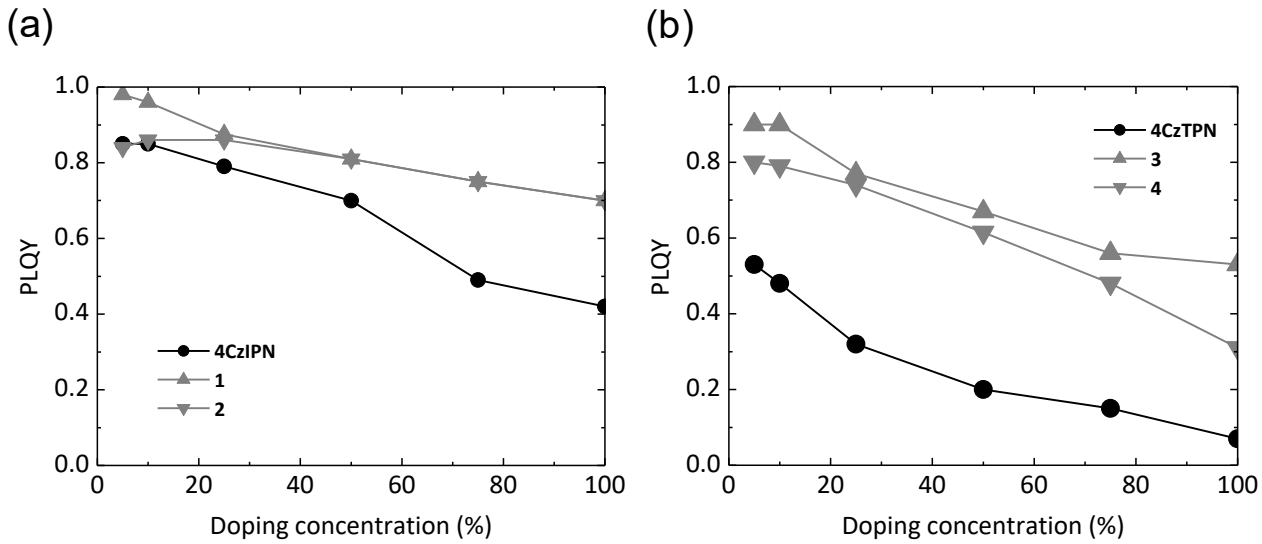

Figure 2-8 PLQY of doped **PPT** films with various doping concentrations (5, 10, 25, 50, 75 wt%) and pristine film (100 wt%); (a) **4CzIPN**, **1**, and **2**; (b) **4CzTPN**, **3**, and **4**.

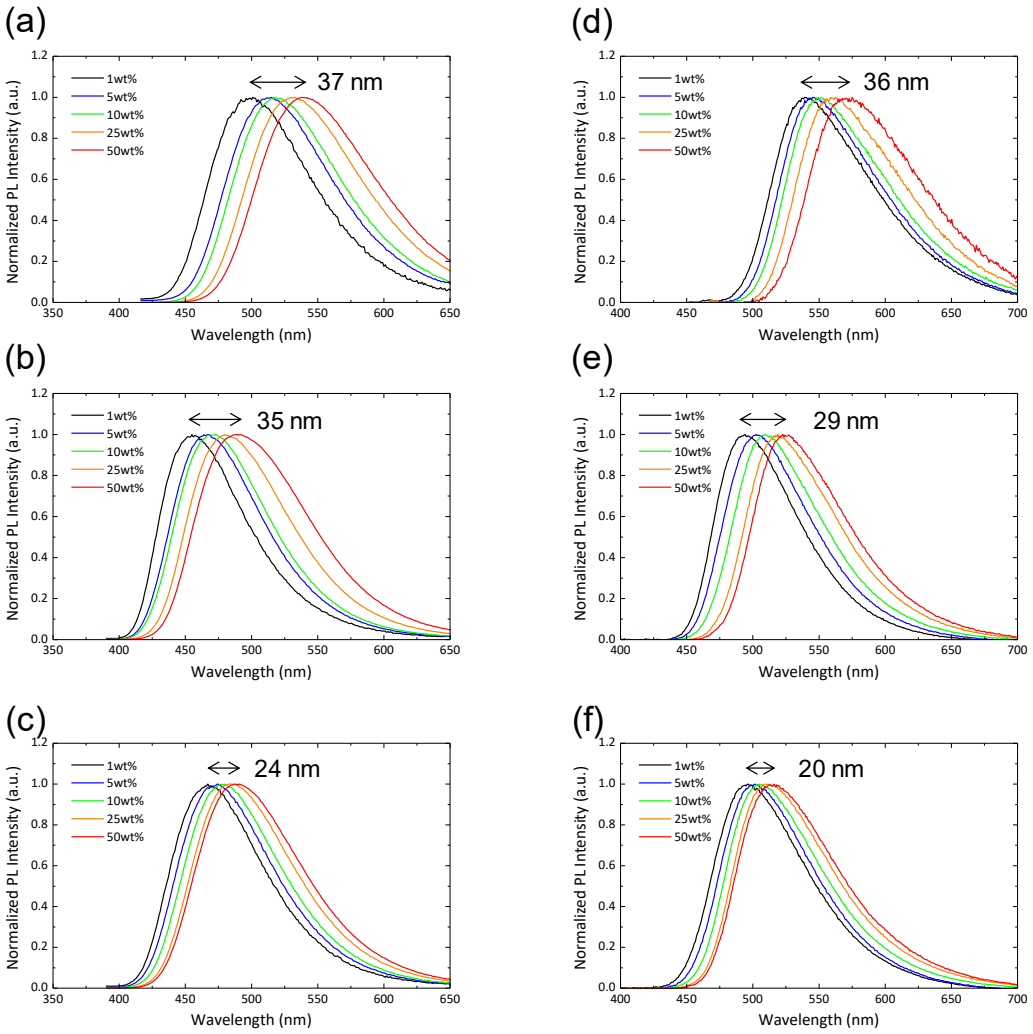

Figure 2-9 PL spectra of emitter doped **PPT** films with various doping concentrations; (a) **4CzIPN**; (b) **1**; (c) **2**; (d) **4CzTPN**; (e) **3**; (f) **4**.

2-2-4. OLED performance

To demonstrate the impact of an increased PLQY on OLED performance, I fabricated OLEDs using **1**–**4** as emitters. Chemical structures of the organic semiconductor materials used in the devices are presented in **Section 2-4-2**. EQE-current density (EQE-J) characteristics, current density-voltage-luminance (J-V-L) characteristics, the EL spectra, and Commission Internationale de l'Éclairage (CIE) coordinates of the devices are shown in **Figure 2-10**. The maximum EQE (EQE_{max}), EQE at 100 cd m^{-2}, and CIE coordinates were 12.1%, 8.48%, and (0.15, 0.15) for **1**, respectively; 9.88%, 6.95%, and (0.16, 0.22) for **2**, respectively; 15.1%, 13.2%, and (0.23, 0.52) for **3**, respectively; and 12.6%, 10.4%, and (0.24, 0.51) for **4**, respectively. Similar trends were observed for the EQE of the OLEDs and PLQYs of the **PPT** films; that is, the emitters with β-substituents (**1** and **3**) showed higher EQEs than those of the materials with γ-substituents (**2** and **4**). However, the effect of CF_3 modification on the device lifetime was not conducted in this study, since the HOMO and LUMO levels of **1**–**4** were too deep to use highly stable host and peripheral materials.

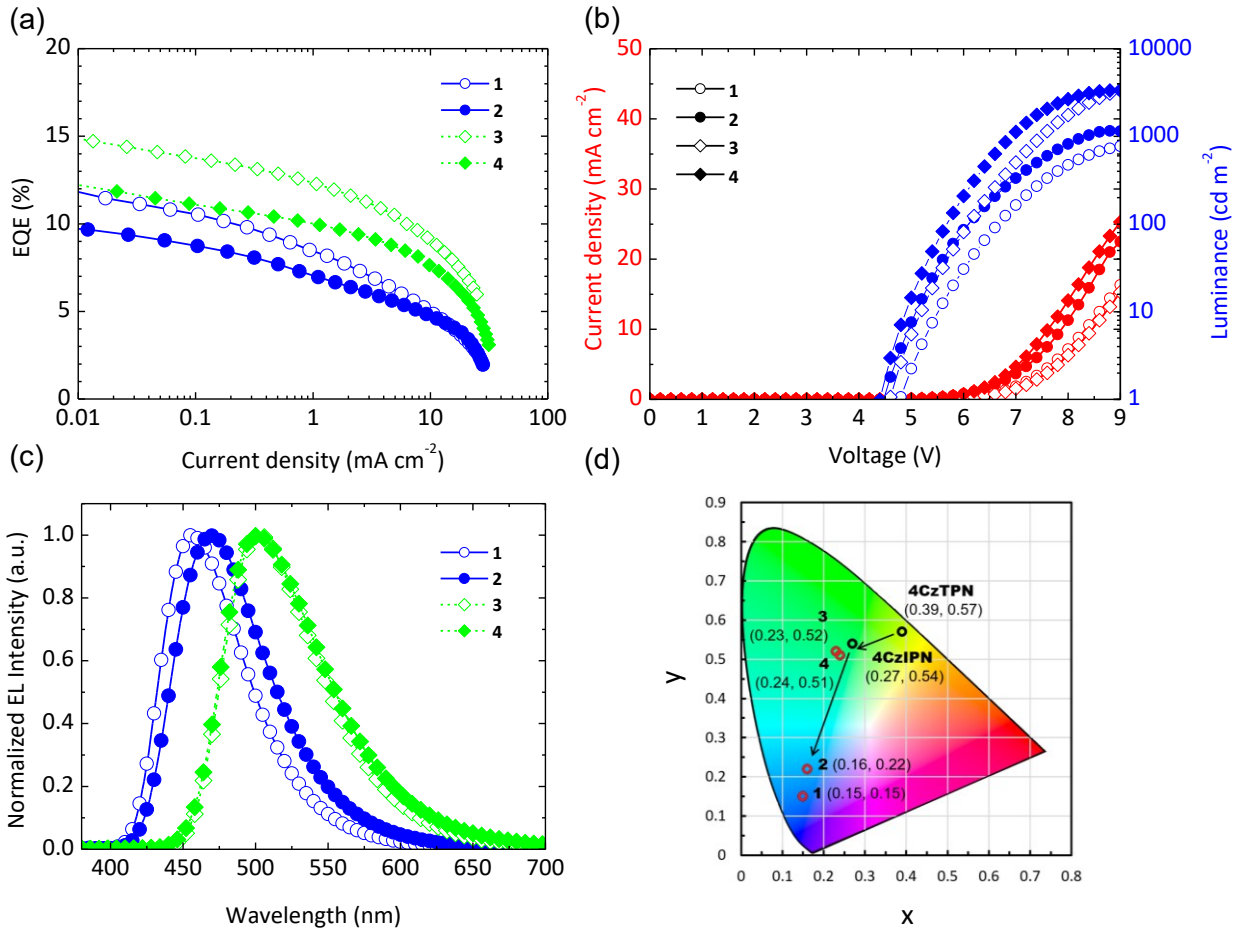

Figure 2-10 Electroluminescence characteristics of OLEDs using **1**–**4** as an emitter; (a) EQE-J characteristics; (b) J-V-L characteristics; (c) EL spectra; (d) CIE diagram (CIE1931).

2-3. Conclusion

I investigated the effect of CF_3 modification of the donor groups of TADF emitters. CF_3 modification of Cz groups provided blue-shifted emission for both **4CzIPN** and **4CzTPN** architectures because the electron-donating ability of the Cz was decreased. As predicted by DFT calculations, all CF_3 modified compounds exhibited 40–55 nm blue-shifted emission compared with the unmodified compounds and high PLQY. I found both of the β-substituted compounds showed longer delayed emission with higher PLQY than both of the γ-substituted ones in toluene. The same trend was observed in the evaporated films. Therefore, I concluded that CF_3 modification on Cz not only blue-shifts the emission but also decreases intermolecular interactions, resulted in the advanced blue-shifted emission properties in the solid-state. In OLEDs using these materials, the β-substituted emitters also exhibited higher EQE than the γ-substituted ones.

2-4. Materials and methods

2-4-1. Measurement of photoluminescence properties

UV–vis absorption spectra and PL spectra were recorded on UV–vis (UV-2550, Shimadzu, Japan) and PL (FluoroMax-4, Horiba Jobin Yvon, Japan)) spectrophotometers. Phosphorescence spectra in solution at 77 K were recorded on a multichannel analyzer (PMA-12, Hamamatsu Photonics, Japan). PLQY was measured under the flow of argon gas using an absolute PL quantum yield measurement system (C11347-01, Hamamatsu Photonics, Japan) with an excitation wavelength of 340 nm. Emission lifetimes were measured using a fluorescence lifetime measurement system (C11367-03 Quantaurus-Tau, Hamamatsu Photonics, Japan). The prompt and delayed PL spectra and phosphorescent spectra of the doped films were measured under vacuum using a streak camera system (C4334, Hamamatsu Photonics, Japan) with an excitation wavelength of 337 nm. The ionic potential of the materials was measured using a photoelectron yield spectrometer (AC-3, Riken Keiki, Japan).

2-4-2. Device fabrication and characterization of OLED performance

OLEDs were fabricated by thermal evaporation onto clean ITO-coated glass substrates. Glass substrates with a pre-patterned, 100 nm thick ITO coating were used as anodes. The hole transport material 4,4-bis[*N*-(1-naphthyl)-*N*-phenylamino]-biphenyl (**α-NPD**), the electron blocking material 1,3-bis(*N*-carbazolyl)benzene (***m*CP**), the host and electron transport material 2,8-bis(diphenylphosphoryl)dibenzo-[*b*,*d*]thiophene (**PPT**) were used in the TADF-OLEDs (**Figure 2-11**). **α-NPD** was purchased from Nipponsteel, ***m*CP** was purchased from NARD Institute, Ltd. **PPT** was synthesized in our laboratory. Organic layers were formed by thermal evaporation. Doped emission layers were deposited by co-evaporation. The bilayer of 0.8 nm LiF / 100 nm Al was used as cathode. After device fabrication, devices were immediately encapsulated with glass lids using epoxy glue in a nitrogen-filled glove box (O_2 < 0.1 ppm, H_2O < 0.1 ppm). Commercial calcium oxide desiccant (Dynic Co., Japan) was included in each encapsulated package. EQE-J and J-V-L characteristics of the OLEDs were evaluated using a source meter (Keithley 2400, Keithley

Instruments Inc., USA) and an absolute external quantum efficiency measurement system (C9920-12, Hamamatsu Photonics, Japan).

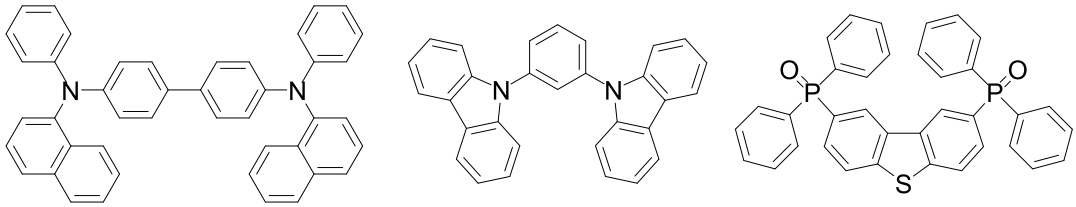

Figure 2-11 Chemical structures of **α-NPD**, ***m*CP**, and **PPT**.

2-4-3. Synthesis and characterization

2,7-bis(trifluoromethyl)carbazole and 3,6-bis(trifluoromethyl)carbazole were synthesized according to literature.[8]

1,2,3,5-tetrakis(2,7-bis(trifluoromethyl)carbazol-9-yl)-4,6-dicyanobenzene (1)

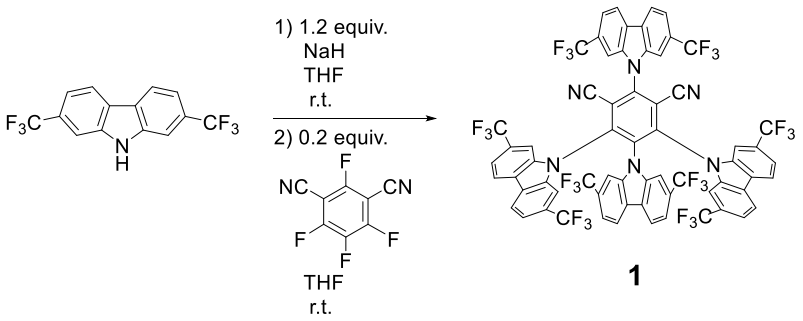

Under the N_2 atmosphere, sodium hydride (480 mg, 60wt% dispersion in mineral oil, 12.0 mmol) was added portionwise to a THF solution (100 ml) of 2,7-bis(trifluoromethyl)carbazole (3.03 g, 10.0 mmol), then the mixture was stirred for 1 h. After stirring, tetrafluoroisophthalonitrile (400 mg, 2 mmol) was added to the solution and the resulted mixture was stirred at room temperature for 18 h. The reaction was quenched by adding water. The precipitates were collected by a filter and washed with water and chloroform to obtain light yellow powder (2.6 g, 99 % yield). The product was further purified by sublimation before measurements. **^{1}H NMR** (500 MHz, acetone-d_6): δ (ppm) = 7.33 (dd, 2H, 8.5, 1.0 Hz), 7.62 (dd, 4H, 8.5, 1.0 Hz), 7.89 (s, 2H), 7.90 (s, 4H), 7.93 (d, 4H, 8.5 Hz), 7.98 (dd, 2H, 8.5, 1.0 Hz), 8.05 (s, 2H), 8.33 (d, 4H, 8.5 Hz), 8.80 (d, 2H, 8.5 Hz). **^{19}F NMR**

(400 MHz, acetone-d_6): δ (ppm) = −61.73, −62.14, −62.21. **MS** (ASAP): *m/z* 1333, M^+. **Elemental analysis**: Calcd. for $C_{64}H_{24}F_{24}N_6$ (%): C 57.67, H 1.81, N 6.31; Found C 57.63, H 1.89, N 6.33.

1,2,3,5-tetrakis(3,6-bis(trifluoromethyl)carbazol-9-yl)-4,6-dicyanobenzene (2)

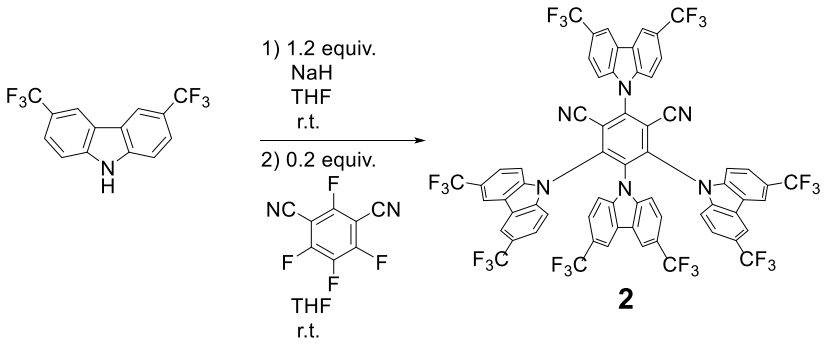

Under the N_2 atmosphere, sodium hydride (336 mg, 60wt% dispersion in mineral oil, 8.40 mmol) was added portionwise to a THF solution (70 ml) of 3,6-bis(trifluoromethyl)carbazole (2.12 g, 7.00 mmol), then the mixture was stirred for 1 h. After stirring, tetrafluoroisophthalonitrile (280mg, 1.4 mmol) was added to the solution, and the resulted mixture was stirred at room temperature for 13 h. The reaction was quenched by adding water. The precipitate was collected by a filter and washed with water and isopropanol to obtain light yellow powder (1.9 g, 99 % yield). The product was further purified by sublimation before measurements. **^{1}H NMR** (500 MHz, DMSO-d_6): δ (ppm) = 7.16 (dd, 2H, 8.5, 1.5 Hz), 7.63 (d, 4H, 8.5 Hz), 7.65 (d, 2H, 1.5 Hz), 7.98 (d, 4H, 8.5 Hz), 8.20 (s, 2H), 8.30 (dd, 2H, 8.5, 1.5 Hz), 8.40 (d, 2H, 8.5 Hz), 8.63 (s, 4H), 9.19 (s, 2H). **^{19}F NMR** (400 MHz, DMSO-d_6): δ (ppm) = −59.12, −59.46, −59.68. **MS** (ASAP): *m/z* 1333, M^+. **Elemental analysis**: Calcd. for $C_{64}H_{24}F_{24}N_6$ (%): C 57.67, H 1.81, N 6.31; Found: C 57.91, H 1.81, N 6.30.

1,2,4,5-tetrakis(2,7-bis(trifluoromethyl)carbazol-9-yl)-3,6-dicyanobenzene (3)

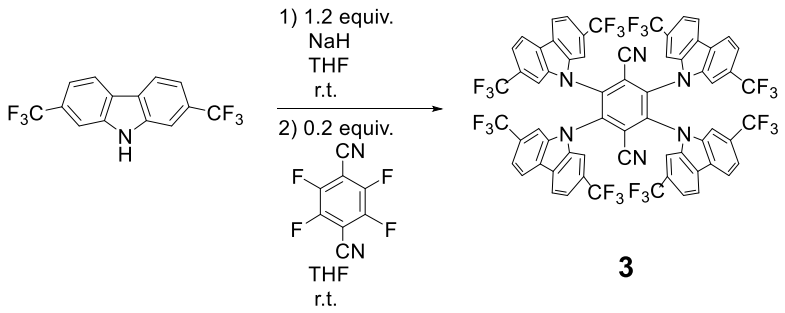

Under the N_2 atmosphere, sodium hydride (480 mg, 60wt% dispersion in mineral oil, 12.0 mmol) was added portionwise to a THF solution (100 ml) of 2,7-bis(trifluoromethyl)carbazole (3.03 g, 10.0 mmol), then the mixture was stirred for 1 h. After stirring, tetrafluoroterephthalonitrile (400 mg, 2 mmol) was added to the solution and the resulted mixture was stirred at room temperature for 18 h. The reaction was quenched by adding water. The precipitate was collected by a filter and washed with water and chloroform to obtain yellow powder (2.6 g, 96 % yield). The product was further purified by sublimation before measurements. **^{1}H NMR** (500 MHz, acetone-d_6): δ (ppm) = 7.66 (dd, 8H, 8.0, 1.5 Hz), 8.04 (d, 8H, 1.5Hz), 8.35 (d, 8H, 8.0 Hz). **^{19}F NMR** (400 MHz, acetone-d_6): δ (ppm) = −61.91. **MS** (ASAP): *m/z* 1333, M^+. **Elemental analysis**: Calcd. for $C_{64}H_{24}F_{24}N_6$ (%): C 57.67, H 1.81, N 6.31; Found C 57.73, H 1.76, N 6.48.

1,2,4,5-tetrakis(3,6-bis(trifluoromethyl)carbazol-9-yl)-3,6-dicyanobenzene (4)

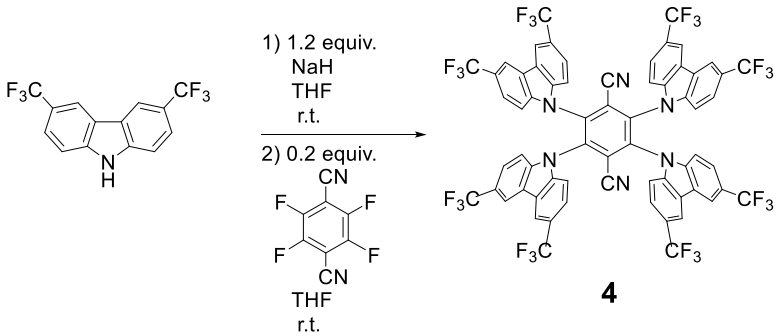

Under the N_2 atmosphere, sodium hydride (336 mg, 60wt% dispersion in mineral oil, 8.40 mmol) was added portionwise to a THF solution (70 ml) of 3,6-bis(trifluoromethyl)carbazole (2.12 g, 7.00 mmol), then the mixture was stirred for 1 h. After stirring, tetrafluoroterephthalonitrile (280

mg, 1.4 mmol) was added to the solution and the resulted mixture was stirred at room temperature for 18 h. The reaction was quenched by adding water. The precipitate was collected by a filter and washed with water and chloroform to obtain yellow powder (2.0 g, 99 % yield). The product was further purified by sublimation before measurements. **^{1}H NMR** (500 MHz, acetone-d_6): δ (ppm) = 7.61 (dd, 8H, 8.5, 2.5 Hz), 7.91 (d, 8H, 8.5 Hz), 8.51 (d, 8H, 2.5 Hz). **^{19}F NMR** (400 MHz, acetone-d_6): δ (ppm) = −61.55. **MS** (ASAP): *m/z* 1333, M^+. **Elemental analysis**: Calcd. for $C_{64}H_{24}F_{24}N_6$ (%): C 57.67, H 1.81, N 6.31; Found C 57.81, H 1.83, N 6.26.

References

(1) Godumala, M.; Choi, S.; Cho, M. J.; Choi, D. H. Thermally Activated Delayed Fluorescence Blue Dopants and Hosts: From the Design Strategy to Organic Light-Emitting Diode Applications. *J. Mater. Chem. C* **2016**, *4* (48), 11355–11381.

(2) Zhang, D.; Cai, M.; Zhang, Y.; Zhang, D.; Duan, L. Sterically Shielded Blue Thermally Activated Delayed Fluorescence Emitters with Improved Efficiency and Stability. *Mater. Horizons* **2016**, *3* (2), 145–151.

(3) Kim, M.; Jeon, S. K.; Hwang, S. H.; Lee, J. Y. Stable Blue Thermally Activated Delayed Fluorescent Organic Light-Emitting Diodes with Three Times Longer Lifetime than Phosphorescent Organic Light-Emitting Diodes. *Adv. Mater.* **2015**, *27* (15), 2515–2520.

(4) Cui, L. S.; Deng, Y. L.; Tsang, D. P. K.; Jiang, Z. Q.; Zhang, Q.; Liao, L. S.; Adachi, C. Controlling Synergistic Oxidation Processes for Efficient and Stable Blue Thermally Activated Delayed Fluorescence Devices. *Adv. Mater.* **2016**, *28* (35), 7620–7625.

(5) Kretzschmar, A.; Patze, C.; Schwaebel, S. T.; Bunz, U. H. F. Development of Thermally Activated Delayed Fluorescence Materials with Shortened Emissive Lifetimes. *J. Org. Chem.* **2015**, *80* (18), 9126–9131.

(6) Jiao, L.; Pang, W.; Zhou, J.; Wei, Y.; Mu, X.; Bai, G.; Hao, E. Regioselective Stepwise Bromination of Boron Dipyrromethene (BODIPY) Dyes. *J. Org. Chem.* **2011**, *76* (24), 9988–9996.

(7) Scerba, M. T.; Bloom, S.; Haselton, N.; Siegler, M.; Jaffe, J.; Lectka, T. Interaction of a C-F Bond with the π-System of a C=C Bond or "Head on" with a Proximate C-H Bond. *J. Org. Chem.* **2012**, *77* (3), 1605–1609.

(8) Gantenbein, M.; Hellstern, M.; Le Pleux, L.; Neuburger, M.; Mayor, M. New 4,4'-Bis(9-Carbazolyl)-Biphenyl Derivatives with Locked Carbazole-Biphenyl Junctions: High-Triplet State Energy Materials. *Chem. Mater.* **2015**, *27* (5), 1772–1779.

Chapter 3

Partial modification of electron-withdrawing groups in thermally-activated delayed fluorescence materials aimed to improve efficiency and stability

Yokoyama, M.; Tsuchiya, Y.; Nakanotani, H.; Adachi, C.

Chemistry Letters, accepted (doi.org/10.1246/cl.200435).

Abstract

Highly efficient and stable blue-green thermally-activated delayed fluorescence molecules with CF_3 groups were developed. Partial modification with CF_3 groups at the appropriate position of the donor moiety improved the luminescence efficiency and excited-state stability. OLEDs using modified emitters showed improved EQE and operational lifetime compared with unmodified one.

3-1. Introduction

In **Chapter 2**, I demonstrated that all CF_3 modification of the Czs substituents for **4CzIPN** and **4CzTPN** resulted in high efficiency with the blue-shifted emission. In this chapter, I used **5CzBN** as a model scaffold to understand the effect of the partial CF_3 modification (**Figure 3-1**) because the photophysical properties of **5CzBN** has been well investigated in the previous literatures.[1,2] Further, the modified **5CzBN** derivatives can emit blue emission because a benzonitrile acts as a weak acceptor compared with phthalonitrile. Therefore, fully modified **5CzBN** with CF_3 groups (**5CF5**) are expected to emit in the deep blue region. However, according to the discussion in **Chapter 2**, the HOMO and LUMO levels of fully CF_3 modified emitters would be too deep to apply the conventional device structures that can be expected to have high durability. To increase the HOMO and LUMO levels of the emitters, I further investigated partially CF_3 modified emitters with a reduction in the number of CF_3 groups (**5CF1**, **5CF2**, and **5CF4**). TADF materials containing both CF_3 modified Cz and unmodified Cz substituents in the structure have not been reported so far. The effects of partial modification on photophysical properties and stability are highly interesting. In addition, to investigate the effect of the modification position and the kinds of electron-withdrawing groups on the photophysical properties, I also synthesized the γ-position modified ones, (**5CF1γ** and **5CF5γ)** and the cyano group modified one, **5CN1**.

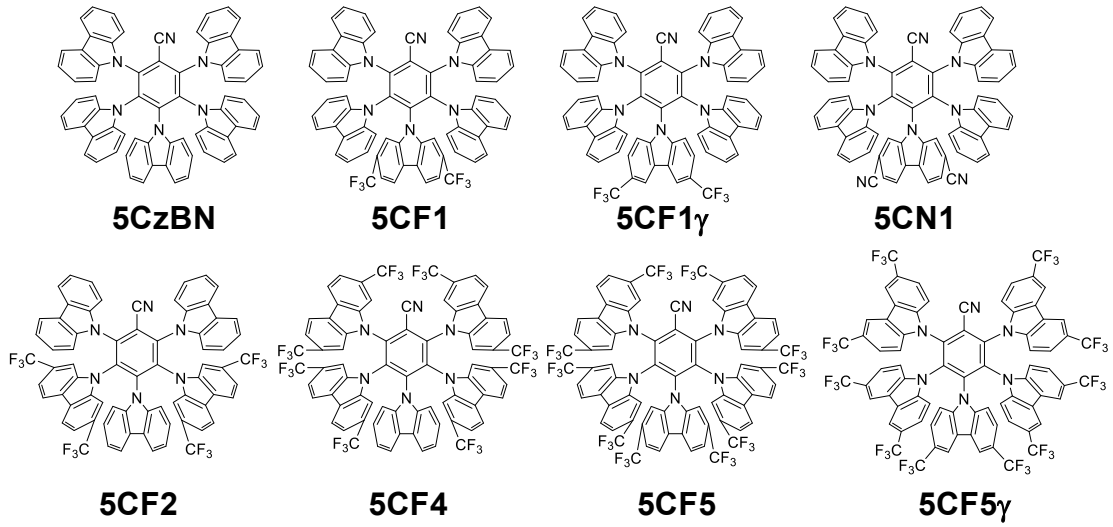

Figure 3-1 Schematic chemical structures of **5CzBN** based emitters.

3-2. Results and discussion

3-2-1. DFT calculations

To investigate the effect of CF_3 modification on the electronic state, HOMO-LUMO levels, and S_1 / T_1 energies were calculated using the Gaussian 16 program package. The S_0 geometry was optimized at the B3LYP/6-31G(d) level of theory, and the S_1 and T_1 were calculated with TD-DFT and B3LYP/6-31+G(d) methods using the optimized S_0 geometry. **Table 3-1** shows the HOMO and LUMO levels, exciton energies, and oscillator strength between S_1 and S_0 for **5CzBN** based materials by the DFT calculations. All of the CF_3 modified materials showed a deeper HOMO and LUMO levels than those of **5CzBN**. For the S_1 and T_1 energies, the higher energies were estimated for the fully CF_3 modified ones (**5CF5**) as predicted from the results of **Chapter 2**. In comparison, the similar or lower energies were estimated for the partially CF_3 modified materials (**5CF1**, **5CF2**, and **5CF4**) than those of **5CzBN**. This can be explained by the difference of HOMO distributions; HOMO of **5CF5** distributed on the CF_3 modified Cz units but those of partially CF_3 modified materials distributed on the unmodified Cz units (**Figure 3-2**). The modification of electron-withdrawing CF_3 substituents greatly weakened the electron-donating ability of Cz to which they were bonded, and also somewhat reduced the electron density of the BN unit and unmodified Cz by their inductive effect. Therefore, the fully CF_3 modified **5CF5** showed a large HOMO level drop and a little LUMO level drop, which provided a larger optical energy gap (E_g) and the blue-shifted emission. Meanwhile, partially CF_3 modified emitter showed a small HOMO drop and a large LUMO drop because the inductive effect was a distance-dependent phenomenon. The BN unit, which was closer to the CF_3 group was more susceptible to the induction effect than unmodified Cz, which was farther away from. This induced smaller E_g and the red-shifted emission in the partially modified materials by increasing the numbers of CF_3 modified Cz.

Table 3-1 DFT calculations of 5CzBN derivatives (B3LYP/6-31+G(d)) using Gaussian 16, Rev. A.03.

Emitter	HOMO (eV)	LUMO (eV)	E_g (eV)	S_1 (eV)	T_1 (eV)	ΔE_{ST} (eV)	f
5CzBN	−5.56	−2.20	3.35	2.73	2.53	0.19	0.034
5CF1	−5.68	−2.39	3.29	2.65	2.53	0.12	0.007
5CF1γ	−5.75	−2.46	3.30	2.67	2.53	0.13	0.007
5CN1	−5.77	−2.52	3.25	2.60	2.49	0.11	0.006
5CF2	−5.81	−2.53	3.27	2.61	2.53	0.07	0.021
5CF4	−6.05	−2.90	3.15	2.53	2.38	0.15	0.053
5CF5	−6.67	−3.31	3.36	2.74	2.64	0.10	0.031
5CF5γ	−6.79	−3.37	3.42	2.79	2.60	0.19	0.029

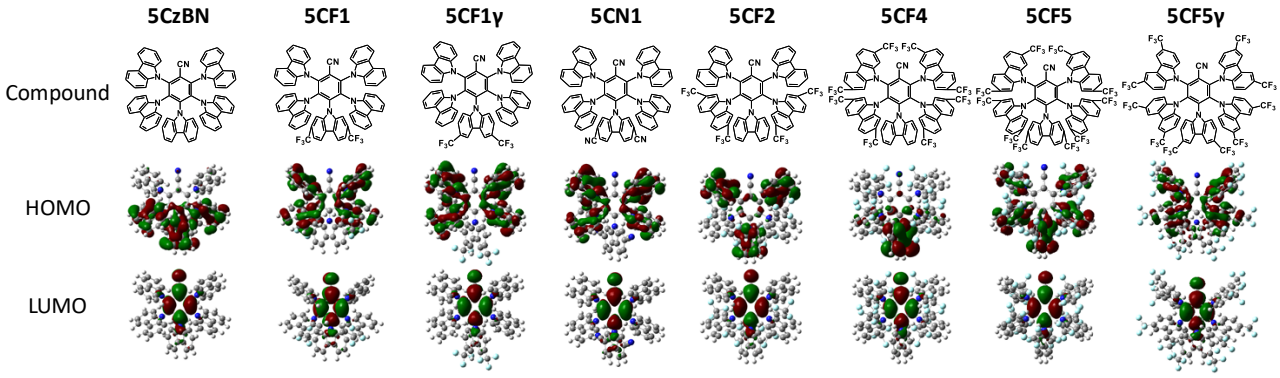

Figure 3-2 HOMO and LUMO distributions for 5CzBN derivatives (B3LYP/6-31+G(d)) using Gaussian 16, Rev. A.03.

3-2-2. Fully CF_3 modified 5CzBN derivatives

The absorption, fluorescence, and phosphorescence spectra of **5CF5** and **5CF5γ** in toluene (1.0×10^{-5} mol L^{-1}) were shown in **Figure 3-3**. Both **5CF5** and **5CF5γ** showed blue-shifted absorption and emission spectra compared with those of the unmodified **5CzBN**, as expected from DFT calculations. Their emission colors were in the deep blue region; λ_{em} were 445 and 453 nm with the PLQY of 32% and 29% for **5CF5** and **5CF5γ**, respectively (**Table 3-2**). On the other hand, **5CF5** showed high PLQY (81%) in a **PPT** film. This was higher than **5CF5γ** (50%) and **5CzBN** (75%). In **PPT** films, the emission spectra of **5CF5** and **5CF5γ** were slightly redshifted comparing to those of toluene solutions, however, the emission colors were still kept in deep blue; λ_{em} = 468 and 466 nm,

respectively. The delayed fluorescence lifetimes of **5CF5** and **5CF5γ** were almost the same as that of the unmodified one (**Figure 3-4**). By the modification position of the CF_3 on the Cz group, **5CF5** and **5CF5γ** showed the large difference in PL efficiency, but I could scarcely find any difference in other photophysical properties for those of the **PPT** films. This difference should be based on the larger steric overlap between the Cz and CF_3 groups of the β-substituent than that of the γ-substituent.[3,4] The large steric hindrance of CF_3 arising from its F-π repulsion would lead to reduce the intramolecular interaction of adjacent Cz groups due to the large dihedral angle between benzonitrile and Cz, resulting in the high PLQY.

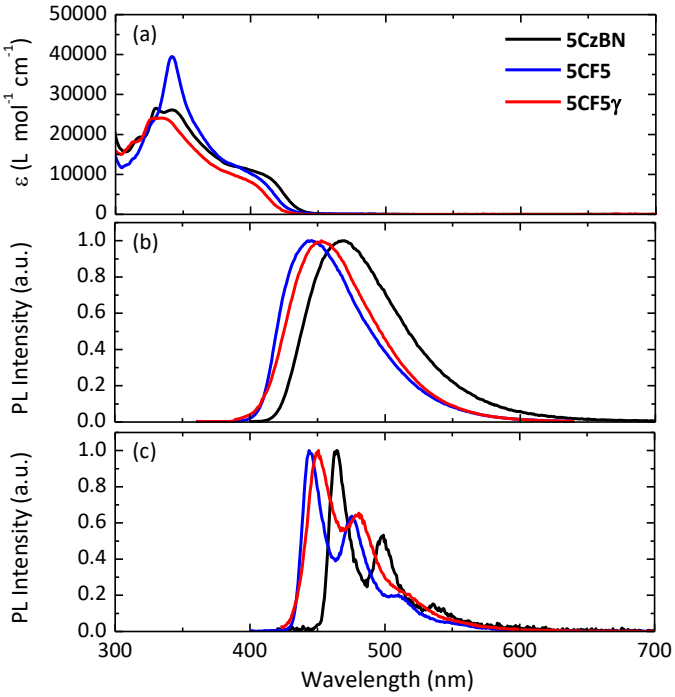

Figure 3-3 Photophysical properties of 1.0×10^{-5} mol L^{-1} toluene solution for **5CzBN**, **5CF5**, and **5CF5γ** (a) UV–vis absorption, (b) Fluorescent spectra, (c) Phosphorescent spectra.

Table 3-2 Photophysical properties of 5CzBN derivatives.

	Emitter	λ_{em}[a] (nm)	FWHM (nm)	PLQY[b] (%)	S_1[c] (eV)	T_1[c] (eV)	ΔE_{ST} (eV)	τ_p (ns)	τ_d[b] (μs)	k_{rs} (10^7 s^{-1})	k_{ISC} (10^8 s^{-1})	k_{RISC} (10^6 s^{-1})	k_{nrT} (10^4 s^{-1})
Solution (toluene)	**5CzBN**	468	78	75 (7)	2.97	2.75	0.22	3.8	47 (0.4)	1.9	2.4	0.2	0.6
	5CF1	489	100	90 (13)	2.90	2.76	0.13	5.5	6.0 (0.3)	1.6	1.7	1.7	1.9
	5CF1γ	480	83	93 (12)	2.92	2.80	0.15	5.1	8.2 (0.4)	1.7	1.8	1.3	1.0
	5CN1	491	91	75 (15)	2.86	2.74	0.12	7.4	5.3 (0.3)	1.7	1.2	1.1	5.3
	5CF2	494	92	81 (10)	2.88	2.76	0.12	8.9	7.2 (0.3)	1.0	1.0	1.2	3.0
	5CF4	521	132	13 (8)	2.87	2.75	0.12	12	3.6 (0.3)	0.5	0.8	0.3	26
	5CF5	445	68	32 (7)	3.08	2.88	0.20	2.6	36 (0.2)	1.6	3.7	0.2	2.0
	5CF5γ	453	71	29 (9)	3.09	2.94	0.15	4.1	10 (0.9)	1.8	2.3	0.3	7.6
Film 5 w% **PPT**	**5CzBN**	480	85	75	2.90	2.78	0.12	7.6	12	0.6	1.3	1.4	2.2
	5CF1	483	84	85	2.90	2.80	0.10	6.6	6.1	0.7	1.5	3.1	2.5
	5CF1γ	482	86	81	2.89	2.79	0.10	6.9	6.6	0.7	1.4	2.7	3.0
	5CN1	486	87	76	2.87	2.75	0.12	7.9	7.6	0.8	1.2	1.6	3.4
	5CF2	491	88	69	2.88	2.80	0.08	9.9	8.4	0.5	1.0	1.8	3.8
	5CF4	512	99	55	2.79	2.74	0.05	17	6.8	1.1	0.5	0.4	8.1
	5CF5	468	76	81	2.95	2.82	0.13	3.9	11	1.1	2.5	1.7	1.8
	5CF5γ	466	78	50	3.01	2.84	0.17	4.2	12	0.9	2.3	1.1	4.3
5 wt% ***m*** **CBP**	**5CF1**	483	80	97	2.83	2.69	0.14	5.9	3.0	0.9	1.6	5.7	0.3
10 wt% ***m*** **CBP**	**5CF1**	491	86	98	2.83	2.69	0.14	5.9	3.0	0.9	1.4	5.4	0.3
20 wt% ***m*** **CBP**	**5CzBN**	491	84	78	2.83	2.69	0.14	7.2	9.7	0.7	1.3	1.6	2.4
	5CF1	507	96	85	2.78	2.71	0.07	10.7	2.9	0.7	0.9	3.8	5.7
	5CF1γ	495	84	79	2.88	2.78	0.10	6.6	5.0	0.8	1.5	3.1	4.4
	5CN1	506	92	66	2.78	2.70	0.08	13	3.5	0.6	0.7	2.2	11
	5CF2	505	98	73	2.78	2.73	0.05	15	3.9	0.4	0.6	3.4	7
	5CF4	529	118	41	2.74	2.64	0.10	25	6.1	0.1	0.4	2.6	10

[a] Peak maximum value; [b] under Ar-saturated condition, before deoxygenation values were in parenthesis; [c] estimated from emission onset of fluorescent or phosphorescent spectra.

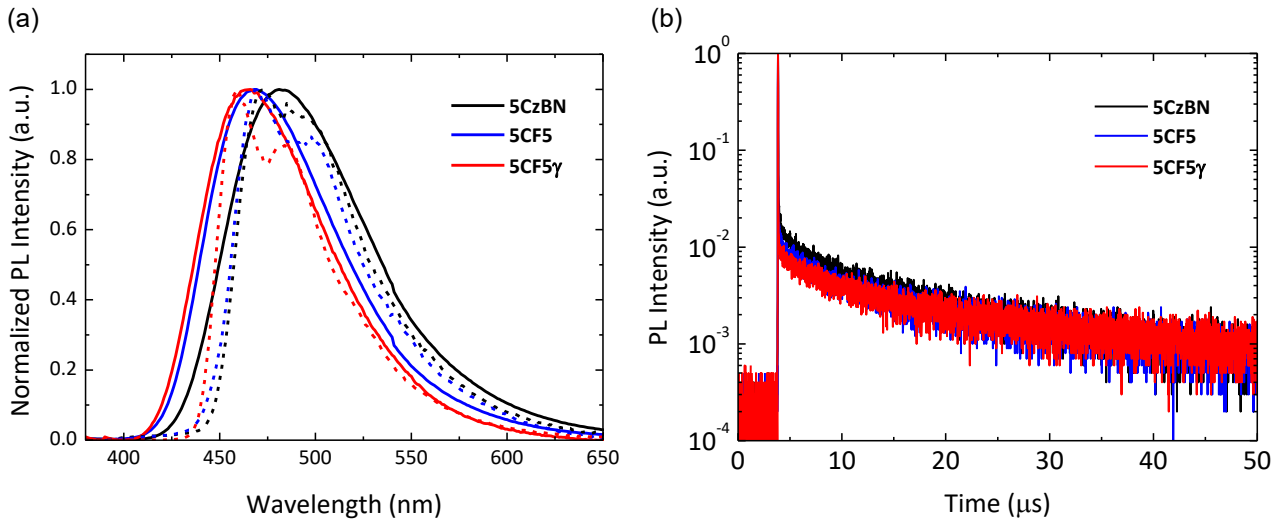

Figure 3-4 Photophysical properties of 5 wt% doped **PPT** films for **5CzBN**, **5CF5**, and **5CF5γ**; (a) Fluorescence spectra at room temperature (solid line) and phosphorescence spectra at 77 K (broken line), (b) Transient PL decay curves.

The modification position of CF_3 on the Cz group also has a critical effect on their photostability. I compared the photostability for **5CzBN**, **5CF5**, and **5CF5γ** in the argon- (Ar-) saturated toluene (**Figure 3-5**). The β-substituent (**5CF5**) showed better photostability than unmodified **5CzBN**, while the γ-substituent (**5CF5γ**) showed a large drop in its photostability.

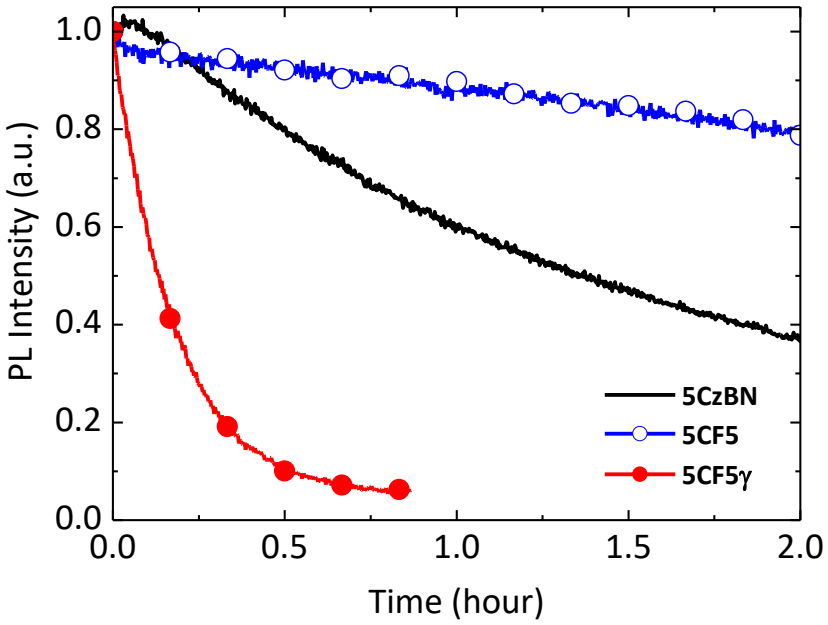

Figure 3-5 Photodegradation curves of argon gas saturated toluene solution of various emitters (1.0×10^{-5} mol L^{-1}) irradiated 365 nm UV light at 0.8 mW cm^{-2}.

When 3,3'-Di(9*H*-carbazol-9-yl)-1,1'-biphenyl (***m*CBP**) was employed as a host material, **5CF5** showed strongly red-shifted spectrum with increased FWHM compared with that in the **PPT** film (**Figure 3-6**). This was caused by the exciplex formation between **5CF5** and ***m*CBP** because of the deeper HOMO level of **5CF5** than ***m*CBP**. Therefore, **PPT** should be used as a host material to fabricate OLEDs for the fully CF_3 modified materials, **5CF5** and **5CF5γ**.

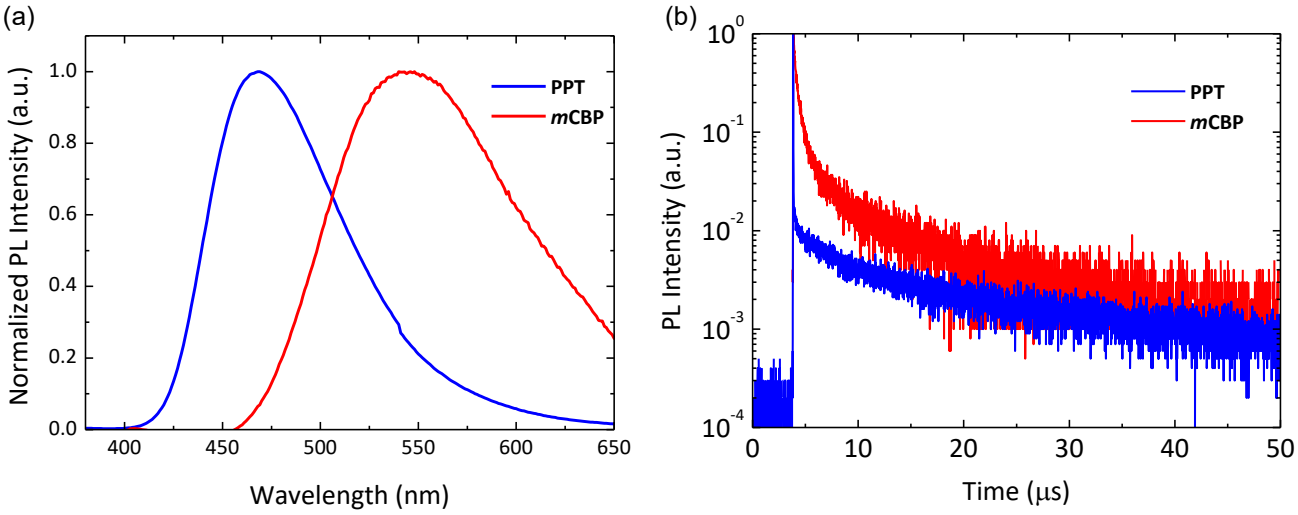

Figure 3-6 (a) PL spectra of 5 wt% **5CF5** doped films in **PPT** (blue line), ***m*CBP** (red line), (b) Transient PL decay curves of 5 wt% **5CF5** doped films in **PPT** (blue line), ***m*CBP** (red line).

To evaluate the EL properties of **5CF5** and **5CF5γ**, OLEDs were fabricated employing device structure (A) using **PPT** as the host material. **Figure 3-7** shows EQE-J characteristics, J-V-L characteristics, EL spectra and CIE coordinates for the device using **5CzBN**, **5CF5**, and **5CF5γ** as an emitter. The results are summarized in **Table 3-3**. The devices using **5CF5** and **5CF5γ** showed the deep-blue emissions, which were the shorter wavelength of 470 and 468 nm than that of the **5CzBN** based OLED (477 nm). The CIE coordinates were (0.17, 0.30), (0.15, 0.21), and (0.15, 0.20) for **5CzBN**, **5CF5**, and **5CF5γ**, respectively. Since the PLQY of **5CF5** was higher than **5CzBN**, the OLED based on **5CF5** should provide a high EQE. However, the observed EQE_{max} was 12.4% which was slightly lower than that of the OLED based on **5CzBN** (13.8%). This EQE drop would be caused by the deeper LUMO levels of the fully CF_3 modified emitters than that of the unmodified one. Electrons were easily trapped due to the deep LUMO level of the emitter, leading to the decrease of EQE.[5] In fact, the turn-on voltages (V_{on}) of the device for **5CF5** and **5CF5γ** showed higher values of 6.6 and 8.0 V than that of **5CzBN** (5.4 V).

Table 3-3 Device performance of OLEDs using 5CzBN derivatives as an emitter.

Device structure	Emitter	λ_{em}[a] (nm)	V_{on}[b] (V)	EQE[c] (%)	CIE[d]	LT_{50}[e] (hours)
(A)	**5CzBN**	477	5.4	13.8 / 11.6 / 8.5	(0.17, 0.30)	-
	5CF1	478	6.0	16.1 / 13.7 / 10.9	(0.16, 0.28)	-
	5CF1γ	478	6.6	9.4 / 8.8 / 6.5	(0.16, 0.27)	-
	5CN1	482	7.2	7.8 / 6.5 / 4.6	(0.18, 0.32)	-
	5CF2	482	6.0	10.8 / 9.8 / 6.9	(0.18, 0.34)	-
	5CF4	500	6.2	9.9 / 8.0 / 5.0	(0.24, 0.47)	-
	5CF5	470	6.6	12.4 / 7.6 / -	(0.15, 0.21)	-
	5CF5γ	468	8.0	9.1 / 6.8 / -	(0.15, 0.20)	-
(B)	**5CzBN**	486	3.2	14.1 / 13.3 / 11.2	(0.20, 0.40)	86
	5CF1	500	3.6	17.2 / 15.6 / 13.3	(0.24, 0.48)	276
	5CF1γ	491	3.8	12.1 / 11.7 / 10.2	(0.21, 0.42)	19
	5CN1	502	3.4	13.1 / 11.4 / 9.6	(0.24, 0.49)	231
	5CF2	501	3.8	9.3 / 6.9 / 5.4	(0.24, 0.48)	171
	5CF4	532	4.0	5.4 / 4.9 / 3.4	(0.34, 0.54)	29

[a] Peak maximum values ; [b] turn-on voltage, which reached the luminance of 1 cd m^{-2} ; [c] maximum value, obtained at 100, 1000 cd m^{-2}, respectively; [d] values at 100 cd m^{-2} ; [e] initial luminance of 1000 cd m^{-2}, device structure (A): ITO / **HAT-CN** (10 nm) / **α-NPD** (20 nm) / ***m*CP** (10 nm) / 5 wt% emitter: **PPT** (30 nm) / **PPT** (40 nm) / **Liq** (2 nm) / Al (100 nm), (B): ITO / **HAT-CN** (60 nm) / **TrisPCz** (30 nm) / ***m*CBP** (5 nm) / 20 wt% emitter: ***m*CBP** (30 nm) / **SF3TRZ** (10 nm) / 30 wt% **Liq**:**SF3TRZ** (30 nm) / **Liq** (2 nm) / Al (100 nm).

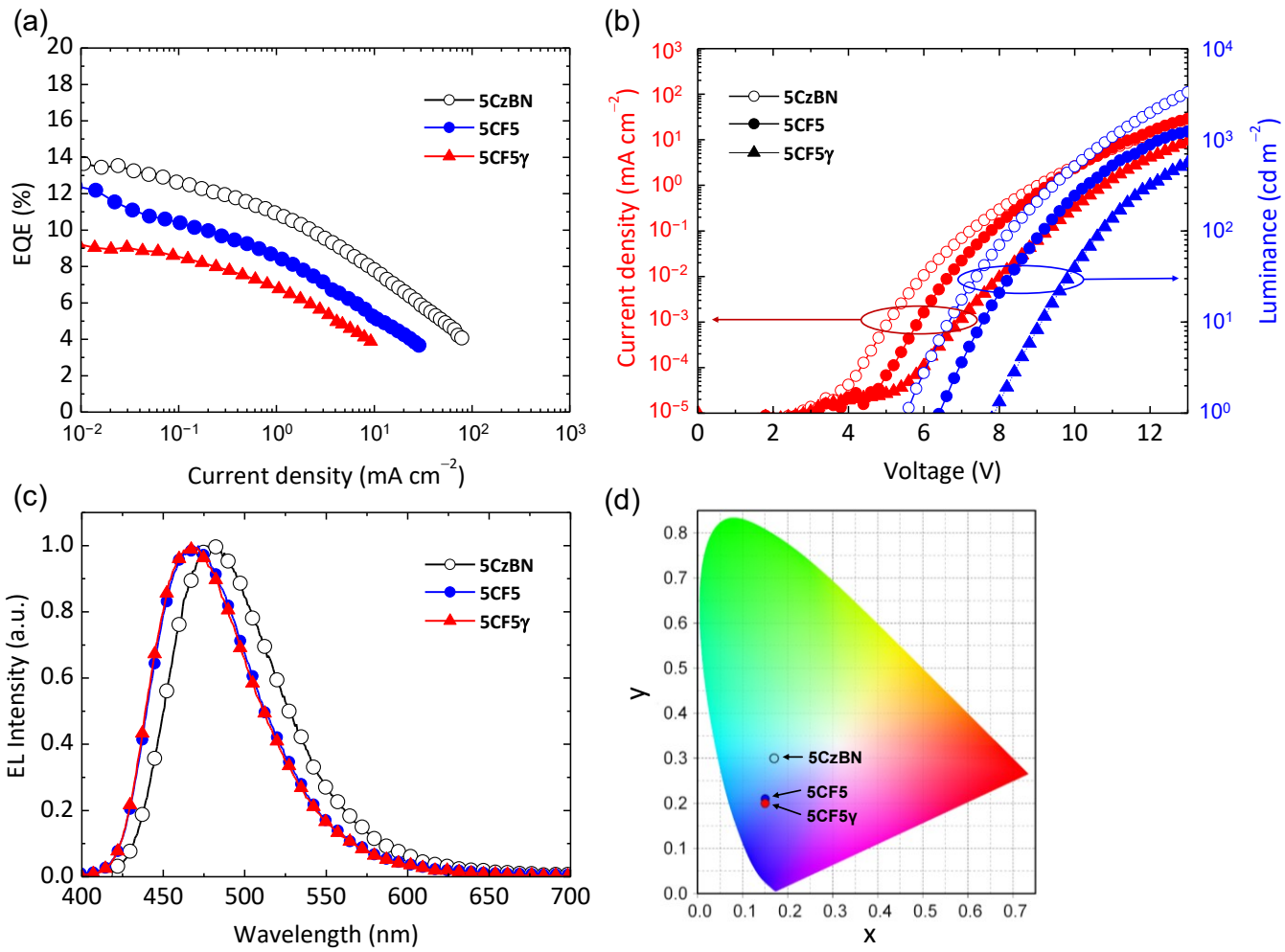

Figure 3-7 Electroluminescence characteristics of OLEDs using **5CzBN**, **5CF5**, and **5CF5γ** as an emitter; (a) EQE-J characteristics; (b) J-V-L characteristics; (c) EL spectra; (d) CIE 1931 coordinate. Device structure (A).

These results suggest that using the CF_3 modified Cz especially on the β-positions is a good strategy to obtain stable deep-blue TADF emitters with high PLQY. However, it is not a good strategy for OLEDs. Because their HOMO and LUMO levels are too deep, only limited host and peripheral materials can be employed. To improve the device performances, I should develop a suitable host and carrier transport materials applicable to the emitters having deep HOMO and LUMO levels.

3-2-4. Partially CF_3 modified 5CzBN derivatives

The CF_3 modification at the β-position of all Cz groups on **5CzBN** showed the blue-shifted emission and high molecular stability, however, their HOMO levels were too deep to apply to the promising device structure having high device durability. Thus, it is required that the HOMO level of the emitter should be designed shallower. The 5CzBN derivatives decreasing the number of CF_3 modified Cz groups provided the shallower HOMO levels than those of fully CF_3 modified ones. The synthesized partially CF_3 modified derivatives, **5CF1**, **5CF2**, and **5CF4** have shallower HOMO levels by decreasing the number of CF_3 modified Cz in cyclic voltammetry (CV) measurement (**Figure 3-8**). The partially CF_3 modified emitters showed a linear relationship between the number of CF_3 modified Cz and the HOMO and LUMO levels. On the other hand, the HOMO level of fully CF_3 modified **5CF5** slightly deviated from this relationship because its HOMO distributed on the CF_3 modified Cz. These trends in the experimental results agreed with the calculated value (**Figure 3-8**). In addition, these values were somewhat shallower than that of ***m*CBP** (−6.00 eV), the representative TADF host material.

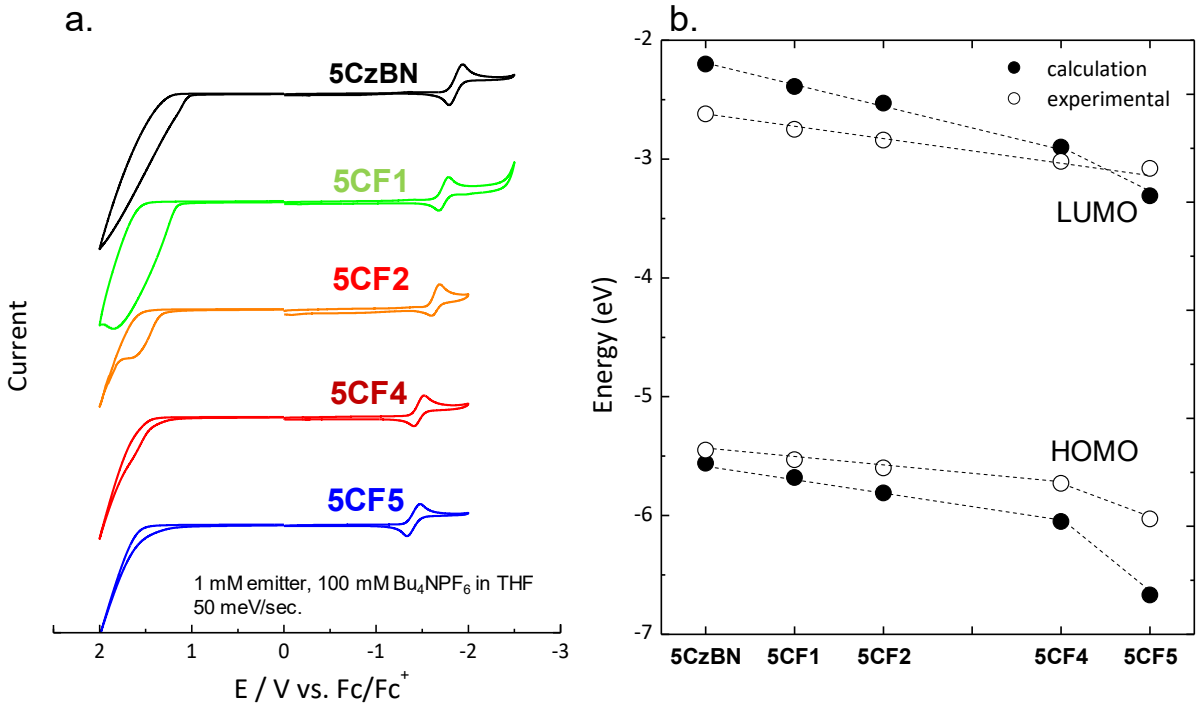

Figure 3-8 (a) Cyclic voltammograms, (b) HOMO and LUMO energy diagram for **5CzBN**, **5CF1**, **5CF2**, **5CF4**, and **5CF5**.

Although I also tried to compare the HOMO levels by AC3 measurements, the HOMO levels of **5CF4** and **5CF5** were deeper than the measurement limit of AC3 (~ −6.4 eV) and could not be estimated accurately. Focusing on the chemical shift in ^{1}H NMR, the distance from the cyano group of benzonitrile in 5CzBN had a significant effect on the chemical shift of Czs. In other words, Czs at the *ortho*-, *meta*-, and *para*-position of the cyano group were more affected by the electron-withdrawing effect of the cyano group, in that order, and the electron density was decreased. However, quantitative comparison of all compounds by ^{1}H NMR chemical shifts was not possible because the introduction position of the CF_3 modified Cz differs from compound to compound. Meanwhile, **5CzBN**, **5CF1**, and **5CF2** both had unmodified Czs at the *ortho*-position of the cyano group, ^{1}H NMR chemical shifts of them could be compared (**Table 3-4**). The results showed that as increasing the number of CF_3 modified Cz, NMR peaks of unmodified Cz shifted downfield slightly, indicating that the electron density of the unmodified Cz decreased. There was not much correlation between the ^{19}F NMR chemical shift and the HOMO levels.

Table 3-4 Chemical shift of ^{1}H, ^{19}F NMR spectra for **5CzBN**, **5CF1**, **5CF2**, **5CF4**, and **5CF5**.

	δ (ppm)			
	^{1}H NMR (Cz at *ortho*-position of CN)			^{19}F NMR
	a	d	b, c	
5CzBN	7.71 (d)	7.24 (d)	7.04-7.08 (m)	-
5CF1	7.73 (d)	7.31 (d)	7.06-7.11 (m)	−61.25
5CF2	7.75 (d)	7.32 (d)	7.07-7.14 (m)	−61.25
5CF4	-	-	-	−61.79
5CF5	-	-	-	−61.70, −62.36, −62.46

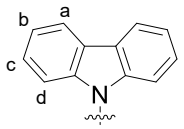

Increasing the number of CF_3 modified Cz on 5CzBN scaffold provided the red-shifted emission. S_1 energies were 2.97, 2.90, 2.88, 2.87, and 3.08 eV for **5CzBN, 5CF1**, **5CF2**, **5CF4**, and **5CF5**, respectively (**Figure 3-9**, **Tables 3-2**). These tendencies showed a good agreement with the calculated values (**Table 3-1**). PLQY of partially modified emitters tended to decrease with an increasing number of modified Cz. However, **5CF1** showed higher PLQY (90%) than that of

unmodified **5CzBN** (75%). Interestingly, I found the partially CF_3 substituted emitters showed one order of magnitude shorter lifetime of delayed fluorescence (τ_d) than that of the unmodified **5CzBN** (47 μs); they were 6.0, 7.2, and 3.6 μs for **5CF1**, **5CF2**, and **5CF4**, respectively in toluene solution. In the case of the fully CF_3 substituted **5CF5**, τ_d was a similar value (36 μs) to that of **5CzBN** (**Table 3-2**).

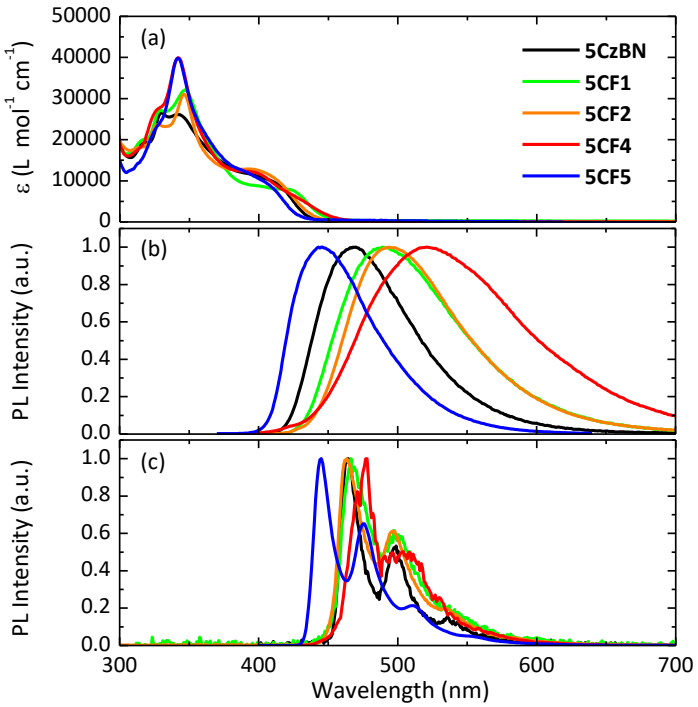

Figure 3-9 Photophysical properties of 1.0×10^{-5} mol L^{-1} toluene solution for **5CzBN**, **5CF1**, **5CF2**, **5CF4**, and **5CF5** (a) UV−vis absorption, (b) Fluorescent spectra, (c) Phosphorescent spectra.

Highest occupied and lowest unoccupied natural transition orbitals (HONTO and LUNTO) at S_1 and T_1 are shown in **Figure 3-10**, while molecular orbital distribution of HOMO, HOMO−1, HOMO−2, and LUMO in the ground state are summarized in **Figure 3-11**. Regarding the emission from S_1 to S_0, in addition to HOMO-LUMO transition, the transition from HOMO−1 or HOMO−2 to LUMO were also included for **5CzBN**, **5CF1**, **5CF1γ**, and **5CF2**. On the other hand, for **5CF4** and **5CF5**, almost only HOMO-LUMO transition contributed to the emission. Since LUMO+1 level was far from the LUMO level, its contribution to emission was small.

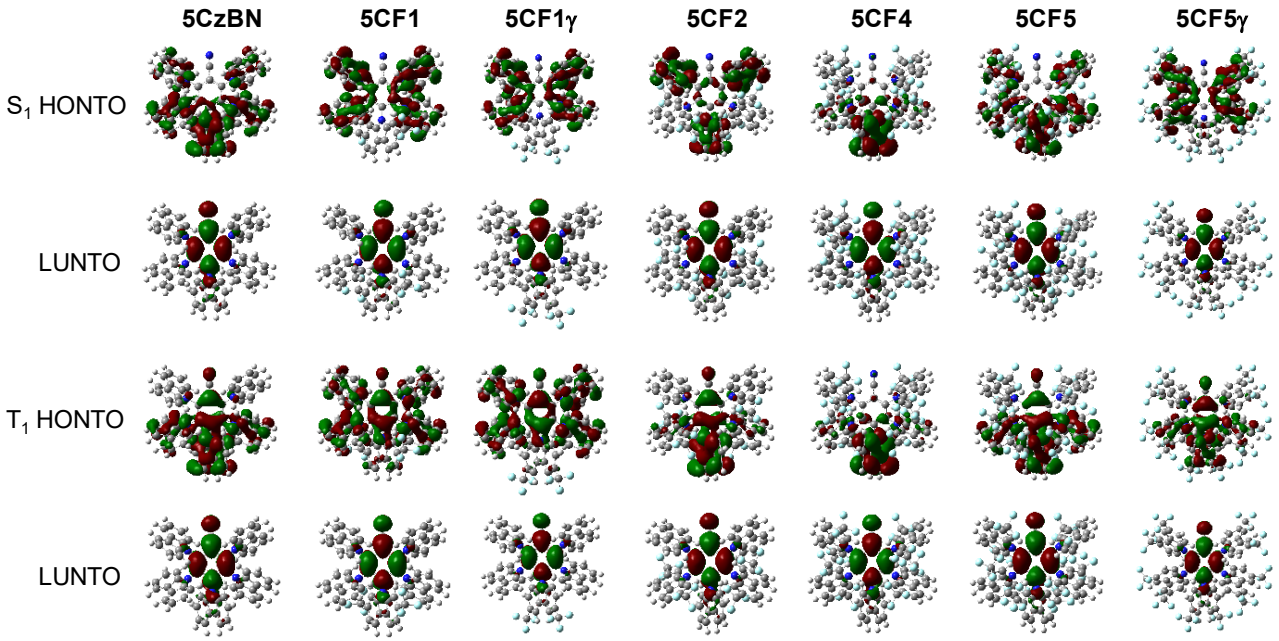

Figure 3-10 Distribution of HONTO and LUNTO at S_1 and T_1.

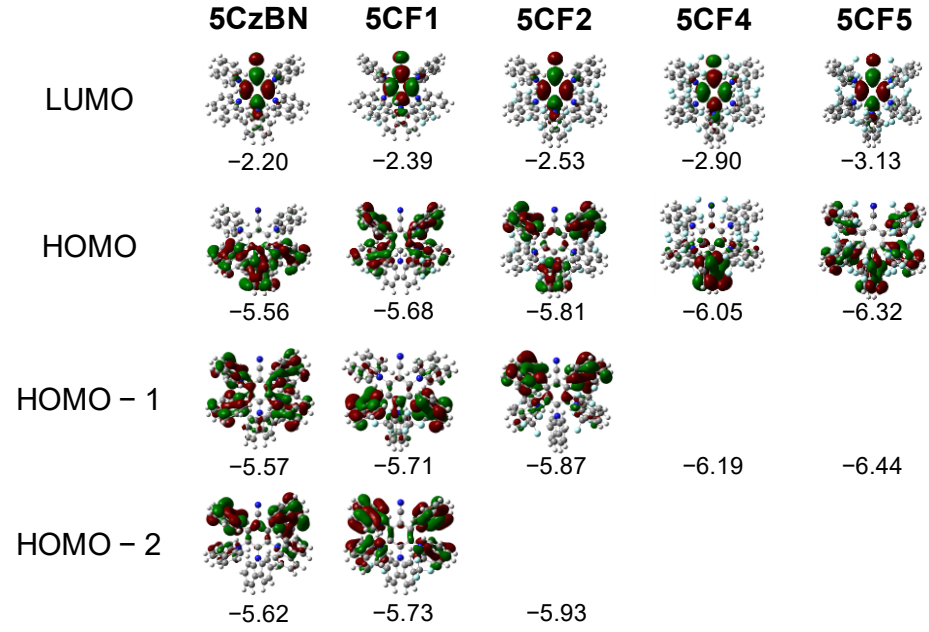

Figure 3-11 Distribution of HOMO, HOMO−1, HOMO−2, and LUMO.

Regarding the modification position of CF_3 on the Cz group, I could not find a large difference between **5CF1** and **5CF1γ**. This indicates the modification position of CF_3 on the Cz did not affect the photophysical properties so much in the 5CzBN platform. On the other hand, the modification position had a critical effect on their photostability. I compared the photostability for **5CzBN**, β-substituents (**5CF1**, **5CF2**, **5CF4**, and **5CF5**), and γ-substituents **(5CF1γ)** in the Ar

saturated toluene (**Figure 3-12**). All the β-substituents showed better photostability than that of unmodified **5CzBN**, while the γ-substituents showed similar stability (**5CF1γ**). Especially, **5CF1** having one CF_3 modified Cz group at the *para*-position of BN showed the best performance of the photostability among all materials in the 5CzBN platform. To find a universality for the modification effect of the electron-withdrawing groups on the β-position of the Cz group, I also synthesized **5CN1** which have a 2,7-dicyanocarbazolyl group on *para*-position on benzonitrile instead of CF_3 modified Cz. **5CN1** showed more red-shifted emission, lower PLQY, and k_{RISC} than **5CF1** (**Tables 3-2**) but it also enhanced the photostability well (**Figure 3-12** b). I can conclude that the strategy of electron-withdrawing group modification on the β-position of the Cz group enhances the photostability of TADF materials, regardless of full or partial modification and the kinds of a functional group.

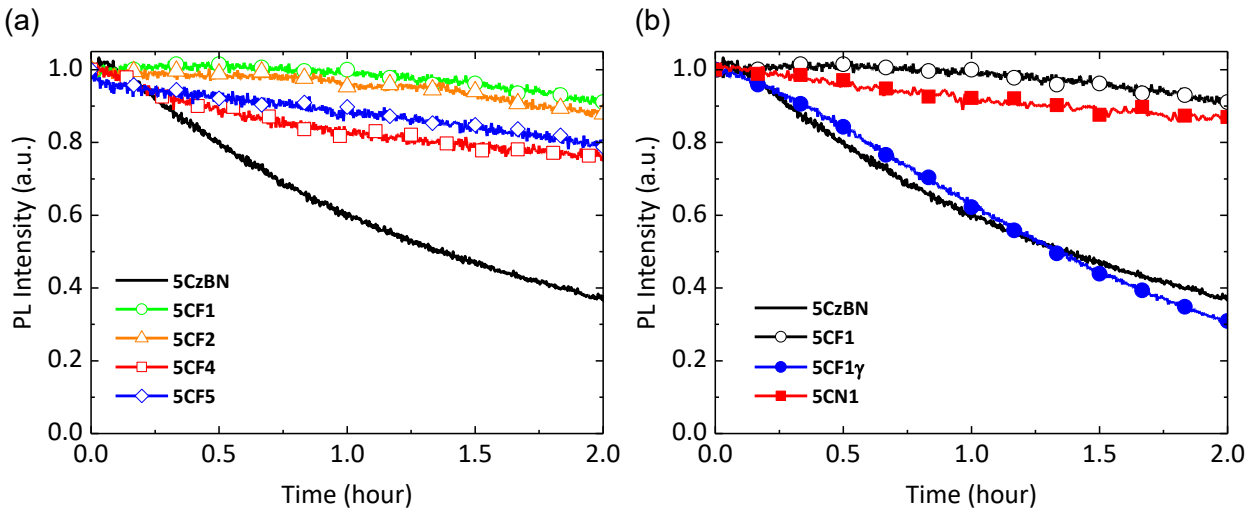

Figure 3-12 Photodegradation curves of argon gas saturated toluene solution of 5CzBN derivatives (1.0×10^{-5} M) irradiated 365 nm UV light at 0.8 mW cm^{-2}.

To investigate the film properties of these emitters, ***m*CBP** was employed as a host material because the HOMO levels of partially CF_3 modified 5CzBN derivatives were shallower than that of ***m*CBP**.The same trend in the toluene solution was observed in ***m*CBP** films. To compare the effect of changing the host material, the various concentration of **5CF1** (5-20 wt%) doped ***m*CBP** films were prepared. These emission spectra and PLQY were summarized in **Figure 3-13** and **Table 3-2**. Comparing between the **PPT** and ***m*CBP** hosts with the doping concentration of 5 wt%, the ***m*CBP** film showed slightly longer emission than the **PPT** film. By increasing the doping concentration,

5CF1 showed a red-shifted emission with the larger FWHM. The spectra of 20 wt% doped film for each partially CF_3 modified emitters were summarized in **Table 3-2**. The **5CF4** showed the red-shifted emission (λ_{em} = 529 nm) and broader FWHM (118 nm). Since these values were similar to those of its solution (λ_{em} = 521 nm, FWHM = 132 nm), this was not caused by the exciplex formation between **5CF4** and ***m*CBP**.

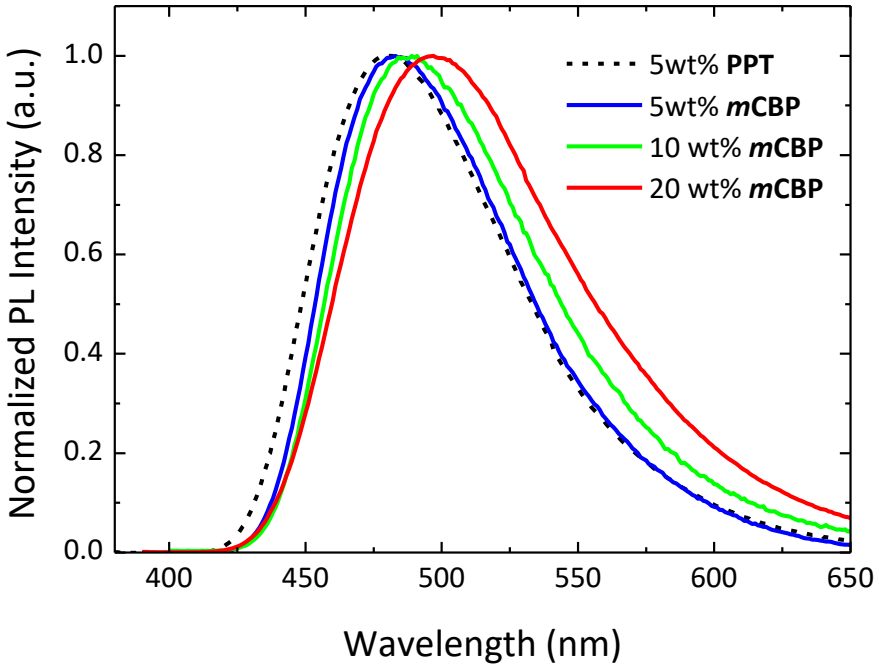

Figure 3-13 PL spectra of **5CF1** doped films; 5wt% in **PPT**, 5, 10, 20 wt% in ***m*CBP**.

The doping concentration of 20 wt% was often selected for the reported OLEDs to measure their durability because the device lifetime is improved by increasing the doping concentration of emitters.[1,5] This should be caused by the improvement of the electron transporting ability of the emission layer (EML). Therefore, I fabricated OLEDs using **5CzBN**, **5CF1**, **5CF2**, **5CF4**, **5CF1γ**, and **5CN1** as an emitter with the device structure (B) having 20 wt% emitters in ***m*CBP** as an EML (the results of device structure (A) using **PPT** host were shown in **Table 3-3**). The results of EQE-J, J-V-L, EL spectra, and device durability test for each emitter were shown in **Figures 3-14**, **3-15**. The device operational durability test was recorded as the EL intensity decay of the device from the initial luminance (1000 cd m^{-2}) under the driving condition of constant current. The values of EQE_{max}, EQE@1000 cd m^{-2}, CIE coordinates, and LT_{50} were summarized in **Table 3-3**. EQE of the devices

correlated with PLQY of the emitter and **5CF1** showed the highest EQE of 17.2%. Comparing the devices of **5CzBN**, **5CF1**, **5CF2**, and **5CF4**, V_{on} was increased by increasing the number of CF_3 modified Cz groups. This would be due to the electron trapping by the deep LUMO level of the emitters. The device lifetimes of **5CF1**, **5CN1**, and **5CF2** were significantly improved over **5CzBN**, while **5CF1γ** declined as predicted by the photostability test.

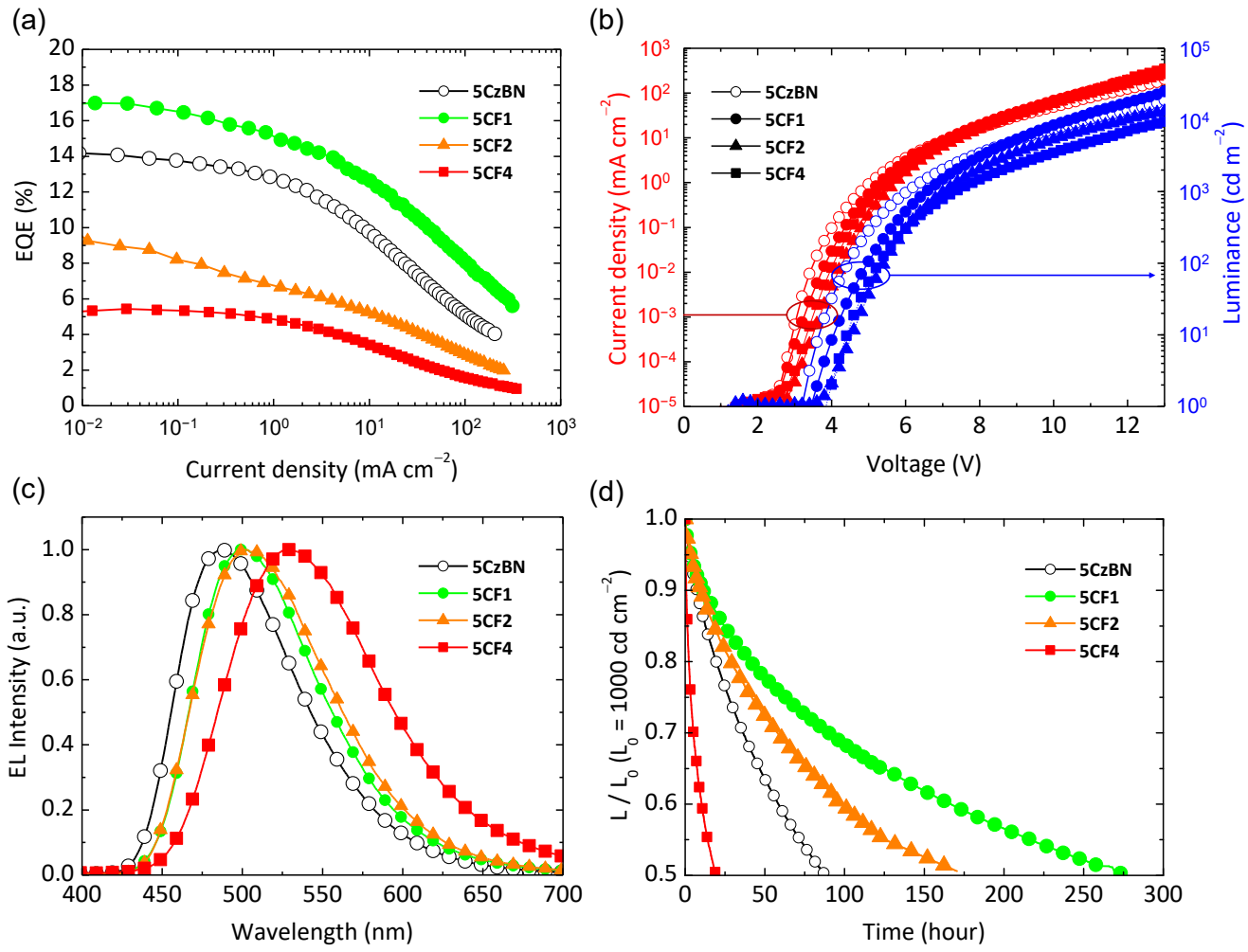

Figure 3-14 Electroluminescence characteristics of OLEDs using **5CzBN**, **5CF1**, **5CF2**, and **5CF4** as an emitter; (a) EQE-J characteristics; (b) J-V-L characteristics; (c) EL spectra; (d) Luminance decay (at an initial luminance of 1000 cd m^{-2}). Device structure (B).

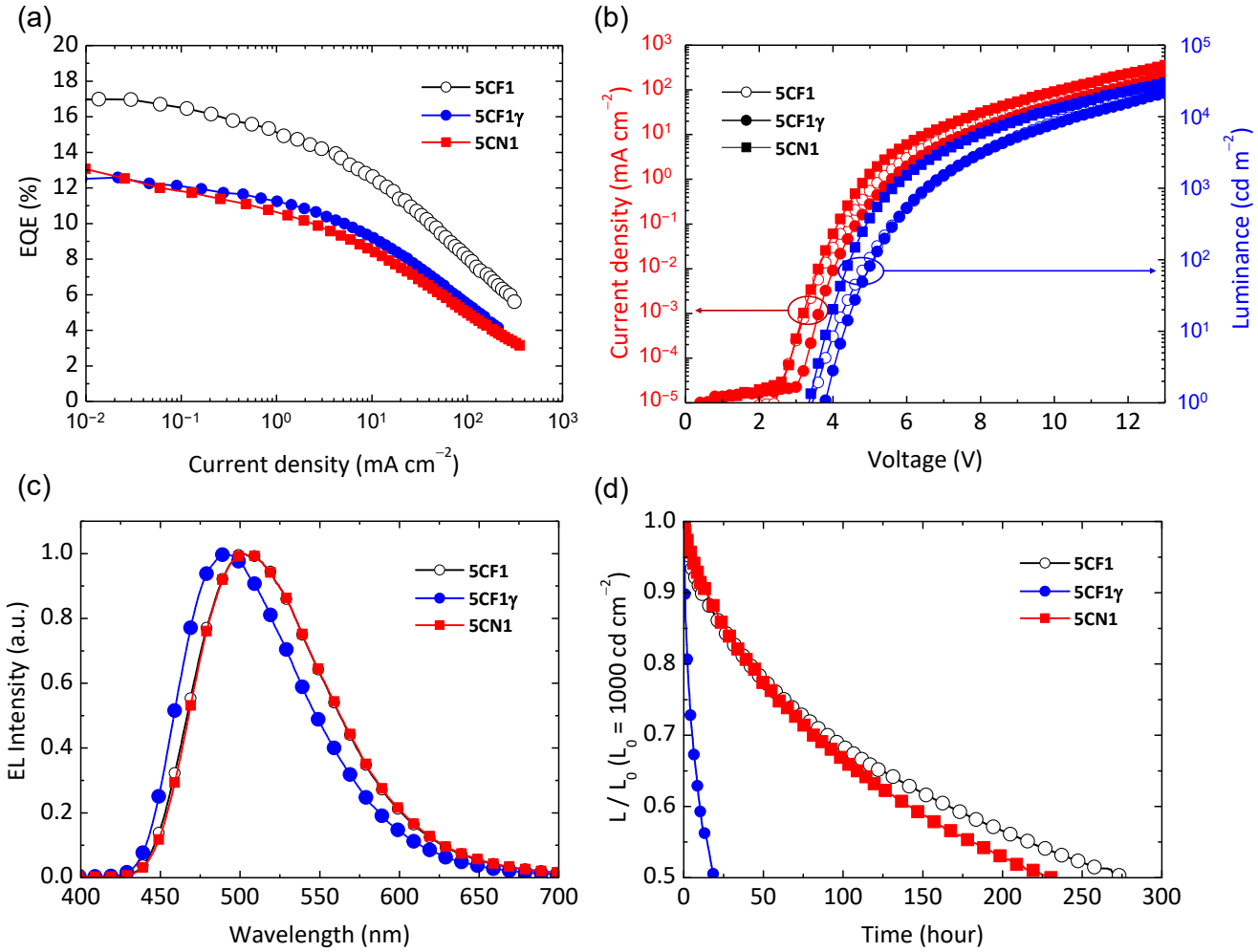

Figure 3-15 Electroluminescence characteristics of OLEDs using **5CF1**, **5CF1γ**, and **5CN1** as an emitter; (a) EQE-J characteristics; (b) J-V-L characteristics; (c) EL spectra; (d) Luminance decay (at an initial luminance of 1000 cd m^{-2}). Device structure (B).

3-2-5. Discussion

The electron-withdrawing groups modification of **5CzBN** intensivcly affected on their device stablity. As mentioned in **Chapter 1**, device degradation is originated from the inherently poor stability of organic materials used in the carrier transport or emission layers of OLEDs. In addition, improper management of device structures acceralates material degradation. Therefore, both material and device related degradation routes should be considered at the same time (**Figure 3-16**). Material related degradation in OLEDs can be largely divided into photochemical degradation and electrochemical degradation. Photochemical degradation is the inherent degradation of organic materials, which is thought to be mainly caused by the long-lived triplet excitons.[6] The triplet excitons

having high energy and long lifetime could cause the bond cleavage and various intra- or inter-molecular reactions. Therefore, the photochemical stability (photostability) of an emitter is often judged by its triplet energy, triplet lifetime,[7,8] and its bond dissociation energy (BDE).[9] For improved photostability, emitters composed of strong bonds with low triplet energy and short delayed fluorescence lifetime should be promissing. In addition, for improved electrochemical stabiliy, the emitters should be reversible to redox because organic materials are continuously oxidized or reduced during device operation. Here, I discuss the reasons why the number of CF_3 modified Cz and their modification positions affected the device stability in terms of material stability and device structures.

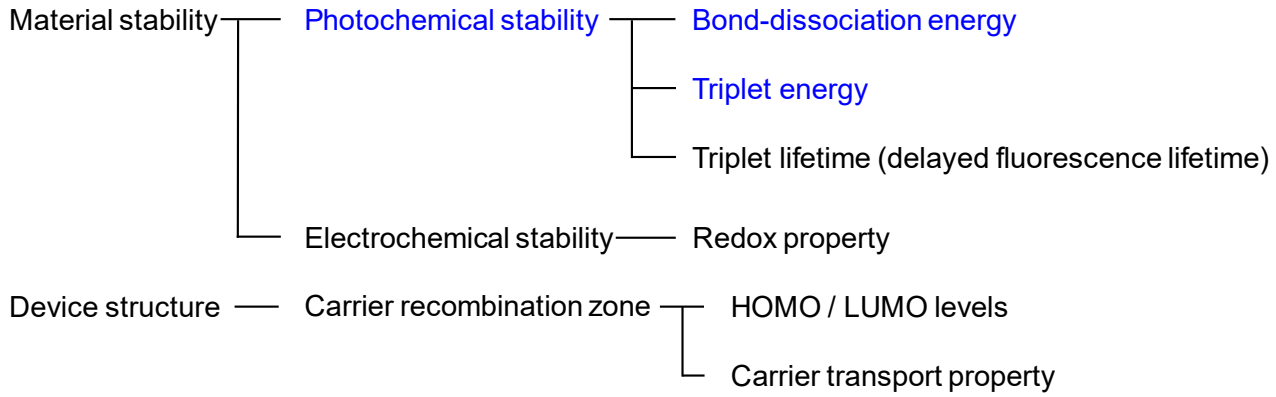

Figure 3-16 Cause and effect diagram for the stability of OLEDs.

a) Material stability

The number of electron-withdrawing group-modified Cz and their modification positions had a significant impact on their photostability of the emitters. On the other hand, CF_3 modification did not affect the electrochemical stability of emitters. Although emitters with reversible redox function are preferable, the γ-position of Cz is electrochemically active and irreversible to oxidation.[10] This problem was not resolved by partial CF_3 modification. Both **5CF1** and **5CF1γ** showed irreversible oxidation. This should be due to the presence of unprotected carbazolyl groups at γ-position in the molecular structure. Then, the differences in the material stability of these emitters were mainly affected by their photostability. Factors affecting photostability are discussed below.

<Triplet energy and lifetime>

The RISC process of **5CzBN** was reported to involve the triplet energy states of their substructures, for examples 2,3,5,6-tetra(9*H*-carbazol-9-yl)benzonitrile (**4CzBN**) as an intermediate state (**Figure 3-17** a).[11] Besides, the enhanced k_{RISC} of partially phenyl group modified 5CzBN derivative involves the locally excited states of 9-phenyl-3,6-diphenylcarbazole (**Figure 3-17** b).[1]

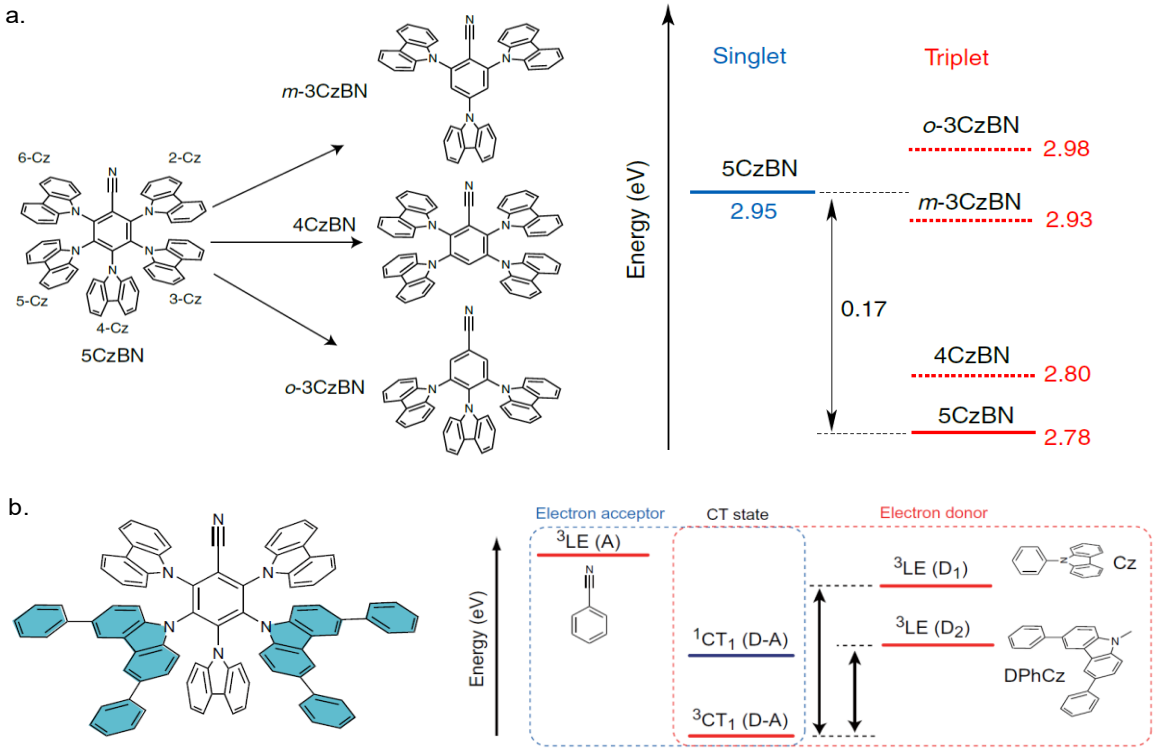

Figure 3-17 Schematic illustration of the intermediate state for RISC process. (a) **5CzBN**, (b) partially phenyl groups modified **5CzBN**.

Thus, by introduction of electron-withdrawing groups in **5CzBN**, different triplet intermediate states could be involved in RISC process. Actually, the partially CF_3 substituted emitters showed one order of magnitude shorter lifetime of delayed fluorescence (τ_d) than that of unmodified **5CzBN**, while that of fully CF_3 substituents were similar values in toluene solution (**Table 3-2**). To understand the RISC processes in these compounds, the temperature dependence of k_{RISC} and k_{ISC} were measured. Activation energies for RISC (E_a^{RISC}) and ISC (E_a^{ISC}) were estimated from Arrhenius plots of k_{RISC} and k_{ISC} (**Figure 3-18**). E_a^{RISC} values were 0.13, 0.08, 0.09, 0.04, and 0.08 eV for

5CzBN, **5CF1**, **5CF1γ**, **5CN1**, and **5CF2**, respectively. These values were smaller than ΔE_{ST} of each compound (**Table 3-2**), and partially electron-withdrawing groups modified emitters (**5CF1**, **5CF1γ**, **5CN1**, and **5CF2**) showed smaller E_a^{RISC} than **5CzBN**. **5CF4** and **5CF5** showed no temperature dependance of transient PL decay curves, and would not be able to estimate the k_{RISC} and k_{ISC} correctly due to their low PLQY. E_a^{ISC} values were 0.01, 0.03, 0.03, 0.03, and 0.03 eV for **5CzBN**, **5CF1**, **5CF1γ**, **5CN1**, and **5CF2**, respectively. These results indicated that there were some intermediate triplet states (T_n) between S_1 and T_1, which were involved in the RISC process (**Figure 3-19**).

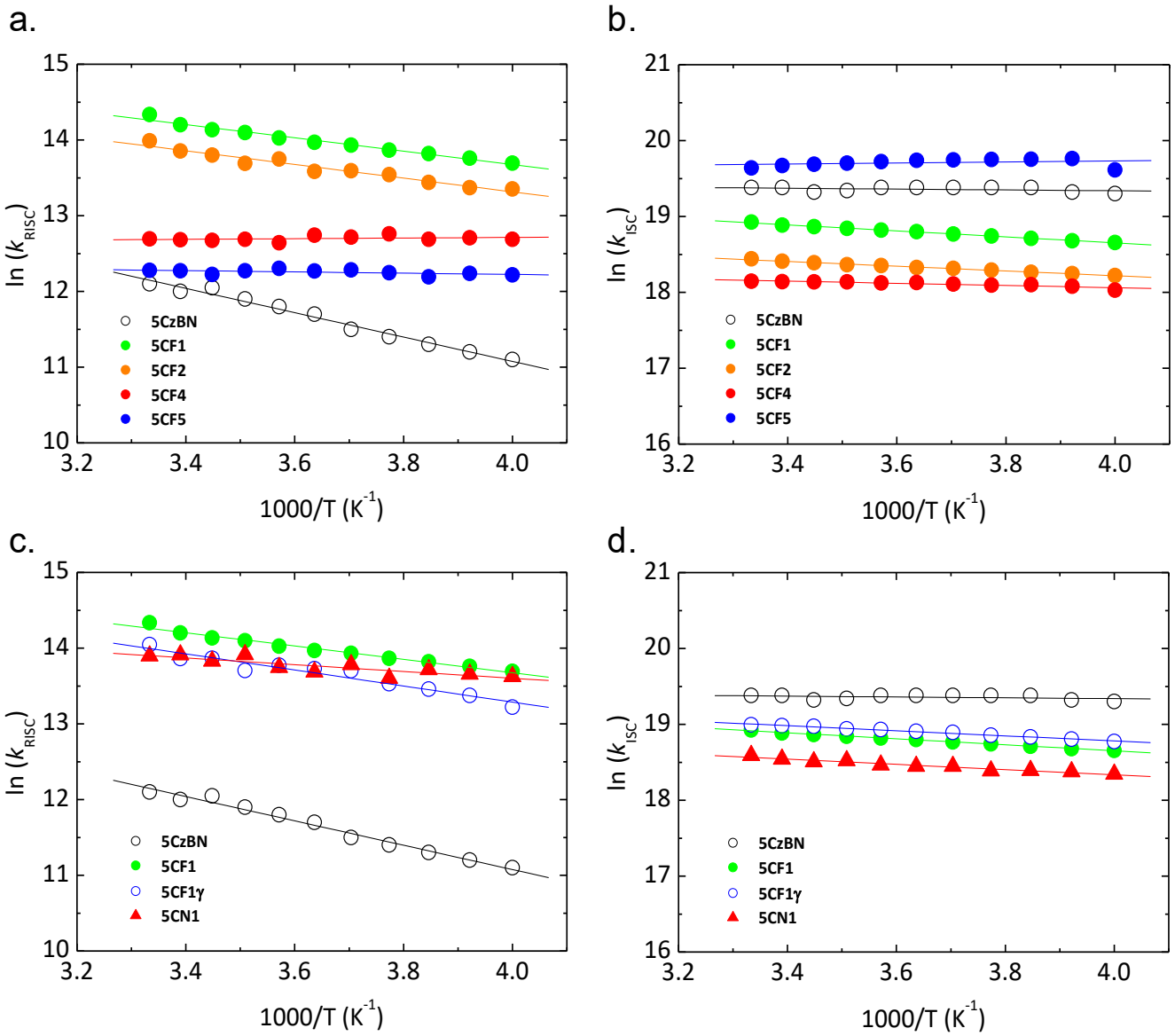

Figure 3-18 Arrhenius plots of RISC and ISC for **5CzBN**, **5CF1**, **5CF1**, **5CN1**, **5CF2**, **5CF4**, and **5CF5**.

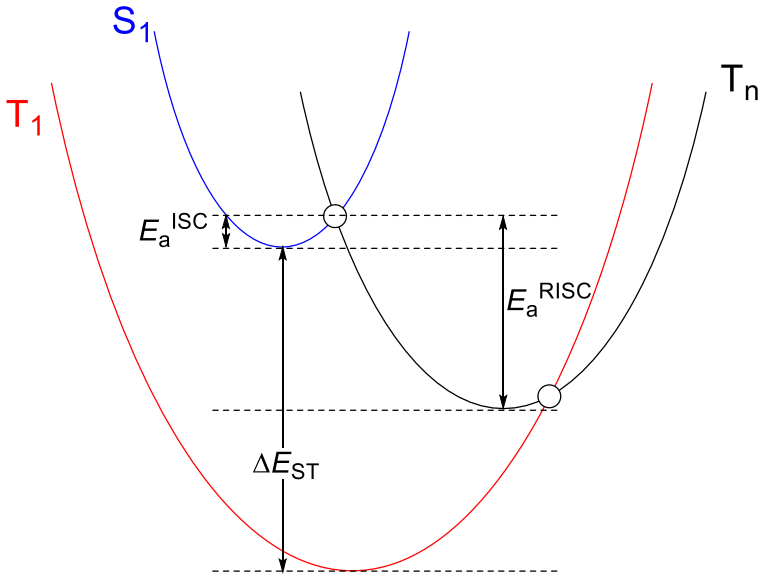

Figure 3-19 Supposed RISC and ISC process of 5CzBN derivatives.

It was reported that E_a^{RISC} of **5CzBN** was similar to the energy difference between S_1 and T_n.[11] According to a previous finding, the rate-determing process in RISC was assumed to be a transition from T_n to S_1 in **Figuer 3-19**. The transition from T_1 to T_n by the conformational conversion without spin-flips (ps order) should be much faster than the transition from T_n to S_1 with spin-flips (μs order).[12]. Based on **Figure 3-19**, I estimated the energy of T_n, using the following equation;

$$T_n = S_1 + E_a^{ISC} - E_a^{RISC}$$

The results are shown in **Table 3-5**. The estimated T_n were 2.85, 2.80, and 2.86 eV for **5CzBN**, **5CF1**, and **5CF1γ**, respectively. These results indicated that T_n was decreased for β-modification and increased for γ-modification.

Table 3-5 Photophysical properties of 5CzBN derivatives.

	S_1 (eV)	T_1 (eV)	ΔE_{ST} (eV)	E_a^{ISC} (eV)	E_a^{RISC} (eV)	k_{ISC} (10^8 s^{-1})	k_{RISC} (10^6 s^{-1})	T_n (eV)
5CzBN	2.97	2.75	0.22	0.01	0.13	2.4	0.2	2.85
5CF1	2.90	2.76	0.13	0.03	0.08	1.7	1.7	2.80
5CF1γ	2.92	2.89	0.15	0.03	0.09	1.8	1.3	2.86
5CN1	2.86	2.74	0.12	0.03	0.04	1.2	1.1	2.85
5CF2	2.88	2.76	0.12	0.03	0.08	1.0	1.2	2.83

At present, the substructure corresponding to T_n is unclear. However, to clarify the effect of the electron-withdrawing groups modification on triplet energies, the phosphorescence spectra of the substructures, **PhCz**, **PhβCF**, **PhγCF**, and **PhβCN**, were measured (**Figure 3-20**); these values were 3.04, 2.98, 3.07, and 2.73 eV, respectively. T_1 of **PhCz** was also found to be decreased for β-position electron-withdrawing modification and increased for γ-position modification.

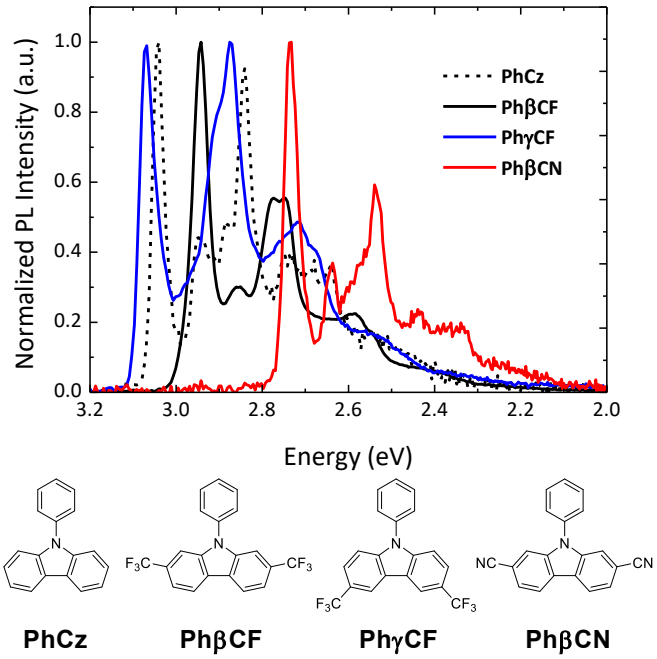

Figure 3-20 Phosphorescence spectra of toluene solutions for 9-phenylcarbazole derivatives.

The delayed fluorescence lifetime of partially modified emitters was uniformly shortened, while that of fully modified ones showed only a little change. Therefore, the triplet lifetime would not be the only factor for the difference in photostability. Considering triplet energies, T_1 and T_n decreased by β-modification and increased by γ-modification. The lower triplet energy of β-substituents would stabilize their excited states (**Figure 3-21**).

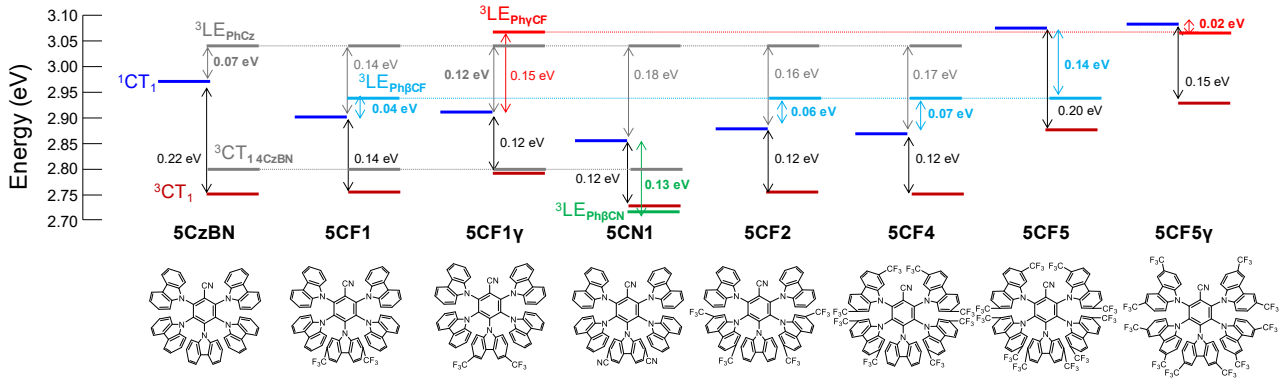

Figure 3-21 Schematic illustration of the intermediate state for RISC process for 5CzBN derivatives.

<Bond dissociation energy (BDE)>

The C−N single bond between donor and accrptor moieties is the weakest bond in most donor-acceptor type TADF materials. Therefore, dissociation of the C−N bond is easy.[13] For examples, The excited-state stability and decomposition products of **4CzIPN** have been reported.[14] LC/MS analysis of the toluene solution after UV irradiation has been performed and homocleaved decomposition products between Cz and phthalonitrile were observed. It has been also reported that homocleavage of the C−N bond linking Cz and phenylene occurs in the case of host materials and hole transport materials containing Cz in the structure.[15] In addition, this literature showed that the neutral radicals generated from homocleavage could react with the surrounding molecules and accelerate the degradation by addition reactions. BDE calculations for these molecules also suggested that the C−N bond is the weakest bond in the structure. Quio et al. reported that the electron-withdrawing substituents on Cz of 9-phenylcarbazole provided the higher BDE of C−N bond (CF_3; 3.64-3.65 eV, CN; 3.68 eV) compared with that of unmodified one (3.54 eV).[16] The increase of the BDE for modified emitters would also be a possible reason to the high photostability. Then, the BDE of C−N bond for 5CzBN derivatives were calculated using the Gaussian 16 program package. BDE was calculated at the UB3LYP/6-31G(d) level of theory using the optimized S_0 geometry. The results were summarized in **Table 3-6**. In **5CzBN**, there are three kinds of C−N bonds in *ortho*-, *meta*-, and

para-positions for the nitrile group, and they had different BDE (3.44, 3.39, and 3.36 eV, respectively). The BDE of C−N bond in *para*-position was the weakest (3.36 eV) and improved by the electron-withdrawing groups modification; the BDE of modifed C−N bonds were 3.45, 3.46, and 3.46 eV for **5CF1**, **5CF1γ**, and **5CN1**, respectively. In addition, electron-withdrawing group modification of one carbazole improves not only the BDE of modified C−N bond but also the BDE of the unmodified C−N bond to some extent (0.01 ~ 0.04 eV).[17,18] In the case of **5CF2**, CF_3 modification also improved the BDE of modifed and unmodifed C−N bonds. On the other hand, the BDE of C−N bonds of *ortho*- and *meta*-positon for **5CF4** were smaller than those of **5CzBN**. That would be due to the large dihedral angles between Cz and BN units. Because of the large steric hindrance of CF_3 groups, their conjugations were much reduced.[16] Among the partial modified emitters, **5CF1** showed the highest photostability, suggesting that increasing the BDE of the weakest bond in the molecule (*para*-position of **5CzBN**) was effective in improving its stability. The slightly lower photostability of **5CF5** than **5CF1** would be due to its reduced conjugation of C−N bond, higher triplet energy, and longer delayed fluorescence lifetime.

Table 3-6 BDE calcurations of C−N bond for 5CzBN derivatives (UB3LYP/6-31G(d)) using Gaussian 16, Rev. A.03.

C−N bond	BDE (eV)					
	5CzBN	**5CF1**	**5CF1γ**	**5CN1**	**5CF2**	**5CF4**
ortho	3.44	3.47	3.47	3.48	3.47	3.43
meta	3.39	3.40	3.41	3.42	3.46	3.36
para	3.36	3.45	3.46	3.46	3.38	3.41

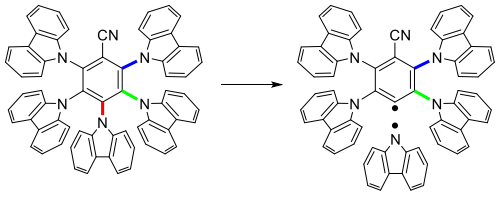

Therefore, the high stability of **5CF1** should be based on its lower triplet energy, shorter delayed fluorescence lifetime, and stabilized C−N bond between Cz and BN unit.

b) Device structure

The durability of **5CF4** based OLED was decreased in spite of its improved photostability. This may be due to the change in carrier balance, which is the main degradation process in 5CzBN-based OLEDs.[19] The EL spectral change around 630 to 680 nm region during degradation testing was observed for all emitters and grew over time (**Figure 3-22**). This red emission is thought to be electromer emission from a hole blocking material, indicating that the carrier recombination zone was shifted from the anode side to the hole blocking layer side. The changes were the largest for **5CF4**, suggesting the reduced electron transporting ability in the **5CF4** device. Among these emitters, **5CF4** had the deepest LUMO level, which tends to trap electrons, and the charge recombination zone was shifted toward the hole-blocking layer to reduce the device lifetime. The reason why **5CF1** showed the highest device stability among these emitting materials should be due to its high photostability.

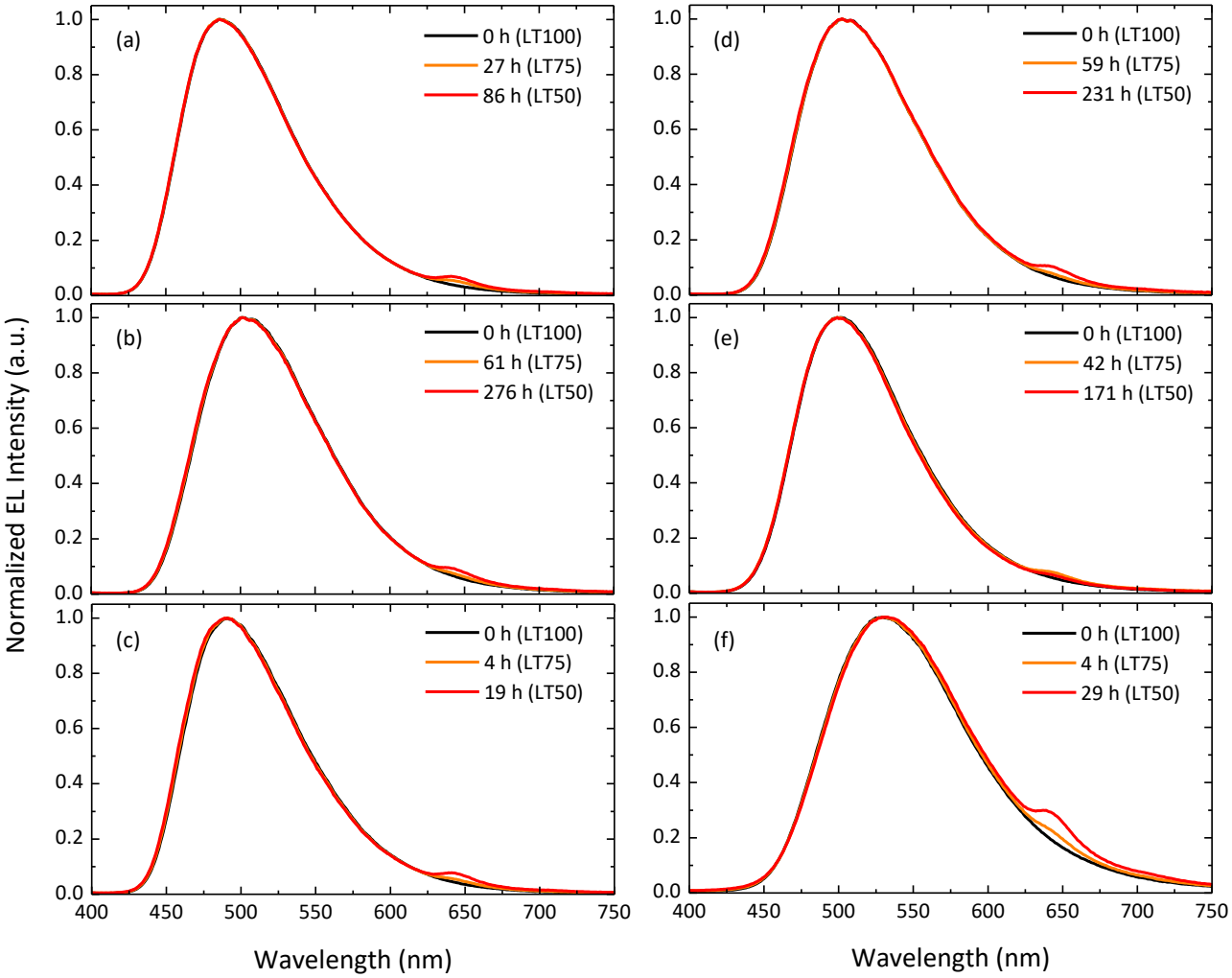

Figure 3-22 Normalized EL spectra with various driving times (a) **5CzBN**, (b) **5CF1**, (c) **5CF1γ**, (d) **5CN1**, (e) **5CF2**, (f) **5CF4**.

3-3. Conclusion

These results clearly indicate that the partially CF_3 modification of the Cz group on the TADF material improves the EQE and durability of the device. I found the replacement of only one Cz group to CF_3 modified Cz on β-position dramatically improve the device operational durability. Considering the energy drop of HOMO and LUMO levels and the increase of CIE-y value by the CF_3 modification, the replacement of only one Cz group is the best in the partially CF_3 modification strategy.

For further discussion of their photostability, I plan to try following experiments; (1) calculation of T_2 states for modified emitters, (2) the synthesis of considerable substractures and measurement of their T_1 energies.

3-4. Materials and methods

3-4-1. Measurement of photoluminescence and electrochemical properties

UV–vis absorption spectra were recorded on UV–vis spectrophotometer (Lambda 950-KPA, Perkin-Elmer, USA). Fluorescent and Phosphorescent spectra were recorded on a Photoluminescence spectrometer (FP-8600, JASCO, Japan) at r.t or 77 K. PLQY was measured under the flow of argon gas using an absolute PL quantum yield measurement system (C11347-01, Hamamatsu Photonics, Japan) with an excitation wavelength of 340 nm. Emission lifetimes were measured using a fluorescence lifetime measurement system (C11367-03 Quantaurus-Tau, Hamamatsu Photonics, Japan). The photo-degradation was measured by light irradiation using a Xe lamp (MAX-303, Asahi Spectra, Japan) with a 365 nm bandpass filter and light intensity control feedback unit. The initial irradiation light intensity was measured by a UV power meter (C9536_H9958, Hamamatsu Photonics, Japan) and the emission was continuously recorded on a multichannel analyzer (PMA-12, Hamamatsu Photonics, Japan). CV measurements were performed using an electrochemical analyzer (ALS608D, BAS, Japan) with a glassy carbon working electrode, platinum counter electrode, and Ag/Ag^+ reference electrode. Values were corrected by using ferrocene as an external standard and expressed against Fc/Fc^+. Argon-purged THF was used as a solvent with tetrabutylammonium hexafluorophosphate ($TBAPF_6$) (0.1 mmol L^{-1}) as the supporting electrolyte. The sweep rate used for the measurements was 0.05 V s^{-1}. For the CV measurements, the half potentials ($E_{1/2}$) observed in the negative potential region based on the reduction of materials were defined as LUMO level with the equation of $E_{1/2} - 4.8$ (eV). HOMO level was estimated by using the band gap from the UV absorption edge and estimated LUMO level.

3-4-2. Device fabrication and characterization of OLED performance

OLEDs were fabricated by thermal evaporation onto clean ITO-coated glass substrates. Glass substrates with a pre-patterned, 100 nm thick ITO coating were used as anodes. Hole injection

material dipyrazino[2,3-*f*:20,30-*h*]quinoxaline-2,3,6,7,10,11-hexacarbonitrile (**HAT-CN**), hole transport material 9,9',9"-triphenyl-9*H*,9'*H*,9"*H*-3,3':6',3"-tercarbazole (**TrisPCz**), electron blocking material and host 3,3-di(9*H*-carbazol-9-yl)biphenyl (***m*CBP**), hole blocking and electron transport material 2-(9,9'-spirobi[fluoren]-3-yl)-4,6-diphenyl-1,3,5-triazine (**SF3TRZ**) were used in the TADF-OLEDs (**Figure 3-23**). **HAT-CN**, **TrisPCz**, and ***m*CBP** were purchased from NARD Institute, Ltd. The **SF3TRZ** was synthesized in our laboratory. Organic layers were formed by thermal evaporation. Doped emission layers and electron transport were deposited by co-evaporation. The bilayer of 2 nm **Liq** / 100 nm Al was used as cathode. After device fabrication, devices were immediately encapsulated with glass lids using epoxy glue in a nitrogen-filled glove box (O_2 < 0.1 ppm, H_2O < 0.1 ppm). Commercial calcium oxide desiccant (Dynic Co., Japan) was included in each encapsulated package. The characteristics of the OLEDs were evaluated using a source meter (Keithley 2400, Keithley Instruments Inc., USA) and an absolute external quantum efficiency measurement system (C9920-12, Hamamatsu Photonics, Japan). The operational lifetime was measured using a luminance meter (SR-3AR, TOPCON, Japan) with the devices operated at a constant direct current.

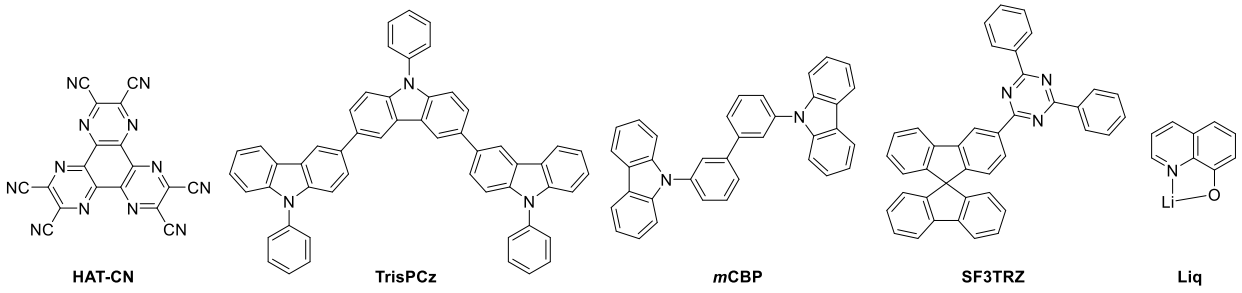

Figure 3-23 Chemical structures of perihedral materials.

3-4-3. Synthesis and characterization

2,7-bis(trifluoromethyl)carbazole and 3,6-bis(trifluoromethyl)carbazole were synthesized according to literature.[20] 2,7-dicyanocarbazole was synthesized according to literature.[21] **pre5CF2** and **pre5CF4** were synthesized according to literature.[1]

2,3,4,5,6-penta(2,7-bis(trifluoromethyl)-9*H*-carbazol-9-yl) benzonitrile (5CF5).

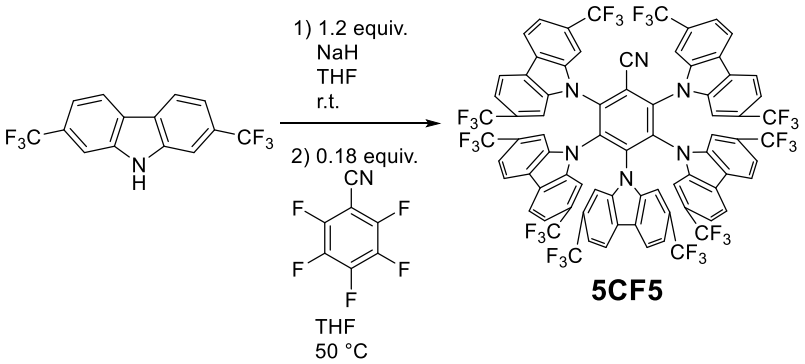

2, 7-bis(trifluoromethyl)carbazole (1.52 g, 5.00 mmol) was dissolved in dry THF (40 mL), then NaH (60wt% oil dispersion, 240 mg, 6.00 mmol) was added. The reaction mixture was stirred at room temperature for an hour. After that, pentafluorobenzonitrile (174 mg, 0.900 mmol) was added and the reaction was heated to 50 °C for 16 h. The reaction was quenched with water. The precipitate was filtered and washed with water and acetone to obtain white powder (1.41 g, 97% yield). **^{1}H NMR** (500 MHz, $CDCl_3$): δ (ppm) = 7.97 (d, 4H, 8.5 Hz), 7.64 (s, 4H), 7.56 (d, 4H, 8.0 Hz), 7.51 (d, 2H, 8.0 Hz), 7.46–7.48 (m, 4H), 7.37 (s, 2H), 7.34 (s, 4H), 7.12 (d, 4H, 8.0 Hz), 7.12 (d, 2H, 8.0 Hz). **^{19}F NMR** (400 MHz, $CDCl_3$): δ (ppm) = −61.70, −62.36, −62.46. **Elemental analysis**: Calcd. for $C_{77}H_{30}F_{30}N_6$ (%): C 57.48, H 1.88, N 5.22; Found C 57.63, H 1.87, N 5.18. **HRMS** (FAB, *m/z*): Calcd. for $C_{77}H_{30}F_{30}N_6$:1608.2053; Found 1608.2052 M^+.

2,3,4,5,6-penta(3,6-bis(trifluoromethyl)-9*H*-carbazol-9-yl) benzonitrile (5CF5γ)

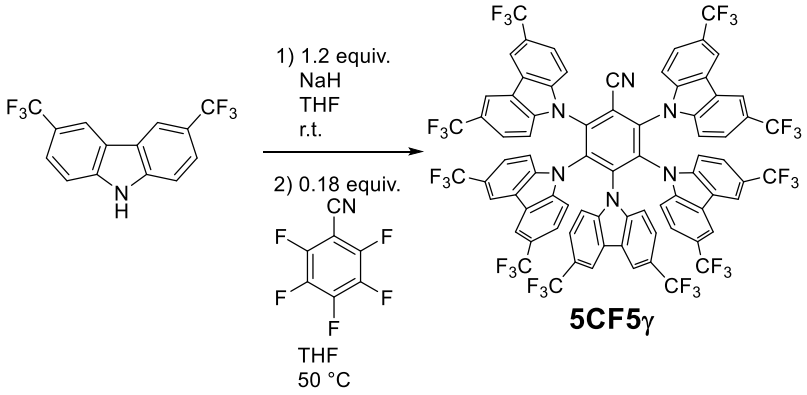

3, 6-bis(trifluoromethyl)carbazole (1.52 g, 5.00 mmol) was dissolved in dry THF (40 mL), then NaH (60wt% oil dispersion, 240 mg, 6.00 mmol) was added. The reaction mixture was stirred at room temperature for an hour. After that, pentafluorobenzonitrile (174 mg, 0.900 mmol) was added and the reaction was heated to 50 °C for 22 h. The reaction was quenched with water. The precipitate was filtered and washed with water and hexane/IPA = 1/1 (vol.) to obtain white powder (950 mg, 66% yield). **^{1}H NMR** (500 MHz, acetone-d_6): δ (ppm) = 8.53 (s, 4H), 8.11 (s, 2H + 4H), 7.97−8.01 (m, 2H + 4H), 7.80 (d, 4H, 9.0 Hz), 7.58 (d, 4H, 9.0 Hz), 7.18 (d, 2H, 9.0 Hz), 7.14 (d, 4H, 9.0 Hz). **^{19}F NMR** (400 MHz, acetone-d_6): δ (ppm) = −61.51, −61.73, −61.76. **Elemental analysis**: Calcd. for $C_{77}H_{30}F_{30}N_6$ (%): C 57.48, H 1.88, N 5.22; Found C 57.43, H 1.86, N 5.49. **HRMS** (FAB, *m/z*): Calcd. for $C_{77}H_{30}F_{30}N_6$:1608.2053; Found 1608.2049 M^+.

4-(2,7-bis(trifluoromethyl)-9*H*-carbazol-9-yl)-2,3,5,6-tetrafluorobenzonitrile (pre5CF1).

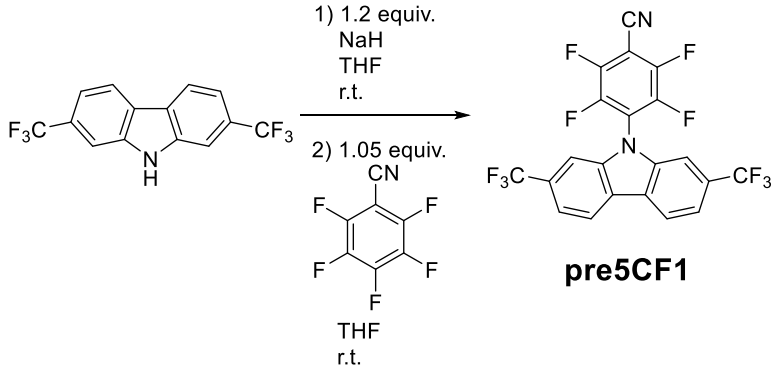

2, 7-bis(trifluoromethyl)carbazole (364 mg, 1.20 mmol) was dissolved in dry THF (5 mL), then NaH (60wt% oil dispersion, 58 mg, 1.44 mmol) was added. The reaction mixture was stirred at room temperature for an hour. After that, this mixture was added to solution of pentafluorobenzonitrile (243 mg, 1.26 mmol) in dry THF (5 mL). The reaction stirred at room temperature for 18 h. The reaction was quenched with water. The precipitate was filtered and washed with water and methanol to obtain white powder (303 mg, 59% yield). **^{1}H NMR** (500 MHz, $CDCl_3$): δ (ppm) = 8.31 (d, 2H, 8.5 Hz), 7.71 (d, 2H, 8.5 Hz), 7.42 (s, 2H). **^{19}F NMR** (500 MHz, $CDCl_3$): δ (ppm) = −61.55, −129.07, −129.09. **Elemental analysis**: Calcd. for $C_{21}H_6F_{10}N_2$ (%): C 52.96, H 1.27, N 5.88; Found C 52.73, H 1.26, N 5.68. **HRMS** (FAB, *m/z*): Calcd. for $C_{21}H_6F_{10}N_2$ 476.0371; Found 476.0410 M^+.

4-(2,7-bis(trifluoromethyl)-9H-carbazol-9-yl)-2,3,5,6-tetra(9*H*-carbazol-9-yl)benzonitrile (5CF1).

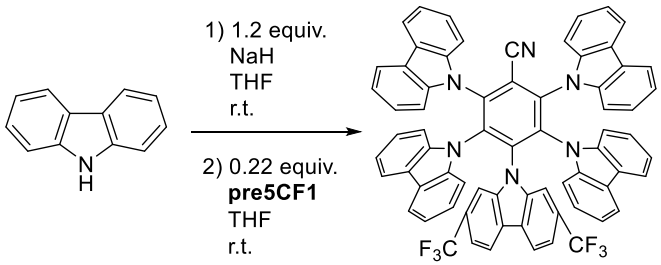

5CF1

Carbazole (447 mg, 2.67 mmol) was dissolved in dry THF (7.5 mL), then NaH (60wt% oil dispersion, 128 mg, 3.20 mmol) was added. The reaction mixture was stirred at room temperature for an hour. After that, **pre5CF1** (280 mg, 0.59 mmol) was added. The reaction stirred at room temperature for 14 h. The reaction was quenched with water. The precipitate was filtered and washed with water and methanol to obtain light yellow powder (393 mg, 63% yield). **^{1}H NMR** (500 MHz, $CDCl_3$): δ (ppm) = 7.73 (d, 4H, 8.0 Hz), 7.45−7.47 (m, 2H + 2H), 7.31 (d, 4H, 8.0 Hz), 7.26−7.29 (2, 4H), 7.06−7.11 (m, 2H + 4H + 4H), 6.93 (d, 4H, 8.0 Hz), 6.78 (t, 4H, 8.0 Hz), 6.59 (t, 4H, 8.0 Hz). **^{19}F NMR** (400 MHz, $CDCl_3$): δ (ppm) = −61.25. **Elemental analysis**: Calcd. for $C_{69}H_{38}F_6N_6$ (%): C

77.81, H 3.60, N 7.89; Found C 77.76, H 3.55, N 7.91. **HRMS** (FAB, *m/z*): Calcd. for $C_{69}H_{38}F_6N_6$ 1064.3062; Found 1064.3084 $[M]^+$.

3,5-bis(2,7-bis(trifluoromethyl)-9*H*-carbazol-9-yl)-2,4,6-tri(9*H*-carbazol-9-yl)benzonitrile (5CF2).

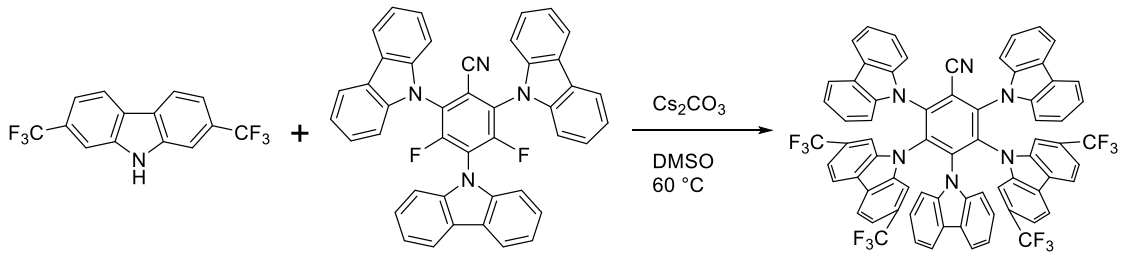

pre5CF2 **5CF2**

2, 7-bis(trifluoromethyl)carbazole (239 mg, 0.79 mmol), **pre5CF2** (200 mg, 0.32 mmol) and cesium carbonate (308 mg, 0.95 mmol) were dissolved in dry DMSO (7 mL). The reaction mixture was stirred at 60 °C for 22 h. The reaction was quenched with water. The precipitate was filtered and washed with water and methanol to obtain yellow powder (137 mg, 36% yield). **^{1}H NMR** (500 MHz, $CDCl_3$): δ (ppm) = 7.75 (d, 4H, 8.0 Hz), 7.51 (d, 4H, 8.0 Hz), 7.38 (s, 4H), 7.25−7.32 (m, 2H + 4H), 7.07−7.14 (m, 4H + 4H + 4H), 6.93 (d, 2H, 8.0 Hz), 6.75 (t, 2H, 8.0 Hz), 6.56 (t, 2H, 8.0 Hz). **^{19}F NMR** (400 MHz, $CDCl_3$): δ (ppm) = −61.25. **Elemental analysis**: Calcd. for $C_{71}H_{36}F_{12}N_6$ (%): C 71.00, H 3.02, N 7.00; Found C 71.00, H 2.95, N 7.01. **HRMS** (FAB, *m/z*): Calcd. for $C_{71}H_{36}F_{12}N_6$ 1200.2810; Found 1200.2820 M^+.

2,3,5,6-tetra(2,7-bis(trifluoromethyl)-9*H*-carbazol-9-yl)-4-(9*H*-carbazol-9-yl)benzonitrile (5CF4).

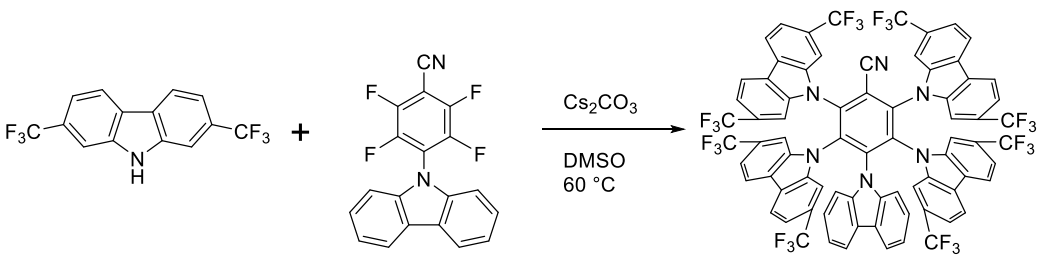

pre5CF4 **5CF4**

2, 7-bis(trifluoromethyl)carbazole (455 mg, 1.5 mmol), **pre5CF4** (112 mg, 0.33 mmol) and cesium carbonate (586 mg, 1.8 mmol) were dissolved in dry DMSO (10 mL). The reaction mixture was stirred at 60 °C for 19 h. The reaction was quenched with water. The precipitate was filtered and washed with water and methanol to obtain orange powder (268 mg, 55% yield). **^{1}H NMR** (500 MHz, $CDCl_3$): δ (ppm) = 7.98 (d, 4H, 8.0 Hz), 7.64 (s, 4H), 7.56 (d, 4H, 8.0 Hz), 7.48 (d, 4H, 8.0 Hz), 7.37 (s, 4H), 7.29 (d, 2H, 8.0 Hz), 7.17 (d, 4H, 8.0 Hz), 6.91 (d, 2H, 8.0 Hz), 6.77 (t, 2H, 8.0 Hz), 6.51 (t, 2H, 8.0 Hz). **^{19}F NMR** (500 MHz, $CDCl_3$): δ (ppm) = −61.75. **Elemental analysis**: Calcd. for $C_{75}H_{32}F_{24}N_6$ (%): C 61.15, H 2.19, N 5.71; Found C 60.99, H 2.08, N 5.84. **HRMS** (FAB, *m/z*): Calcd. for $C_{75}H_{32}F_{24}N_6$ 1472.2305; Found 1472.2319 M^+.

4-(3,6-bis(trifluoromethyl)-9*H*-carbazol-9-yl)-2,3,5,6-tetrafluorobenzonitrile (pre5CF1γ).

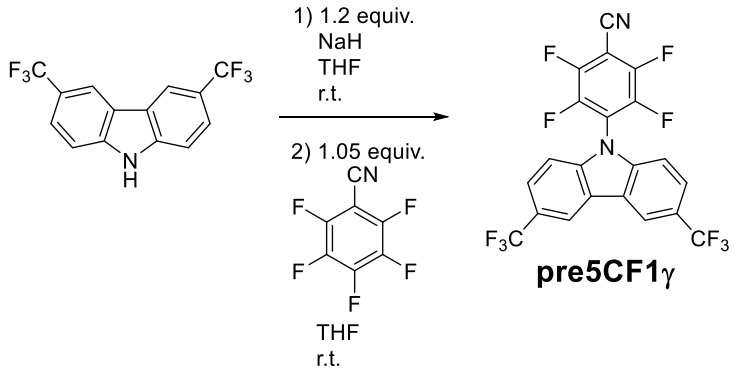

3, 6-bis(trifluoromethyl)carbazole (364 mg, 1.20 mmol) was dissolved in dry THF (5 mL), then NaH (60wt% oil dispersion, 58 mg, 1.44 mmol) was added. The reaction mixture was stirred at room temperature for an hour. After that, this mixture was added to solution of pentafluorobenzonitrile (243 mg, 1.26 mmol) in dry THF (5 mL). The reaction stirred at room temperature for 23 h. The reaction was quenched with water. The precipitate was filtered and washed with water and methanol to obtain white powder (160 mg, 28% yield). **^{1}H NMR** (500 MHz, DMSO-d_6): δ (ppm) = 9.04 (s, 2H), 7.95 (d, 2H, 8.5 Hz), 7.76 (d, 2H, 8.5 Hz). **^{19}F NMR** (400 MHz, DMSO-d_6): δ (ppm) = −60.97, −129.16, −138.35. **Elemental analysis**: Calcd. for $C_{21}H_6F_{10}N_2$ (%): C 52.96,

H 1.27, N 5.88; Found C 52.94, H 1.26, N 5.43. **HRMS** (FAB, *m/z*): Calcd. for $C_{21}H_6F_{10}N_2$ 476.0371; Found 476.0415 M^+.

4-(3,6-bis(trifluoromethyl)-9*H*-carbazol-9-yl)-2,3,5,6-tetra(9*H*-carbazol-9-yl)benzonitrile (5CF1γ).

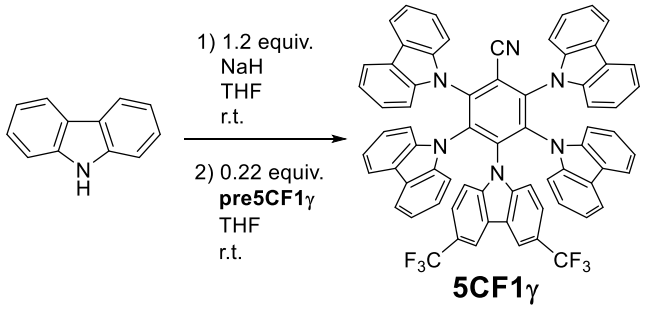

Carbazole (239 mg, 1.43 mmol) was dissolved in dry THF (5.0 mL), then NaH (60wt% oil dispersion, 69 mg, 1.73 mmol) was added. The reaction mixture was stirred at room temperature for an hour. After that, **pre5CF1γ** (150 mg, 0.32 mmol) was added. The reaction stirred at room temperature for 16 h. The reaction was quenched with water. The precipitate was filtered and washed with water and chloroform to obtain light yellow powder (260 mg, 86% yield). **^{1}H NMR** (500 MHz, acetone-d_6): δ (ppm) = 7.94 (s, 2H), 7.84−7.87 (m, 2H + 4H), 7.77 (d, 4H, 8.0 Hz), 7.62 (d, 4H, 8.0 Hz), 7.39 (d, 4H, 8.0 Hz), 7.08−7.16 (m, 8H), 6.94 (d, 2H, 8.0 Hz), 6.78 (t, 4H, 8.0 Hz), 6.68 (t, 4H, 8.0 Hz). **^{19}F NMR** (400 MHz, acetone-d_6): δ (ppm) = −61.30. **Elemental analysis**: Calcd. for $C_{69}H_{38}F_6N_6$ (%): C 77.81, H 3.60, N 7.89; Found C 77.84, H 3.54, N 7.89. **HRMS** (FAB, *m/z*): Calcd. for $C_{69}H_{38}F_6N_6$ 1064.3062; Found 1064.3077 M^+.

4-(2,7-dicyano-9*H*-carbazol-9-yl)-2,3,5,6-tetra(9*H*-carbazol-9-yl)benzonitrile (5CN1).

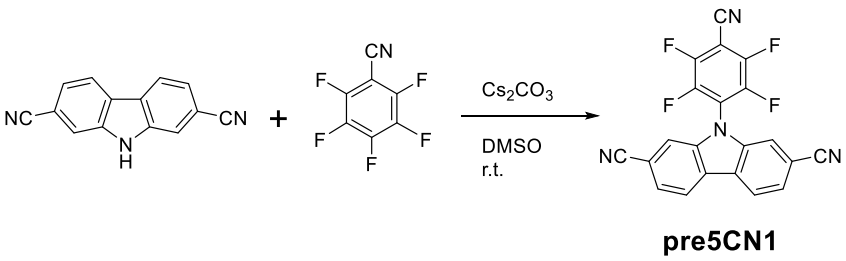

2, 7-dicyanocarbazole (108 mg, 0.5 mmol), pentafluorobenzonitrile (193 mg, 1.0 mmol) and cesium carbonate (196 mg, 0.60 mmol) were dissolved in dry DMSO (7 mL). The reaction mixture was stirred at room temperature for 3 h. The reaction was quenched with water. The precipitate was filtered and washed with water and methanol to obtain **pre5CN1** (190 mg, 97% crude yield). The crude product was used to the next reaction without further purification.

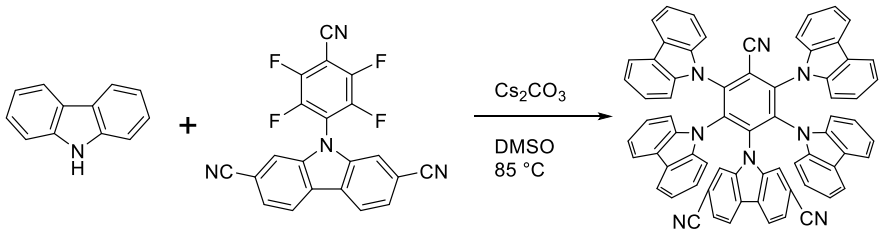

pre5CN1 **5CN1**

Carbazole (167 mg, 1.0 mmol), **pre5CN1** (78 mg, 0.20 mmol) and cesium carbonate (391 mg, 1.2 mmol) were dissolved in dry DMSO (3 mL). The reaction mixture was stirred at 85 °C for 4 h. The reaction was quenched with water. The precipitate was filtered and washed with water and chloroform to obtain yellow powder (58 mg, 30% yield). **^{1}H NMR** (500 MHz, DMSO-d_6): δ (ppm) = 8.23 (s, 2H), 7.92 (d, 4H, 8.5 Hz), 8.87 (d, 4H, 8.5 Hz), 7.75 (d, 4H, 8.5 Hz), 7.66 (d, 2H, 8.5 Hz), 7.43 (d, 2H, 8.5 Hz), 7.25 (t, 4H, 8.5 Hz), 7.11−7.18 (m, 2H + 4H). **^{13}C NMR** (500 MHz, DMSO-d_6): δ (ppm) = 142.2, 141.2, 139.8, 138.7, 138.5, 125.8, 125.0, 124.6, 124.3, 123.4, 122.8, 121.9, 121.4, 121.0, 120.7, 119.9, 119.0, 118.7, 117.0, 113.2, 111.9, 111.6. **Elemental analysis**: Calcd. for $C_{69}H_{38}N_8$ (%): C 84.64, H 3.91, N 11.44; Found C 84.20, H 3.95, N 11.31. **HRMS** (FAB, *m/z*): Calcd. for $C_{69}H_{38}N_8$ 978.3219; Found 978.3229 M^+.

References

(1) Noda, H.; Nakanotani, H.; Adachi, C. Excited State Engineering for Efficient Reverse Intersystem Crossing. *Sci. Adv.* **2018**, *4* (6), eaao6910.

(2) Balijapalli, U.; Tanaka, M.; Auffray, M.; Chan, C. Y.; Lee, Y. T.; Tsuchiya, Y.; Nakanotani, H.; Adachi, C. Utilization of Multi-Heterodonors in Thermally Activated Delayed Fluorescence Molecules and Their High Performance Bluish-Green Organic Light-Emitting Diodes. *ACS Appl. Mater. Interfaces* **2020**, *12* (8), 9498–9506.

(3) Yokoyama, M.; Inada, K.; Tsuchiya, Y.; Nakanotani, H.; Adachi, C. Trifluoromethane Modification of Thermally Activated Delayed Fluorescence Molecules for High-Efficiency Blue Organic Light-Emitting Diodes. *Chem. Commun.* **2018**, *54* (59), 8261–8264.

(4) Scerba, M. T.; Bloom, S.; Haselton, N.; Siegler, M.; Jaffe, J.; Lectka, T. Interaction of a C-F Bond with the π-System of a C=C Bond or "Head on" with a Proximate C-H Bond. *J. Org. Chem.* **2012**, *77* (3), 1605–1609.

(5) Nakanotani, H.; Masui, K.; Nishide, J.; Shibata, T.; Adachi, C. Promising Operational Stability of High-Efficiency Organic Light-Emitting Diodes Based on Thermally Activated Delayed Fluorescence. *Sci. Rep.* **2013**, *3*, 2127.

(6) Zheng, Q.; Lavis, L. D. Development of Photostable Fluorophores for Molecular Imaging. *Curr. Opin. Chem. Biol.* **2017**, *39* (1), 32–38.

(7) Lee, J.; Jeong, C.; Batagoda, T.; Coburn, C.; Thompson, M. E.; Forrest, S. R. Hot Excited State Management for Long-Lived Blue Phosphorescent Organic Light-Emitting Diodes. *Nat. Commun.* **2017**, *8*, 15566.

(8) Jacquemin, D.; Escudero, D. The Short Device Lifetimes of Blue PhOLEDs: Insights into the Photostability of Blue Ir(III) Complexes. *Chem. Sci.* **2017**, *8* (11), 7844–7850.

(9) Zhao, C.; Duan, L. Review on Photo- And Electrical Aging Mechanisms for Neutral Excitons and Ions in Organic Light-Emitting Diodes. *J. Mater. Chem. C* **2020**, *8* (3), 803–820.

(10) Zhang, D.; Cai, M.; Zhang, Y.; Zhang, D.; Duan, L. Sterically Shielded Blue Thermally Activated Delayed Fluorescence Emitters with Improved Efficiency and Stability. *Mater. Horizons* **2016**, *3* (2), 145–151.

(11) Noda, H.; Chen, X. K.; Nakanotani, H.; Hosokai, T.; Miyajima, M.; Notsuka, N.; Kashima, Y.; Brédas, J. L.; Adachi, C. Critical Role of Intermediate Electronic States for Spin-Flip Processes in Charge-Transfer-Type Organic Molecules with Multiple Donors and Acceptors. *Nat. Mater.* **2019**, *18* (10), 1084–1090.

(12) Zewail, A. H. Femtochemistry: Atomic-Scale Dynamics of the Chemical Bond Using Ultrafast Lasers (Nobel Lecture). *Angew. Chemie Int. Ed.* **2000**, *39* (15), 2586–2631.

(13) Scholz, S.; Kondakov, D.; Lüssem, B.; Leo, K. Degradation Mechanisms and Reactions in Organic Light-Emitting Devices. *Chem. Rev.* **2015**, *115* (16), 8449–8503.

(14) Sandanayaka, A. S. D.; Matsushima, T.; Adachi, C. Degradation Mechanisms of Organic Light-Emitting Diodes Based on Thermally Activated Delayed Fluorescence Molecules. *J. Phys. Chem. C* **2015**, *119* (42), 23845–23851.

(15) Schmidbauer, S.; Hohenleutner, A.; König, B. Chemical Degradation in Organic Light-Emitting Devices: Mechanisms and Implications for the Design of New Materials. *Adv. Mater.* **2013**, *25* (15), 2114–2129.

(16) Wang, R.; Wang, Y. L.; Lin, N.; Zhang, R.; Duan, L.; Qiao, J. Effects of Ortho-Linkages on the Molecular Stability of Organic Light-Emitting Diode Materials. *Chem. Mater.* **2018**, *30* (24), 8771–8781.

(17) Oh, C. S.; Choi, J. M.; Lee, J. Y. Chemical Bond Stabilization and Exciton Management by CN Modified Host Material for Improved Efficiency and Lifetime in Blue Phosphorescent Organic Light-Emitting Diodes. *Adv. Opt. Mater.* **2016**, *4* (8), 1281–1287.

(18) Song, W.; Lee, J. Y. Degradation Mechanism and Lifetime Improvement Strategy for Blue Phosphorescent Organic Light-Emitting Diodes. *Adv. Opt. Mater.* **2017**, *5* (9), 1600901.

(19) Tanaka, M.; Noda, H.; Nakanotani, H.; Adachi, C. Effect of Carrier Balance on Device Degradation of Organic Light-Emitting Diodes Based on Thermally Activated Delayed Fluorescence Emitters. *Adv. Electron. Mater.* **2019**, *5* (5), 1800708.

(20) Gantenbein, M.; Hellstern, M.; Le Pleux, L.; Neuburger, M.; Mayor, M. New 4,4'-Bis(9-Carbazolyl)-Biphenyl Derivatives with Locked Carbazole-Biphenyl Junctions: High-Triplet State Energy Materials. *Chem. Mater.* **2015**, *27* (5), 1772–1779.

(21) Song, M.; Park, J. S.; Yoon, K. J.; Kim, C. H.; Im, M. J.; Kim, J. S.; Gal, Y. S.; Lee, J. W.; Lee, J. H.; Jin, S. H. Synthesis and Characterization of Poly(N-Alkyloxyarylcarbazolyl-2,7-Vinylene) Derivatives and Their Applications in Bulk-Heterojunction Solar Cells. *Org. Electron.* **2010**, *11* (6), 969–978.

Chapter 4

Blue thermally-activated delayed fluorescence materials partially modified with trifluoromethyl groups

Yokoyama, M.; Tsuchiya, Y.; Nakanotani, H.; Adachi, C.

manuscript under preparation

Abstract

The partial modification strategy of a CF_3 unit was applied to a deep-blue TADF emitter, **4CzBN**. The partially CF_3 modified emitter (**4CF1**) showed blue emission with a higher PLQY and photostability compared with those of **4CzBN**. The EQE and LT_{50} of OLEDs using these emitters were 5.9% and 3 h for **4CzBN**, and 11.7% and 33 h for **4CF1**. As a result, I succeeded in the enhancement of the EL efficiency and the device operational lifetime of the blue TADF-OLED with the partial modification strategy using the carbazole having CF_3 groups on its β-position.

4-1. Introduction

In **Chapter 3**, I demonstrate the partial CF_3 modification of **5CzBN** enhances the luminescence efficiency and device durability, while it also induced the slightly red-shifted emission; the colors were region in blue-green to green.

In this chapter, I applied the partial CF_3 modification strategy to **4CzBN** scaffold. **4CzBN** is a deep-blue TADF material with a shorter emission wavelength than that of **5CzBN**.[1] Partially CF_3 modification of **4CzBN** is expected to produce blue luminescence with high efficiency and durability. The molecular structures proposed and synthesized in this chapter are shown in **Figure 4-1**.

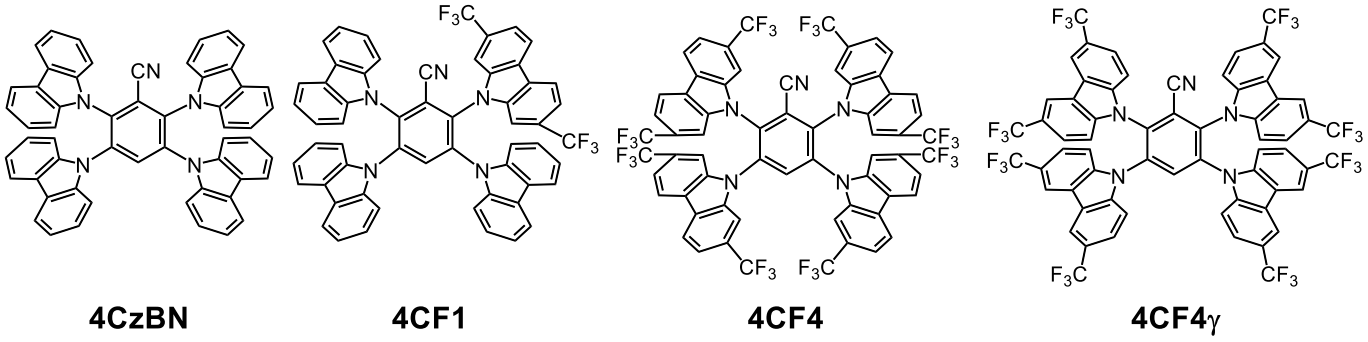

Figure 4-1 Schematic chemical structures of 4CzBN based emitters.

4-2. Results and discussion

4-2-1. DFT calculations

DFT calculations of **4CzBN** derivatives were performed to determine the number and modification positions of the CF_3 groups. HOMO-LUMO levels and S_1 / T_1 energies were calculated using the Gaussian 16 program package. The S_0 geometry was optimized at the B3LYP/6-31G(d) level of theory, and the S_1 and T_1 were calculated with time-dependent density functional theory (TD-DFT) and B3LYP/6-31+G(d) methods using the optimized S_0 geometry. The 4CzBN derivatives with different numbers and positions of CF_3 modified Cz groups showed a similar trend with 5CzBN derivatives as mentioned in **Chapter 3** (**Table 4-1**). S_1 energies were increased for the fully modified emitters (**4CF4** and **4CF4γ**) and decreased for the partially modified ones (**4CF1**, **4CF1'**, and **4CF2**)

compared with that of the naked **4CzBN**. Therefore, the former would emit in deep blue and the latter would emit in blue. Because the replacement of only one Cz group to the CF_3 modified Cz group dramatically improved the photo-stability and device durability in the 5CzBN based material, I chose **4CF1** as a partially CF_3 modified **4CzBN**. This should provide the discreet HOMO drop and red-shift of emission. In addition, I could not find the large difference in the estimated energy levels between **4CF1** and its regioisomer **4CF1'**. As for the distribution of HOMO and LUMO, in both materials, HOMOs were distributed on unmodified Cz units and LUMOs were distributed on benzonitrile (**Figure 4-2**). Both compounds were thought to exhibit similar optical properties from DFT calculation. Then, the BDE of C−N bonds for each compound were calculated (**Table 4-2**). Both compounds showed improved BDE compared with **4CzBN**, but the weakest BDE value of **4CF1** (3.57 eV, bond No. 3) was slightly higher than that of **4CF1'** (3.56 eV, bond No. 4). Here, only **4CzBN** and **4CF1** were synthesized, **4CF1'** and **4CF2** were not synthesized. To investigate the effect of the CF_3 modification position on the Cz group, **4CF4** and **4CF4γ** were also synthesized.

Table 4-1 DFT calculations of 4CzBN derivatives (B3LYP/6-31+G(d)) using Gaussian 16, Rev. A.03.

Emitter	HOMO (eV)	LUMO (eV)	E_g (eV)	S_1 (eV)	T_1 (eV)	ΔE_{ST} (eV)	f
4CzBN	−5.61	−2.08	3.54	2.89	2.69	0.21	0.081
4CF1	−5.74	−2.33	3.42	2.79	2.63	0.16	0.067
4CF1'	−5.67	−2.23	3.44	2.79	2.64	0.15	0.074
4CF2	−5.86	−2.44	3.42	2.78	2.64	0.16	0.006
4CF4	−6.41	−2.83	3.58	2.93	2.77	0.16	0.065
4CF4γ	−6.73	−3.10	3.63	2.99	2.77	0.22	0.088

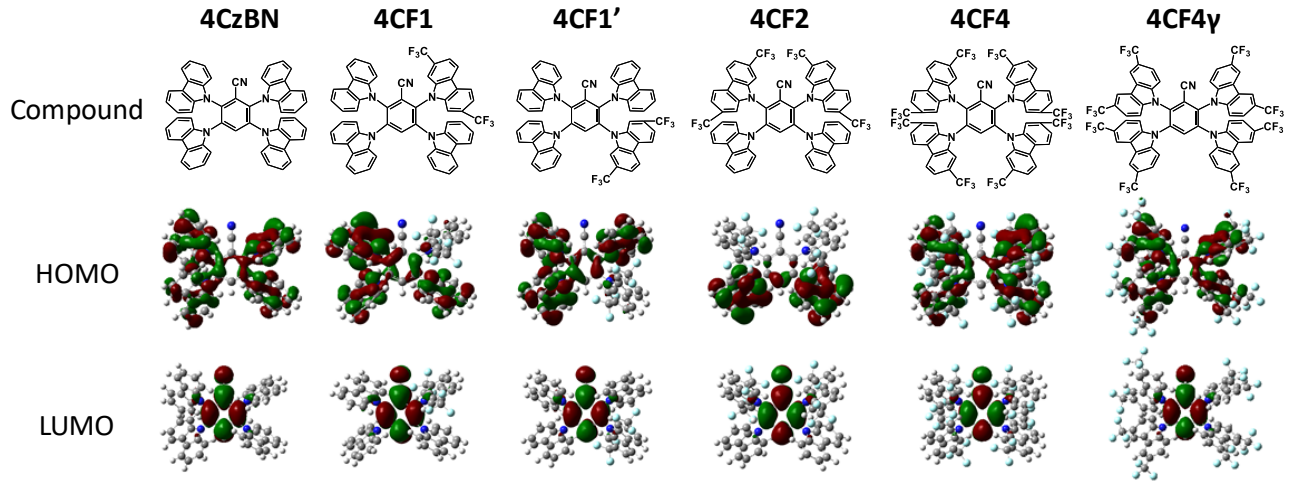

Figure 4-2 HOMO and LUMO distributions for 4CzBN derivatives (B3LYP/6-31+G(d)) using Gaussian 16, Rev. A.03.

Table 4-2 BDE calcurations of C−N bond for 4CzBN derivatives (UB3LYP/6-31G(d)) using Gaussian 16, Rev. A.03.

C−N bond No.	BDE (eV)		
	4CzBN	**4CF1**	**4CF1'**
1	3.54	3.60	3.56
2	3.59	3.60	3.63
3	-	3.60	3.60
4	-	3.57	3.56

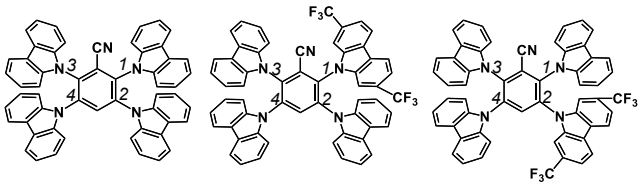

4-2-2. Photophysical properties

In the case of the 4CzBN derivatives, the effects of fully and partially CF_3 modification in their HOMO-LUMO levels, S_1/T_1 energies, and spectra were similar to those of the 5CzBN derivatives. HOMO and LUMO levels of **4CzBN**, **4CF1**, **4CF4**, and **4CF4γ** measured by CV are summarized in **Figure 4-3**. HOMO and LUMO levels decreased as the number of CF_3-modified Cz increased.

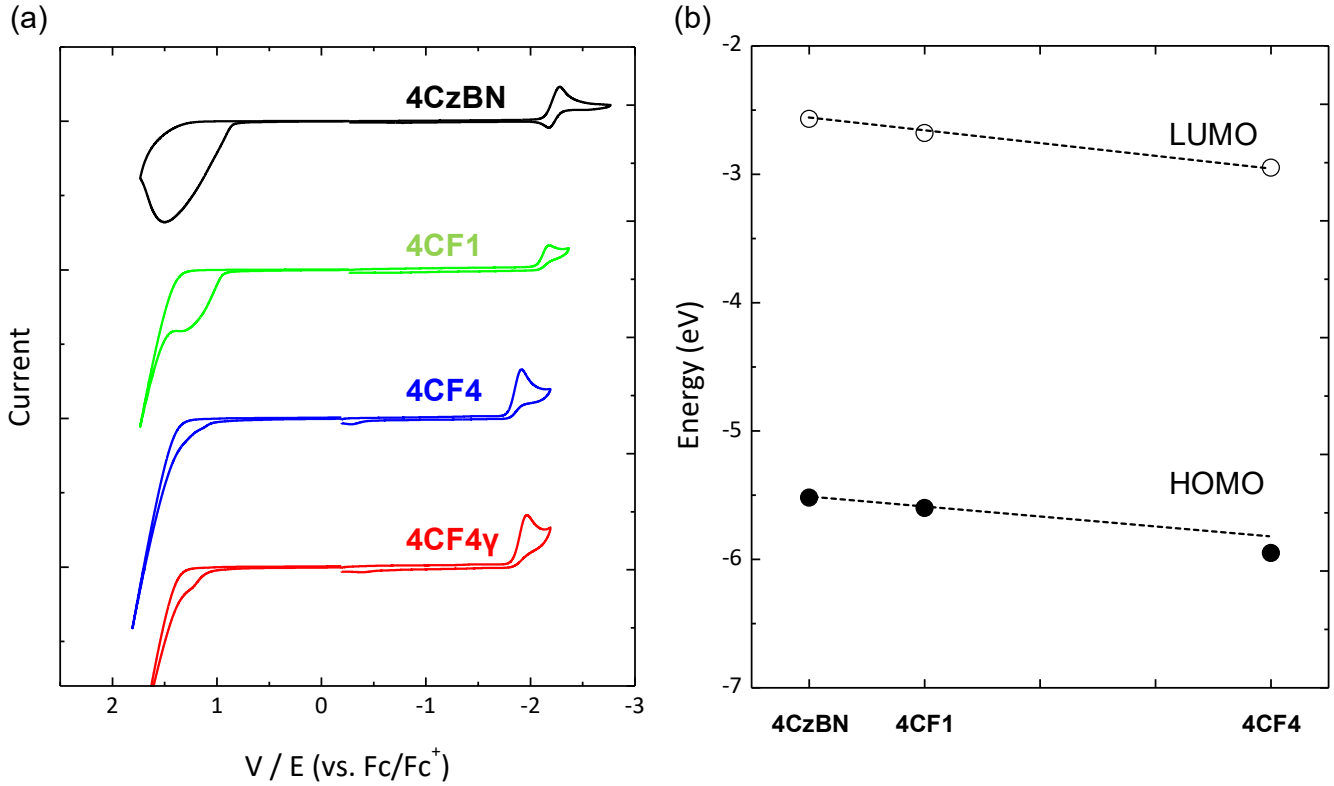

Figure 4-3 (a) Cyclic voltamogram for **4CzBN**, **4CF1**, **4CF4**, and **4CF4γ**, (b) HOMO and LUMO energy diagram of 4CzBN derivatives.

The absorption, fluorescence, and phosphorescence spectra of **4CzBN**, **4CF1**, **4CF4**, and **4CF4γ** in toluene (1.0×10^{-5} mol L^{-1}) were also shown in **Figure 4-4**. Fully modified **4CF4** and **4CF4γ** showed blue-shifted emission compared with that of **4CzBN**. The emission of partially modified **4CF1** was shifted to a longer wavelength than that of **4CzBN**, but it was still in the blue region (λ_{em} = 456 nm) (**Table 4-3**). A similar relationship was observed in the **PPT** doped film. **4CF1** showed a higher PLQY both in the solution (56%) and film states (90%) compared to those of **4CzBN** (the values were 48% and 70%, respectively), due to the increasing of k_r.

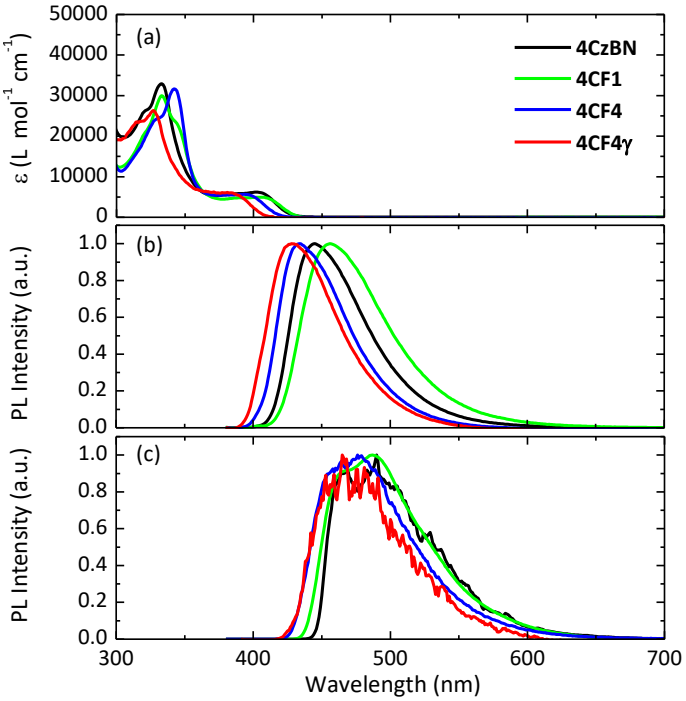

Figure 4-4 Photophysical properties of 1.0×10^{-5} mol L^{-1} toluene solution for **4CzBN**, **4CF1**, **4CF4**, and **4CF4γ** (a) UV–vis absorption, (b) Fluorescent spectra, (c) Phosphorescent spectra.

Table 4-3 Photophysical properties of **4CzBN** derivatives.

	Emitter	λ_{em} [a] (nm)	FWHM (nm)	PLQY [b] (%)	S_1 [c] (eV)	T_1 [c] (eV)	ΔE_{ST} (eV)	τ_p (ns)	τ_d [b] (μs)	k_{rs} (10^7 s^{-1})	k_{ISC} (10^8 s^{-1})	k_{RISC} (10^6 s^{-1})	k_{nrT} (10^4 s^{-1})
Solution (toluene)	**4CzBN**	445	61	48 (10)	3.00	2.78	0.22	1.5	43 (0.3)	0.1	6.6	1.0	0.2
	4CF1	456	70	56 (15)	2.97	2.83	0.14	3.2	37 (0.2)	0.4	3.1	1.1	0.1
	4CF4	434	57	36 (8)	3.08	2.89	0.19	1.1	16 (0.5)	0.1	8.9	1.4	0.4
	4CF4γ	428	60	16 (12)	3.14	2.89	0.25	2.4	17 (0.4)	0.2	4.2	0.4	0.4
Film 5 w% **PPT**	**4CzBN**	462	64	70	2.97	2.80	0.17	2.6	26	0.9	3.8	1.5	4.0
	4CF1	467	81	90	2.95	2.82	0.13	2.5	25	0.8	3.1	1.2	0.9
	4CF4	440	67	64	3.12	2.91	0.21	1.4	35	0.1	7.1	1.9	1.3
	4CF4γ	421	64	14	3.14	2.93	0.21	2.6	7.5	0.1	3.7	1.2	11
20 wt% ***m*CBP**	**4CzBN**	467	104	65	2.94	2.75	0.19	3.6	13	0.9	2.7	1.2	4.1
	4CF1	474	79	90	2.89	2.74	0.15	3.7	17	2.0	2.5	0.7	0.3

[a] Peak maximum value; [b] under Ar-saturated condition, before deoxygenation values were in parenthesis; [c] estimated from emission onset at fluorescent or phosphorescent spectra.

The photostability of **4CF1** and **4CF4** improved compared to **4CzBN**, while **4CF4γ** worsened. As well as the 5CzBN platform, the photostability of **4CzBN** was enhanced by β-modification and decreased by γ-modification.

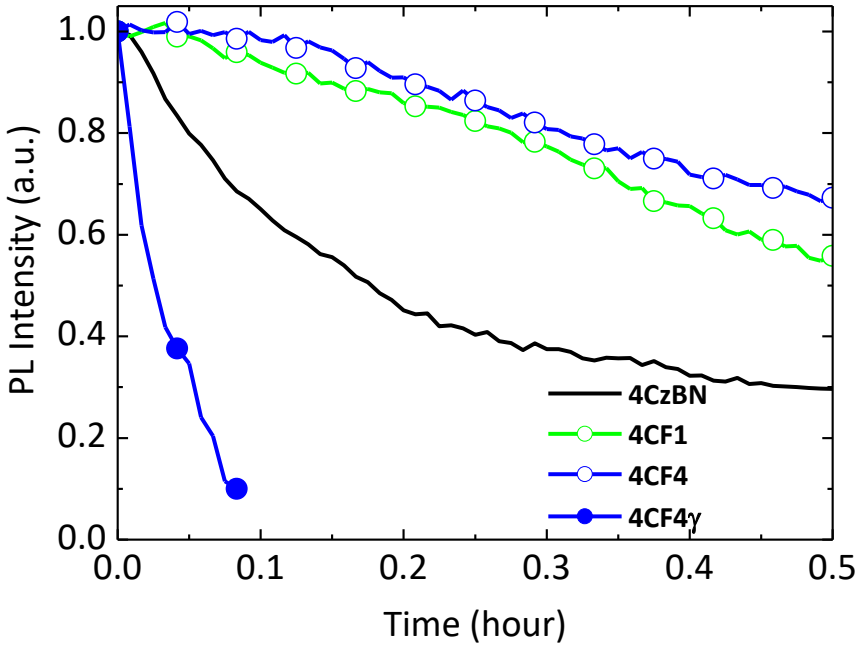

Figure 4-5 Photodegradation curves of argon gas saturated toluene solution of 4CzBN derivatives (1.0×10^{-5} mol L^{-1}) irradiated 365 nm UV light at 0.8 mW cm^{-2}.

4-2-3. OLED performance

To evaluate the OLED performances, OLEDs using **4CzBN** and **4CF1** as an emitter were fabricated. The emitters were evaluated in two different device structures (device structure (A) and (B)). Chemical structures of the organic semiconductor materials used in the devices are presented in **Section 4-4-2**. EQE-J characteristics, J-V-L characteristics, the EL spectra, and device durability of the devices are shown in **Figures 4-6**, **4-7**, and summarized in **Table 4-4**. In device structure (A), the **4CF1** based OLED showed higher EQE of 11.7% and 11 times longer LT_{50} (33 h) than that of the naked **4CzBN** (5.9%, 3 h). The partially CF_3 modification on **4CzBN** improved luminescence efficiency and the operational durability. I also investigated the device structure (B) using **PPT** as the hole blocking and electron transport materials instead of **SF3TRZ**. Higher EQE was obtained in device structure (B) (13.4%) than in device structure (A) (11.7%). This would be because the triplet energy of **SF3TRZ** (2.75 eV) used in a structure (A) was insufficient for these emitters and the excitons were deactivated. Indeed, the 20wt% **4CF1** doped **SF3TRZ** film showed a lower PLQY (28%) than that of **PPT** film (85%). In device structure (B), I obtained the unfavorable result in the

device durability because of the low stability of **PPT**. At least, I confirmed the partial CF_3 modification strategy works well also in the blue TADF material with the device structure (B). Therefore, I believe that further improvement would be obtained in the efficiency and durability by using proper hole blocking materials that possess high chemical stability and sufficiently high triplet energy than that of the TADF emitter.

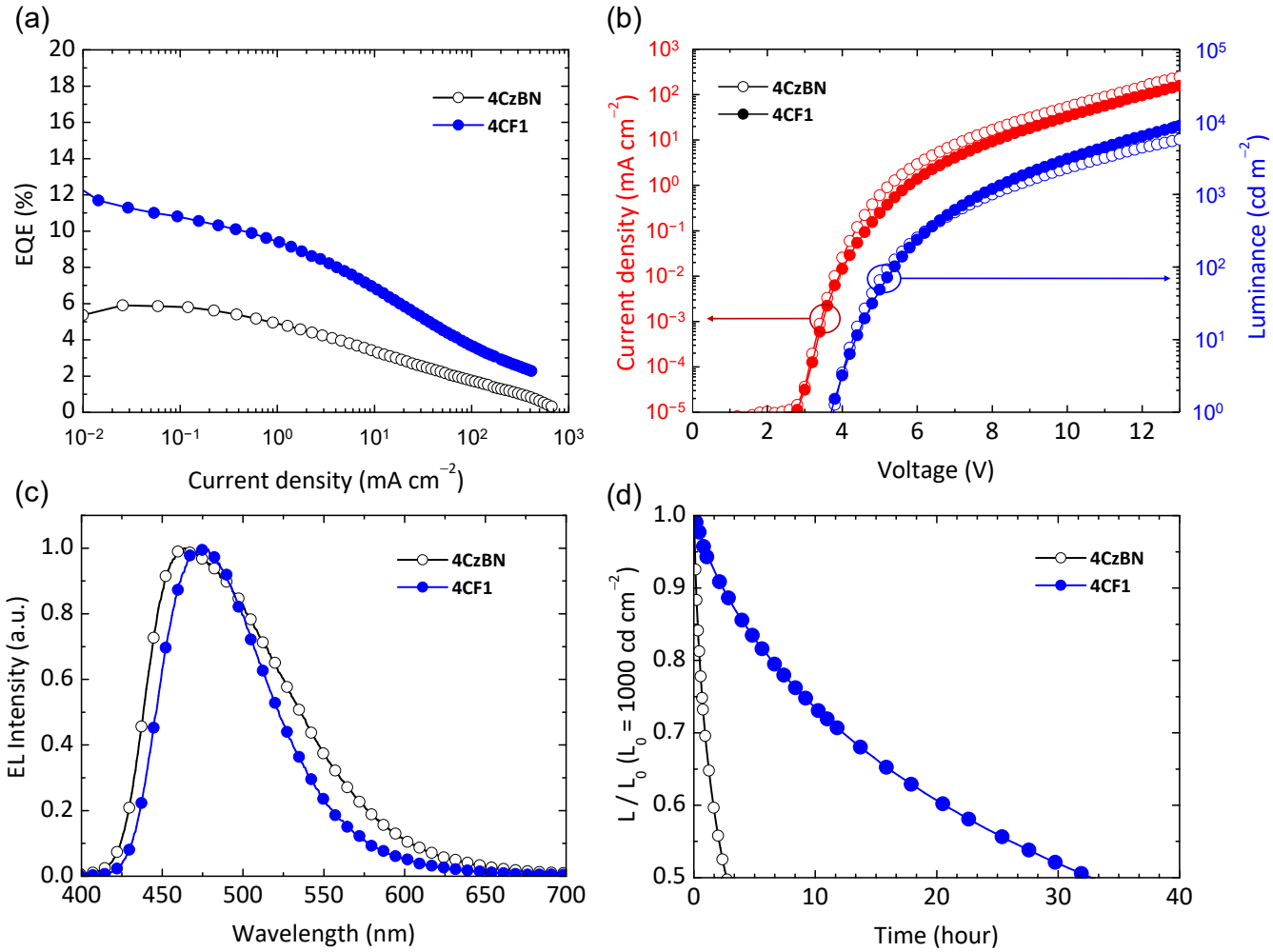

Figure 4-6 Electroluminescence characteristics of OLEDs using **4CzBN** and **4CF1** as an emitter; (a) EQE-J characteristics; (b) J-V-L characteristics; (c) EL spectra; (d) Luminance decay (at an initial luminance of 1000 cd m^{-2}). Device structure (A).

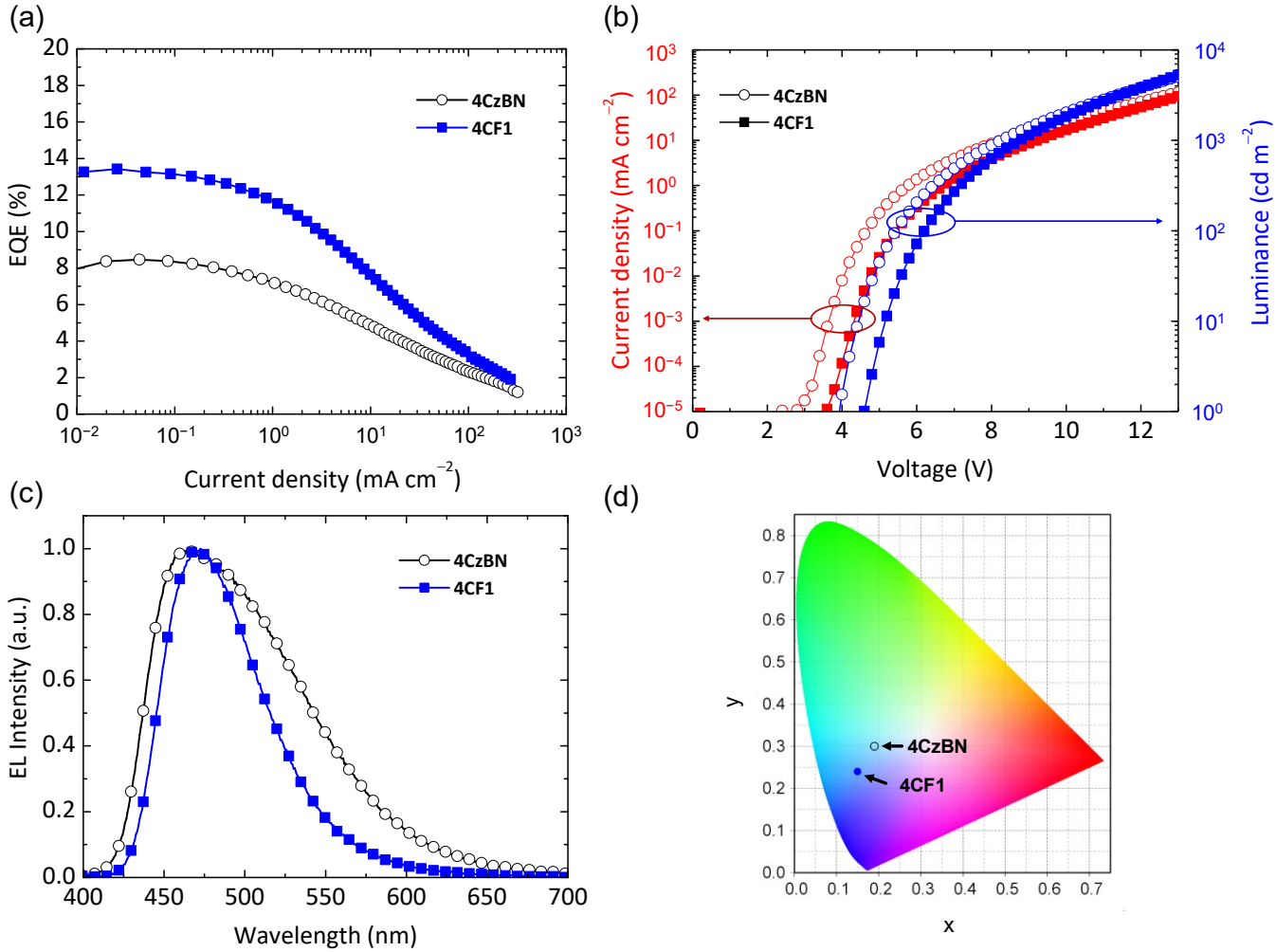

Figure 4-7 Electroluminescence characteristics of OLEDs using **4CzBN** and **4CF1** as an emitter; (a) EQE-J characteristics; (b) J-V-L characteristics; (c) EL spectra; (d) CIE diagram (CIE1931). Device structure (B).

Table 4-4 Device performance of OLEDs using 4CzBN derivatives as an emitter.

Device structure	Emitter	λ_{em} [a] (nm)	V_{on} [b] (V)	EQE [c] (%)	CIE [d]	LT_{50} [e] (hours)
(A)	**4CzBN**	464	3.8	5.9 / 5.0 / 3.0	(0.19, 0.28)	3
	4CF1	474	3.8	11.7 / 9.9 / 7.2	(0.16, 0.27)	33
(B)	**4CzBN**	466	4.0	8.5 / 7.4 / 4.8	(0.19, 0.30)	-
	4CF1	472	4.6	13.4 / 12.4 / 8.2	(0.15, 0.24)	-

[a] Peak maximum values ; [b] turn-on voltage, which reached the luminance of 1 cd m^{-2} ; [c] maximum values, obtained at 100, 1000 cd m^{-2}, respectively; [d] values at 100 cd m^{-2} ; [e] initial luminance of 1000 cd m^{-2}, device structure (A): ITO / **HAT-CN** (60 nm) / **TrisPCz** (30 nm) / ***m*CBP** (5 nm) / 20 wt% emitter: ***m*CBP** (30 nm) / **SF3TRZ** (10 nm) / 30 wt% **Liq**:**SF3TRZ** (30 nm) / **Liq** (2 nm) / Al (100 nm, (B): ITO / **HAT-CN** (60 nm) / **TrisPCz** (30 nm) / ***m*CBP** (5 nm) / 20 wt% emitter: ***m*CBP** (30 nm) / **PPT** (10 nm) / 30 wt% **Liq**:**PPT** (20 nm) / **Liq** (2 nm) / Al (100 nm).

4-2-4. Discussion

Partial CF_3 modification of **4CzBN** improved its device stability as same as **5CzBN**. Introduction of CF_3 groups did not affect the electrochemical stability of the emitters (**Figure 4-3**), and modification at β-position enhanced its photostability as expected (**Figure 4-5**). However, the effect of CF_3 modification on the triplet energies and delayed fluorescence lifetime was different from those of **5CzBN**. In the case of **5CzBN**, the delayed fluorescence lifetime was shortened by partial CF_3 modification and did not change so much by the full modification (**Table 3-2**). On the other hand, in the case of **4CzBN**, the delayed fluorescence lifetime was almost no change by the partial modification and shortened by the full modification (**Table 4-3**). To understand the RISC process of 4CzBN derivatives, $^1CT_1$, $^3CT_1$, and ^3LE energies were shown in **Figure 4-8**. For **4CF1**, **4CF4**, and **4CF4γ**, ^3LE energy of these emitters exists between $^1CT_1$ and $^3CT_1$. Then, ^3LE seems to assist the spin-flip from $^3CT_1$ to $^1CT_1$. However, in the case of **4CF1**, ^3LE of **PhβCF** does not appear to be involved in RISC, while the delayed fluorescence lifetime and k_{RISC} of **4CF1** were nearly equivalent to those of **4CzBN**. Triplet intermediate states other than ^3LE of **PhβCF** may be involved in the RISC process in **4CF1**. For further discussion about the photostability and RISC process, I would like to do additional experiments in my future study; (1) temperature dependence of delayed fluorescence and PLQY to determine activation energies of RISC and ISC, (2) calculation of the electronic state of emitters in excited states.

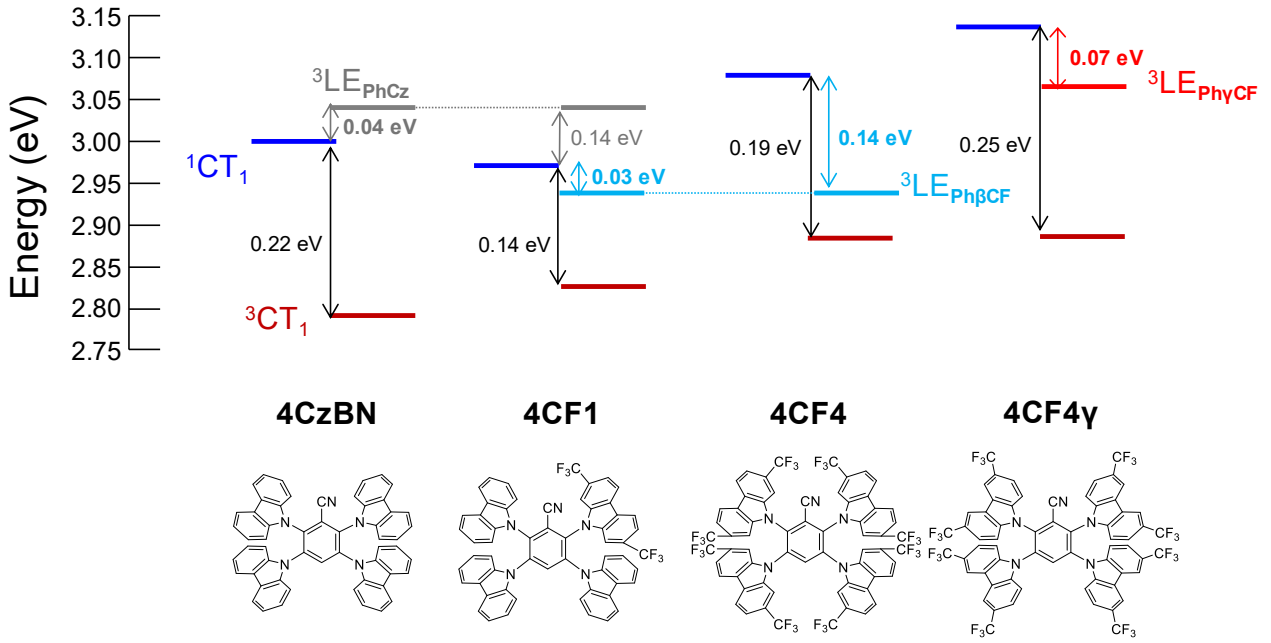

Figure 4-8 Schematic illustration of the intermediate state for RISC process for 4CzBN derivatives.

In order to confirm the effect of the carrier balance on the device stability, the EL spectrum change during operation should be checked as mentioned in **Chapter 3**. Partially modified **4CF1** showed the weak emission originated from the hole-block materials in the region from 630 nm to 680 nm, indicating the shift of recombination site during continuous operation (**Figure 4-9**).

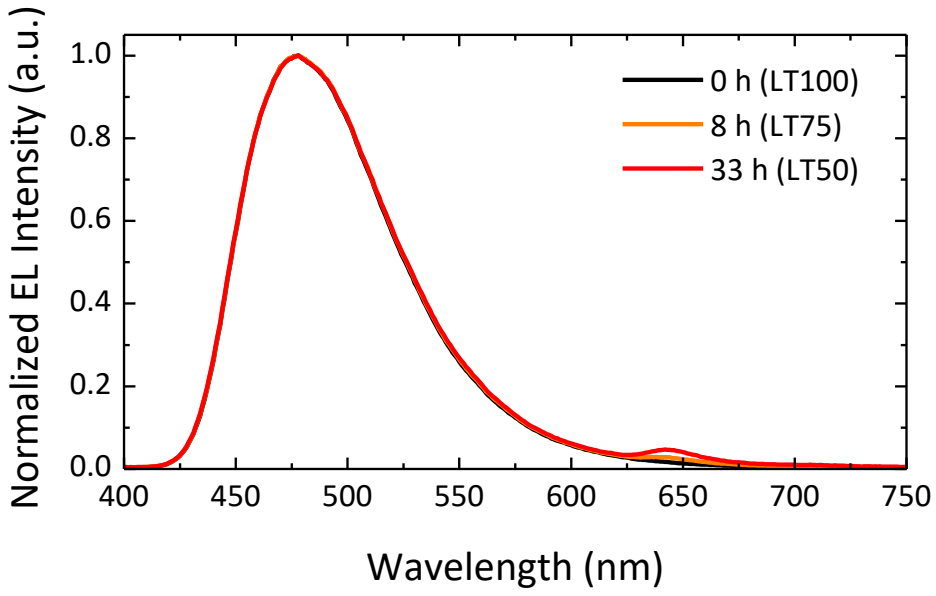

Figure 4-9 Normalized EL spectra with various driving times of **4CF1**.

4-3. Conclusion

In this chapter, partial CF_3 modification was applied to **4CzBN**. **4CzBN** is a deep-blue TADF material and can be expected to emit in blue even when the emission color is red-shifted by the partial CF_3 modification. **4CF1**, in which one of the carbazolyl groups of **4CzBN** was replaced by a CF_3 modified carbazolyl group, showed blue emission with higher PLQY and photostability comparing with that of **4CzBN**. The EQE and LT_{50} of OLEDs using these emitters were 5.9% and 3 h for **4CzBN**, and 11.7% and 33 h for **4CF1**, respectively. I succeeded in the enhancement of the EL efficiency and the operational device lifetime of the blue TADF device with the partial modification strategy using the carbazole having CF_3 groups on its β-position.

4-4. Materials and methods

4-4-1. Measurement of photoluminescence properties

UV–vis absorption spectra were recorded on UV–vis spectrophotometer (Lambda 950-KPA, Perkin-Elmer, USA). Fluorescent and Phosphorescent spectra were recorded on a Photoluminescence spectrometer (FP-8600, JASCO, Japan) at r.t or 77 K. PLQY was measured under the flow of argon gas using an absolute PL quantum yield measurement system (C11347-01, Hamamatsu Photonics, Japan) with an excitation wavelength of 340 nm. Emission lifetimes were measured using a fluorescence lifetime measurement system (C11367-03 Quantaurus-Tau, Hamamatsu Photonics, Japan). The photo-degradation was measured by light irradiation using a Xe lamp (MAX-303, Asahi Spectra, Japan) with a 365 nm bandpass filter and light intensity control feedback unit. The initial irradiation light intensity was measured by a UV power meter (C9536_H9958, Hamamatsu Photonics, Japan) and the emission was continuously recorded on a multichannel analyzer (PMA-12, Hamamatsu Photonics, Japan). CV measurements were performed using an electrochemical analyzer (ALS608D, BAS, Japan) with a glassy carbon working electrode, platinum counter electrode, and Ag/Ag^+ reference electrode. Values were corrected by using ferrocene as an external standard and expressed against Fc/Fc^+. Argon-purged THF was used as a solvent with tetrabutylammonium hexafluorophosphate ($TBAPF_6$) (0.1 mmol L^{-1}) as the supporting electrolyte. The sweep rate used for the measurements was 0.05 V s^{-1}. For the CV measurements, $E_{1/2}$ observed in the negative potential region based on the reduction of materials were defined as LUMO level with the equation of $E_{1/2} - 4.8$ (eV). HOMO level was estimated by using the band gap from the UV absorption edge and estimated LUMO level.

4-4-2. Device fabrication and characterization of OLED performance

OLEDs were fabricated by thermal evaporation onto clean ITO-coated glass substrates. Glass substrates with a pre-patterned, 100 nm thick ITO coating were used as anodes. Hole injection material **HAT-CN**, hole transport material **TrisPCz**, electron blocking material and host ***m*CBP**, hole

blocking and electron transport material **SF3TRZ** or **PPT** were used in the TADF-OLEDs. **HAT-CN**, **TrisPCz**, and ***m*CBP** were purchased from NARD Institute, Ltd. **SF3TRZ** and **PPT** was synthesized in our laboratory. Organic layers were formed by thermal evaporation. Doped emission layers and electron transport were deposited by co-evaporation. The bilayer of 2 nm **Liq** / 100 nm Al was used as cathode. After device fabrication, devices were immediately encapsulated with glass lids using epoxy glue in a nitrogen-filled glove box (O_2 < 0.1 ppm, H_2O < 0.1 ppm). Commercial calcium oxide desiccant (Dynic Co., Japan) was included in each encapsulated package. The characteristics of the OLEDs were evaluated using a source meter (Keithley 2400, Keithley Instruments Inc., USA) and an absolute external quantum efficiency measurement system (C9920-12, Hamamatsu Photonics, Japan). The operational lifetime was measured using a luminance meter (SR-3AR, TOPCON, Japan) with the devices operated at a constant direct current.

4-4-3. Synthesis and characterization

2,7-bis(trifluoromethyl)carbazole and 3,6-bis(trifluoromethyl)carbazole were synthesized according to literature.[2]

2,3,5,6-tetrakis(2,7-bis(trifluoromethyl)-9*H*-carbazol-9-yl)benzonitrile (4CF4).

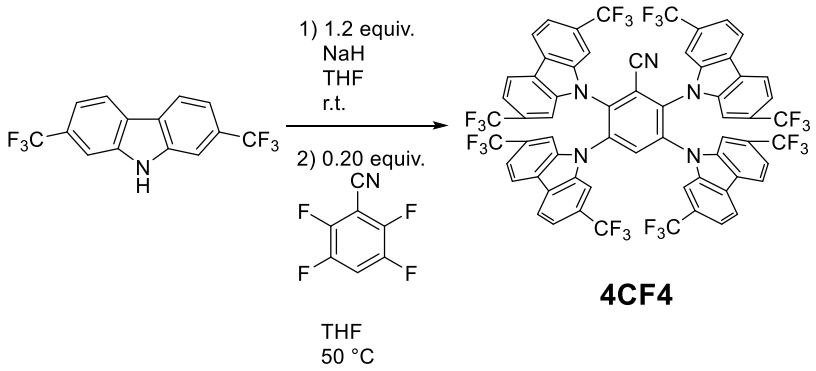

2, 7-bis(trifluoromethyl)carbazole (909 mg, 3.00 mmol) was dissolved in dry THF (40 mL), then NaH (60wt% oil dispersion, 144 mg, 3.60 mmol) was added. The reaction mixture was stirred at room temperature for an hour. After that, 2, 3, 5, 6-tetrafluorobenzonitrile (105 mg, 0.600 mmol) was added and the reaction was heated to 30 °C for 17 h. The reaction was quenched with water. The precipitate was filtered and washed with water and chloroform to obtain white powder (680 mg, 87%

yield). **^{1}H NMR** (500 MHz, acetone-d_6): δ (ppm) = 9.66 (s, 1H), 8.31 (d, 4H, 8.0 Hz), 8.28 (d, 4H, 8.0 Hz), 8.19 (s, 4H), 8.11 (s, 4H), 7.59 (d, 4H, 8.0 Hz), 7.55 (d, 4H, 8.0 Hz). **^{19}F NMR** (400 MHz, acetone-d_6): δ (ppm) = −61.78, −61.81. **Elemental analysis**: Calcd. for $C_{63}H_{25}F_{24}N_5$ (%): C 57.86, H 1.93, N 5.35; Found C 57.88, H 1.88, N 5.34. **HRMS** (FAB, *m/z*): Calcd. for $C_{63}H_{25}F_{24}N_5$ 1307.1727; Found 1307.1725, M^+.

2,3,5,6-tetrakis(3,6-bis(trifluoromethyl)-9*H*-carbazol-9-yl)benzonitrile (4CF4γ).

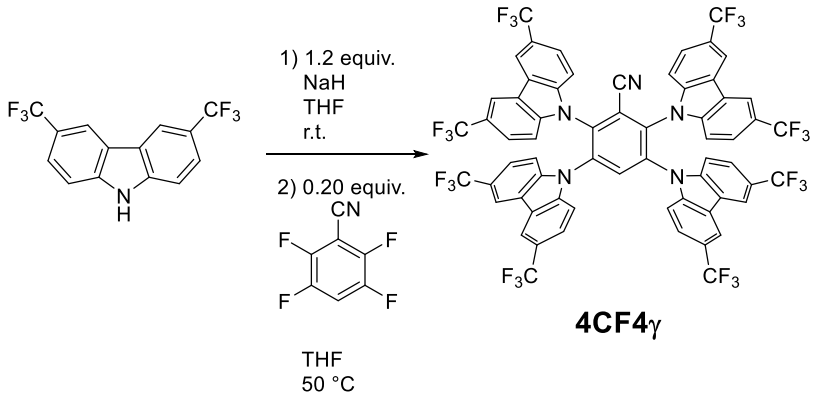

3, 6-bis(trifluoromethyl)carbazole (606 mg, 2.00 mmol) was dissolved in dry THF (40 mL), then NaH (60wt% oil dispersion, 96 mg, 2.40 mmol) was added. The reaction mixture was stirred at room temperature for an hour. After that, 2, 3, 5, 6-tetrafluorobenzonitrile (70 mg, 0.40 mmol) was added and the reaction was heated to 50 °C for 22 h. The reaction was quenched with water. The precipitate was filtered and washed with water and chloroform to obtain white powder (530 mg, 97% yield). **^{1}H NMR** (500 MHz, acetone-d_6): δ (ppm) = 9.56 (s, 1H), 8.53 (s, 4H), 8.50 (s, 4H), 8.01 (d, 4H, 8.5 Hz), 7.95 (d, 4H, 8.4 Hz), 7.62 (d, 4H, 8.5 Hz), 7.58 (d, 4H, 8.5 Hz). **^{19}F NMR** (400 MHz, acetone-d_6): δ (ppm) = −61.29, −61.36. **Elemental analysis**: Calcd. for $C_{63}H_{25}F_{24}N_5$ (%): C 57.86, H 1.93, N 5.35; Found C 57.89, H 1.96, N 5.35. **HRMS** (FAB, *m/z*): Calcd. for $C_{63}H_{25}F_{24}N_5$ 1307.1727; Found 1307.1723, M^+.

2-(2,7-bis(trifluoromethyl)-9*H*-carbazol-9-yl)-3,5,6-trifluorobenzonitrile (pre4CF1).

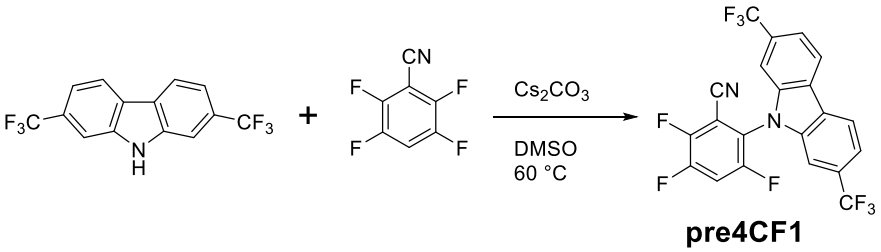

pre4CF1

2, 7-bis(trifluoromethyl)carbazole (303 mg, 1.0 mmol), 2, 3, 5, 6-tetrafluorobenzonitrile (350 mg, 2.0 mmol) and cesium carbonate (390 mg, 1.2 mmol) were dissolved in dry DMSO (7 mL). The reaction mixture was stirred at room temperature for 4 h. The reaction was quenched with water. The precipitate was filtered and washed with water. The crude product was purified by sublimation to obtain white powder (249 mg, 54% yield). **^{1}H NMR** (400 MHz, $CDCl_3$): δ (ppm) = 8.28 (d, 2H, 8.0 Hz), 7.68 (d, 2H, 8.0 Hz), 7.59−7.63 (m, 1H), 7.35 (s, 2H). **^{19}F NMR** (400 MHz, $CDCl_3$): δ (ppm) = −61.43, −114.5, −125.1, −128.7. **Elemental analysis**: Calcd. for $C_{21}H_7F_9N_2$ (%): C 55.04, H 1.54, N 6.11; Found C 55.09, H 1.59, N 6.08. **HRMS** (FAB, *m/z*): Calcd. for $C_{21}H_7F_9N_2$ 458.0466; Found 458.0470, M^+.

2-(2,7-bis(trifluoromethyl)-9*H*-carbazol-9-yl)-3,5,6-tri(9H-carbazol-9-yl)benzonitrile (4CF1).

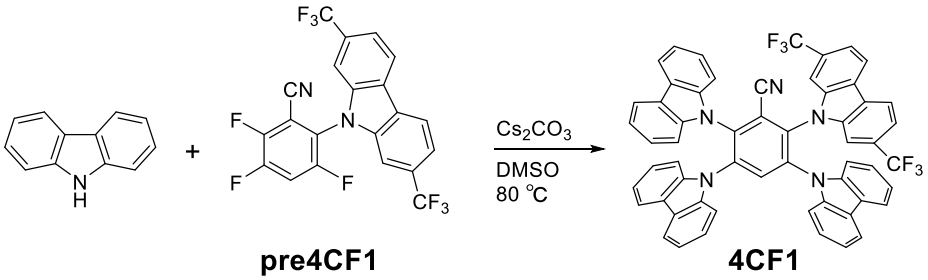

pre4CF1 **4CF1**

Carbazole (292 mg, 1.75 mmol), pre3CzCFBN (200 mg, 0.44 mmol) and cesium carbonate (682 mg, 2.1 mmol) were dissolved in dry DMSO (5 mL). The reaction mixture was stirred at 80 °C for 2 h. The reaction was quenched with water. The precipitate was filtered and washed with water. The crude product was purified by sublimation to obtain white powder (302 mg, 77% yield). **^{1}H NMR** (500 MHz, acetone-d_6): δ (ppm) = 8.94 (s, 1H), 8.29 (s, 2H), 8.26 (d, 2H, 8.0 Hz), 7.82−7.92 (m, 10H), 7.77 (d, 2H, 8.0 Hz), 7.54 (d, 2H, 8.0 Hz), 7.12−7.25 (m, 12H). **^{19}F NMR** (400 MHz, acetone-

d_6): δ (ppm) = −61.62. **Elemental analysis**: Calcd. for $C_{57}H_{31}F_6N_5$ (%): C 76.08, H 3.47, N 7.78; Found C 76.18, H 3.50, N 7.77. **HRMS** (FAB, *m/z*): Calcd. for $C_{57}H_{31}F_6N_5$ 899.2484; Found 899.2480, M^+.

References

(1) Zhang, D.; Cai, M.; Zhang, Y.; Zhang, D.; Duan, L. Sterically Shielded Blue Thermally Activated Delayed Fluorescence Emitters with Improved Efficiency and Stability. *Mater. Horizons* **2016**, *3* (2), 145–151.

(2) Gantenbein, M.; Hellstern, M.; Le Pleux, L.; Neuburger, M.; Mayor, M. New 4,4'-Bis(9-Carbazolyl)-Biphenyl Derivatives with Locked Carbazole-Biphenyl Junctions: High-Triplet State Energy Materials. *Chem. Mater.* **2015**, *27* (5), 1772–1779.

Chapter 5

Summary

In this thesis, I aimed to develop blue TADF materials with high PLQY and durability by controlling HOMO and LUMO levels and the excited-state stability through the modification of an electron-withdrawing group on the electron donor moiety. These properties of TADF materials were intensively improved by CF_3 modification at specific sites.

In **Chapter 2**, I demonstrated a new strategy for a wide HOMO-LUMO energy gap to obtain blue-shifted emission. When I employ an electron donor moiety having a weak electron-donating ability, TADF materials having wide HOMO-LUMO gaps should be obtained. To demonstrate this strategy, I selected **4CzIPN** and **4CzTPN** as a platform. As an electron-withdrawing group for weakening the donor nature, I selected the CF_3 group and introduced it to the β- or γ-position of all Cz on **4CzIPN** and **4CzTPN**. The modification with the electron-withdrawing group on the donor moiety showed the deepened HOMO levels and blue-shifted emission. The modification position of the CF_3 group affected the color purity (FWHM) and emission efficiency of emitters.

In **Chapter 3**, I used a platform of **5CzBN** to demonstrate the full and partial CF_3 modification strategies. Fully CF_3 modified emitter (**5CF5**), in which all the Cz constituting **5CzBN** were modified with CF_3 groups, exhibited highly efficient deep blue emission, as predicted from the discussion in **Chapter 2**. On the other hand, the partially CF_3 modified **5CzBN** derivatives showed red-shifted emission. Interestingly, the modification position of CF_3 on Cz has a critical effect on their photostability, while the HOMO is mainly distributing on the unmodified Cz. The modification on the β position enhanced the photostability but that on the γ position contrastingly worsened. The stability of the excited states also affected the device lifetime. **5CF1** having a CF_3 modified Cz at the *para*-position of the benzonitrile showed higher EQE of 17.6% and 3.2 times longer LT_{50} of 276 h than naked **5CzBN** (14.1%, 86 h).

In **Chapter 4**, partial CF_3 modification was applied to **4CzBN**. **4CzBN** is a deep-blue TADF material and can be expected to emit in blue even when the emission color is red-shifted by the partial CF_3 modification. **4CF1** in which one of the carbazolyl groups of **4CzBN** was replaced by a CF_3 modified carbazolyl group, showed blue emission with higher PLQY and photostability comparing

with **4CzBN**. The EQE and LT_{50} of OLEDs using these emitters were 5.9% and 3 h for **4CzBN**, and 11.7% and 33 h for **4CF1**, respectively. I succeeded in the enhancement of the efficiency and lifetime of the blue TADF device with the partial modification strategy using the carbazole having CF_3 groups on its β position.

Factors affecting device durability include (1) photochemical stability (excited state stability), (2) electrochemical stability, (3) the carrier balance of the device. The CF_3 modification at β-position of Cz improved the device durability due to its improved photochemical stability. However, increasing the number of β-modified Cz makes its HOMO and LUMO levels too deep. This leads to trap electrons and chages carrier balance of the device, resulting in the lower durability. Furthermore, in the case of partial modification, introducing too many β-modified Czs widened FWHM of the emission. Therefore, it is preferable to introduce a small number (1-2) of CF_3-modified Czs.

A future challenge is to understand why the modification of the electron-withdrawing group at the β-position of Cz leads to improve its photochemical stability. For high photochemical stability, it is important to (a) shorten the lifetime of triplet excitons (lower the probability of reaction), (b) reduce the triplet energy (reduce the reaction rate), and (c) increase the minimum BDE of the molecule (increase the energy required for the bond cleavage). For the synthesized compounds, the effects of (a) and (c) enhanced their stability. In other words, (a) the triplet lifetime was shortened by the partial modification, and (c) the BDE was increased by the modification with the electron-withdrawing groups. Therefore, modification with the electron-withdrawing group will increase the photochemical stability of the emitter. However, the effects of (a) and (c) alone could not explain why the stability was increased by the β-modification and decreased by the γ-modification. Hence, the reason for the substitution position affecting the stability should be due to (b) the difference in triplet energy. Recent insights into the TADF mechanism underlined the importance of intermediate triplet states (T_n, $n \geq 2$). Indeed, as the direct spin-flip from ^{3}CT to ^{1}CT is usually prohibited based on the El-Sayed's rule, RISC process of TADF materials are thought to be upconverted from T_1 to S_1 via T_n. Although the substructure involved in RISC has not been identified, if we consider 9-phenylcarbazole derivatives as an example of the substructure, T_1 of 9-phenylcarbazole decreased with the β-modification and

increased with the γ-modification. I assume that the difference in photostability is caused by the difference in triplet energy depending on the modification position.

In conclusion, CF_3 modified carbazole is a promising building block to design TADF materials for blue OLEDs with high efficiency and durability. However, their performances, especially operational device lifetime, are not enough for practical applications. For a further enhancement in performance of OLEDs, both the structural investigation of the emitter and device structure optimization will be needed. The stability of emitters is affected by both their photochemical and electrochemical stabilities.[1] In this thesis, I have reported the photostability-enhancement by CF_3 modification, which would be attributed to the improvement of BDE and lower triplet energy compared with unmodified one. On the other hand, CF_3 modification did not affect the electrochemical stability of emitters. Although emitters with reversible redox function are preferable, the γ-position of Cz is electrochemically active and irreversible to oxidation.[2] This problem was not resolved by the CF_3 modification. Then, for further improvement of stability, not only CF_3 modification on β-position of Cz but also alkyl or aryl modification on γ-position should be applied. In addition, for long operation lifetime, a fast RISC process is crucial to avoid triplet accumulation in the emission layers for the suppression of device degradation.[3–5] Recent studies have revealed the importance of a small energy gap between both charge-transfer and locally excited triplet states, ^{3}CT and ^{3}LE, respectively. As mentioned in **Chapter 1**, the direct spin-flip from ^{3}CT to ^{1}CT is usually prohibited based on the El-Sayed's rule, the additional ^{3}LE assists the RISC efficiently. In this point of view, a multi-donor strategy (for examples, a combination of CF_3-modified Cz with unmodified Cz and electron-donating group-modified Cz) should be effective.[6,7] I believe blue TADF emitters with CF_3-modification put into practical use in the near future by incorporating these advanced molecular design.

References

(1) Song, W.; Lee, J. Y. Degradation Mechanism and Lifetime Improvement Strategy for Blue Phosphorescent Organic Light-Emitting Diodes. *Adv. Opt. Mater.* **2017**, *5* (9), 1600901.

(2) Zhang, D.; Cai, M.; Zhang, Y.; Zhang, D.; Duan, L. Sterically Shielded Blue Thermally Activated Delayed Fluorescence Emitters with Improved Efficiency and Stability. *Mater. Horizons* **2016**, *3* (2), 145–151.

(3) Giebink, N. C.; D'Andrade, B. W.; Weaver, M. S.; MacKenzie, P. B.; Brown, J. J.; Thompson, M. E.; Forrest, S. R. Intrinsic Luminance Loss in Phosphorescent Small-Molecule Organic Light Emitting Devices Due to Bimolecular Annihilation Reactions. *J. Appl. Phys.* **2008**, *103* (4), 044509.

(4) Giebink, N. C.; D'Andrade, B. W.; Weaver, M. S.; Brown, J. J.; Forrest, S. R. Direct Evidence for Degradation of Polaron Excited States in Organic Light Emitting Diodes. *J. Appl. Phys.* **2009**, *105* (12), 124514.

(5) Wang, Q.; Aziz, H. Degradation of Organic/Organic Interfaces in Organic Light-Emitting Devices Due to Polaron-Exciton Interactions. *ACS Appl. Mater. Interfaces* **2013**, *5* (17), 8733–8739.

(6) Noda, H.; Nakanotani, H.; Adachi, C. Excited State Engineering for Efficient Reverse Intersystem Crossing. *Sci. Adv.* **2018**, *4* (6), eaao6910.

(7) Balijapalli, U.; Tanaka, M.; Auffray, M.; Chan, C. Y.; Lee, Y. T.; Tsuchiya, Y.; Nakanotani, H.; Adachi, C. Utilization of Multi-Heterodonors in Thermally Activated Delayed Fluorescence Molecules and Their High Performance Bluish-Green Organic Light-Emitting Diodes. *ACS Appl. Mater. Interfaces* **2020**, *12* (8), 9498–9506.

Table of abbreviations

OLED	Organic light-emitting diode
LED	Light-emitting diode
LCD	Liquid crystal display
ITO	Indium-tin-oxide
EL	Electroluminescence
PL	Photoluminescence
TADF	Thermally-activated delayed fluorescence
IQE	Internal EL quantum efficiency
TTA	Triplet-triplet annihilation
TPA	Triplet-polaron annihilation
ISC	Intersystem crossing
RISC	Reverse intersystem crossing
SOC	Spin-orbit coupling
CT	Charge-transfer
EML	Emission layer
TD-DFT	Time-dependent density functional theory
UV-vis	Ultraviolet-visible
CV	Cyclic voltammetry
CF_3	Trifluoromethyl
Cz	Carbazole

HOMO	Highest occupied molecular orbital
LUMO	Lowest unoccupied molecular orbital
S_0	Singlet ground state
S_1	Lowest singlet excited state
T_1	Lowest triplet excited state
E_g	Optical energy gap
PLQY, ϕ_{PL}	Photoluminescence quantum yield
f	Oscillator strength
λ_{em}	Peak maximum wavelength of emission
FWHM	Full width at half maximum
EQE	External quantum efficiency
EQE_{max}	Maximum EQE
V_{on}	Turn-on voltage
LT_{50}	Half device operational lifetime
CIE	Commission internationale de l'Éclairage
τ_p	Lifetime of prompt fluorescence
τ_d	Lifetime of delayed fluorescence
E_a	Activation energy
BDE	Bond dissociation energy

Publication lists

Original papers

1) **Yokoyama, M.**; Inada, K.; Tsuchiya, Y.; Nakanotani, H.; Adachi, C. Trifluoromethane modification of thermally activated delayed fluorescence molecules for high-efficiency blue organic light-emitting diodes. *Chemical Communications* **2018**, *54*, 8261–8264.

2) **Yokoyama, M.**; Tsuchiya, Y.; Nakanotani, H.; Adachi, C. Partially electron-withdrawing group modification of thermally activated delayed fluorescence materials aimed to improve efficiency and stability. *Chemistry Letters* accepted (doi.org/10.1246/cl.200435).

Patents

1) **Yokoyama, M.**; Hagiya, K.; Adachi, C. 有機発光素子ならびにそれに用いる発光材料および化合物，特許第 06647514 号

2) **Yokoyama, M.**; Hagiya, K.; Adachi, C. Organic electroluminescent material and organic electroluminescent element using same, WO2018/008673

3) **Yokoyama, M.**; Hagiya, K.; Adachi, C. Organic light-emitting lement, and light-emitting material and compound for use therein, WO2018/047948

4) **Yokoyama, M.**; Hagiya, K.; Adachi, C. Compound having-π-electron conjugated unit and carbazole group, WO2019/087936

Acknowledgements

The studies in this thesis were carried out at Adachi laboratory, Department of Chemistry and Biochemistry, Graduate School of Kyushu University, and Toyobo Co., Ltd.

I am deeply grateful to Prof. Chihaya Adachi, for supervising this thesis, excellent experimental environment, helpful discussions, insightful comments and advice for all my work. I am also deeply grateful to Prof. Hiroyuki Furuta and Prof. Ken Onda for co-supervising of this thesis. I would also like to thank Associate Prof. Hajime Nakanotani, and Associate Prof. Youichi Tsuchiya, they gave me useful advice and helped in preparing this thesis and my papers. Especially, Associate Prof. Youichi Tsuchiya helped in preparing this thesis and my papers, in many discussions, and in experiments. I would like to acknowledge Prof. Takuma Yasuda, Prof. Masayuki Yahiro, Associate Prof. Toshinori Matsushima, Assistant Prof. Kenichi Goushi, Assistant Prof. Ryota Kabe (OIST), Assistant Prof. Masashi Mamada, Assistant Prof. Yuya Tanaka (Chiba Univ.), Dr. Chin-Yiu Chan, Dr. Masaki Tanaka, Dr. Naoto Notsuka, Dr. Hiroki Noda, Dr. Yu Esaki, Dr. Munetomo Inoue, Dr. Sunbin Hwang, Dr. Lin-Song Cui, Dr. Hiroshi Fujimoto, Mr. Ko Inada, Mr. Takahiko Yamanaka, Mr. Kazuya Jinnai, Ms. Keiko Kusuhara, Ms. Nozomi Nakamura, helped me in discussions, experiments, and daily life. I also acknowledge Ms. Sachiko Higashikawa, Ms. Yuko Kawahara, Ms. Haruna Kato for supporting my Ph. D. course.

This study was started at Toyobo Co., Ltd. in 2014. I would like to be deeply grateful to Dr. Yasuo Ota, Mr. Satoshi Takase, Mr. Koichi Ono, Dr. Hiroki Murase, Mr. Masaru Kobayashi, Mr. Syoji Tsujii, Dr. Kazutake Hagiya, Mr. Osamu Morimoto, Mr. Hideki Tanaka, my former and present boss who gave me a splendid opportunity. Especially, Dr. Kazutake Hagiya helped my work in various situations. Thanks to their support, I was able to continue and complete this study. I deeply appreciate the members of Toyobo Co., Ltd., Mr. Taichi Toyama for material synthesis, Mr. Yoshihiro Uchida and Mr. Natsuki Ito for their advice on DFT calculations, Mr. Ryohei Yamane for NMR measurements. Because of their help, I was able to perform more useful research.

I also acknowledge all the members of Adachi laboratory, COI members, and all persons who I met through my works for their supports not only for my work but also my daily life.

Finally, I could not have succeeded in my work without the constant support and encouragement of my family. My wife Miyuki and my daughter Momoka sacrificed their time for my research and deserve my sincere thanks for their invaluable assistance. I would also like to express my gratitude to my parents and grandparents for their moral support and warm encouragement.

July, 2020 *Masayuki Yokoyama*